Localization of nitric oxide synthase in the adult rat brain

J. RODRIGO[1], D. R. SPRINGALL[2], O. UTTENTHAL[3], M. L. BENTURA[1], F. ABADIA-MOLINA[2], V. RIVEROS-MORENO[4], R. MARTÍNEZ-MURILLO[1], J. M. POLAK[2] AND S. MONCADA[4]

[1]*Department of Comparative Neuroanatomy, Instituto de Neurobiología Santiago Ramón y Cajal, Dr. Arce 37, 28002 Madrid, Spain*
[2]*Department of Histochemistry, Royal Postgraduate Medical School, Hammersmith Hospital, Du Cane Road, London W12 ONN, U.K.*
[3]*Department of Biochemistry and Molecular Biology, Facultad de Medicina, Universidad de Salamanca, Avda. del Campo Charro s/n., 37007 Salamanca, Spain*
[4]*Wellcome Research Laboratories, Langley Court, Beckenham, Kent BR3 3BS, U.K.*

SUMMARY

The distribution of the immunoreactivity to nitric oxide synthase has been examined from rostral to caudal areas of the rat central nervous system using light microscopy. Endogenous nitric oxide synthase was located using a specific polyclonal antiserum, produced against affinity purified nitric oxide synthase from whole rat brain, following the avidin–biotin peroxidase procedure. Immunoreactive cell bodies and processes showed a widespread distribution in the brain. In the telencephalon, immunoreactive structures were distributed in all areas of the cerebral cortex, the ventral endopiriform nucleus and claustrum, the main and accessory olfactory bulb, the anterior and posterior olfactory nuclei, the precommisural hippocampus, the taenia tecta, the nucleus accumbens, the stria terminalis, the caudate putamen, the olfactory tubercle and islands of Calleja, septum, globus pallidus and substantia innominata, hippocampus and amygdala. In the diencephalon, the immunoreactivity was largely found in both the hypothalamus and thalamus. In the hypothalamus, immunoreactive cell bodies were characteristically located in the perivascular–neurosecretory systems and mamillary bodies. In addition, immunoreactive nerve fibres were detected in the median eminence of the infundibular stem. The mesencephalon showed nitric oxide synthase immunoreactivity in the ventral tegmental area, the interpeduncular nucleus, the rostral linear nucleus of the raphe and the dorsal raphe nucleus. Immunoreactive structures were also found in the nuclei of the central grey, the peripeduncular nucleus and substantia nigra pars lateralis, the geniculate nucleus and in the superior and inferior colliculi. The pons displayed immunoreactive structures principally in the pedunculopontine and laterodorsal tegmental nuclei, the ventral tegmental nucleus, the reticulotegmental pontine nucleus, the parabrachial nucleus and locus coeruleus. In the medulla oblongata, immunoreactive neurons and processes were detected in the principal sensory trigeminal nucleus, the trapezoid body, the raphe magnus, the pontine reticular nuclei, the supragenual nucleus, the prepositus hypoglossal nucleus, the medial and spinal vestibular nuclei, the dorsal cochlear nucleus, the medullary reticular field, the nucleus of the solitary tract, the gracile and cuneate nuclei, the dorsal nucleus of the vagus nerve and the oral, interpolar and caudal parts of the spinal trigeminal nucleus. In the cerebellum, the stellate and basket cells showed immunoreactivity, which was also seen in the basket terminal fibres of the Purkinje cell layer. Isolated immunoreactive Purkinje cells were found in the vermis and paraflocculus regions of the cerebellum. In the granular layer of the cerebellum, the granular cells and glomeruli were also immunoreactive. Numerous positive varicose nerve fibres and occasional neurons were also found in the lateral and interposed cerebellar nuclei. Immunoreactive processes were found close to and penetrating the ependymal cells of the ventricular walls, particularly the lateral ventricles. Immunoreactive cell bodies were also detected in the circumventricular organs, including the subfornical organ and area postrema. Cerebral blood vessels were largely surrounded by varicose immunoreactive neuronal processes forming dense networks. Our demonstration of the widespread distribution of the enzyme nitric oxide synthase in diverse nuclei of the rat brain generally confirms earlier histochemical studies and suggests that this enzyme may affect the function of various neurotransmitter-specific systems. The possible implication of nitric oxide synthase in the regulation of the cerebrospinal fluid system and of cerebral blood circulation is discussed.

Phil. Trans. R. Soc. Lond. B (1994) **345**, 175–221
Printed in Great Britain

1. INTRODUCTION

Nitric oxide (NO) is synthesized from L-arginine in the mammalian brain (Knowles *et al.* 1989; Bredt *et al.* 1990, 1991*b*) as well as in neural structures of invertebrates (Elphick *et al.* 1993) by the enzyme nitric oxide synthase (NO synthase), which has been the subject of extensive study (for reviews, see Moncada & Higgs 1993; Moncada *et al.* 1991).

There is now evidence that at least two forms of NO synthase can be distinguished, the constitutive (cNOS) and the inducible (iNOS) (Hibbs *et al.* 1988; Forstermann *et al.* 1991; Moncada *et al.* 1991). The cNOS isoform is present in vascular endothelial cells (where it is known as eNOS), and in the central and peripheral nervous systems (where it is known as nNOS) (Bredt *et al.* 1990; Moncada *et al.* 1991). It has been purified from the rat brain and cerebellum (Bredt & Snyder 1990; Knowles *et al.* 1990) and cloned from rat (Bredt *et al.* 1991*a*) and human brain (Nakane *et al.* 1993). The nNOS has been described as a soluble homodimer of 155 kDa (Bredt and Snyder 1990; Schmidt & Murad 1991), with sequence similarity to cytochrome P-450 reductase at the carboxy terminal end (Bredt *et al.* 1991*a*). The nNOS has recognition sites for nicotinamide adenine dinucleotide phosphate (NADPH), flavin adenine dinucleotide (FAD), flavin mononucleotide (FMN) and calmodulin (Bredt *et al.* 1991*a*). This form of the enzyme is cytosolic, and totally dependent on Ca^{2+}/calmodulin, L-arginine as substrate and NADPH as co-factor (Knowles *et al.* 1989; Bredt & Snyder 1990, 1992; Garthwaite 1991; Moncada *et al.* 1991).

Biochemical measurements in different regions of the brain have shown that the highest concentration of NO synthase is found in the cerebellum followed by the hypothalamus and midbrain, striatum and hippocampus, with the lowest activity in the medulla oblongata (Forstermann *et al.* 1990).

The iNOS has been purified from the cytosol of activated murine macrophages (Hevel *et al.* 1991; Yui *et al.* 1991) and shown to have a molecular mass of 135 kDa. It has also been identified in mast cells, lymphocytes, neutrophils, hepatocytes, vascular smooth muscle and in tumour, mesangial and endothelial cells (Wright *et al.* 1989; Busse & Mulsch 1990; Marsden & Ballermann 1990; Salvemini *et al.* 1990; Gross *et al.* 1991; Moncada *et al.* 1991). In rodent macrophage cell lines (RAW 264.7 and J774) the synthesis of iNOS is dependent on induction by lipopolysaccharide (LPS) and cytokines (Marletta *et al.* 1988). The enzyme also requires NADPH, FAD and FMN and, to varying degrees, tetrahydrobiopterin (BH_4), and glutathione for full activity (Stuehr *et al.* 1990; Hevel *et al.* 1991). The induction of iNOS can be inhibited by glucocorticoids (Moncada *et al.* 1991). The iNOS from murine macrophages has been cloned (Lyons *et al.* 1992; Xie *et al.* 1992; Lowenstein *et al.* 1993) and found to be distinct from the two known constitutive isoenzymes. Furthermore, human iNOS has recently been cloned, both from chondrocytes (Charles *et al.* 1993) and hepatocytes (Geller *et al.* 1993).

Both the constitutive and inducible forms of NO synthase can be immunoprecipitated with an antibody against neuronal NADPH diaphorase and the activity can be competitively inhibited by nitro blue tetrazolium (Hope *et al.* 1991). Human kidney cells in culture, transfected with NO synthase cDNA, exhibit both NADPH diaphorase and NO synthase activities (Dawson *et al.* 1991). Thus, studies in primate and rat brains have suggested that NADPH diaphorase and nNOS are coincidental (Bredt *et al.* 1991*b*; Dawson *et al.* 1991; Vincent & Kimura 1992).

Nitric oxide is a diffusible gas with the properties of a free radical. Because it is highly lipophilic NO can diffuse through cell membranes without the aid of specific membrane transporters. It then acts on neighbouring cells as a paracrine signal molecule capable of modulating different brain functions (Moncada *et al.* 1991; Garthwaite 1991; Snyder 1992).

Nitric oxide has been shown to stimulate the soluble guanylate cyclase in homogenates of mouse cerebral cortex (Miki *et al.* 1977) and rat cerebellum (Yoshikawa & Kuriyama 1980). Nitric oxide acts on the haem moiety of soluble guanylate cyclase which in turn results in increased levels of cyclic guanosine-5′-monophosphate (cGMP) in target cells (Bredt & Snyder 1989; Knowles *et al.* 1989; East & Garthwaite 1991).

Nitric oxide has also been implicated in various neuropathological disorders, including Huntington's disease (Ferrante *et al.* 1985; Kowall *et al.* 1987), cerebral hypoxia/ischaemia (Ferreiro *et al.* 1988; Halliwell 1989; Uemura *et al.* 1990), Parkinson's disease (Halliwell 1989) and schizophrenia (Karson *et al.* 1991), where NO may mediate the neurotoxic effects of glutamate (Hyman *et al.* 1992; Pauwels & Leysen 1992).

The nNOS has been immunocytochemically localized in discrete neuronal populations in the rat brain and in neurons throughout the body in rat and human (Bredt *et al.* 1990; Bredt & Snyder 1990; Springall *et al.* 1992), but no detailed mapping studies have yet been reported. Many studies on the distribution of nNOS have been carried out using NADPH diaphorase histochemistry, assuming co-localization of nNOS with NADPH diaphorase (Hope *et al.* 1991; Dawson *et al.* 1991). It has been reported that paraformaldehyde fixation affects the NADPH diaphorase activity (Matsumoto *et al.* 1993), leading to a lack of correlation between NADPH diaphorase staining and NO synthase immunocytochemistry (Dun *et al.* 1992). However, the results of Terenghi *et al.* (1993) have shown a good correlation between NADPH diaphorase staining and NO synthase immunocytochemistry in spinal cord tissue fixed with 1% paraformaldehyde.

The aim of this study was to provide a detailed description of the distribution of NO synthase in the central nervous system of the rat using specific immunocytochemical detection, thus enabling a comparison with other reports obtained using NADPH diaphorase activity. This should also provide a basis for the understanding of the involvement of NO in the metabolic activity of the neurons,

their interrelationship and the role of NO in neuropathological disorders.

2. MATERIALS AND METHODS

Tissue was collected from 12 adult male albino Wistar rats (Charles River) (200–250 g body mass). Deeply anaesthetized animals (Equithesin, Jansen Laboratories, 2.5 ml kg^{-1}, i.p.) were ventilated through a tracheal cannula and perfused through the left ventricle with 50 ml of 0.9% saline as a vascular rinse, followed by 500 ml of fixative solution containing 4% paraformaldehyde in 0.1 M phosphate buffer (PB), pH 7.4. The brains were removed, cut into 4–5 mm coronal blocks, and postfixed for a further 4 h (4% paraformaldehyde in 0.1 M PB) at room temperature. Blocks of brains were then rinsed by immersion overnight at 4°C in a solution of 0.1 M PB, containing 30% sucrose, with continuous stirring.

(*a*) *Antibody*

Nitric oxide synthase was purified from rat whole brain according to the method of Bredt & Snyder (1990) and injected into rabbits as described elsewhere (Springall *et al.* 1992; Riveros-Moreno *et al.* 1993). The antiserum thus obtained has been shown to react immunocytochemically with neurons in different species (Springall *et al.* 1992; Martinez *et al.* 1994; Terenghi *et al.* 1993) and to cross-react at high concentration with pig, human and bovine endothelium, and only weakly with rat endothelium (Springall *et al.* 1992). In Western blots of different tissue homogenates a protein band of 155 kDa molecular mass is visible, corresponding to neuronal NO synthase and in tissues rich in blood vessels, a protein band of 135 kDa can be detected, corresponding to the constitutive endothelial form (Springall *et al.* 1992).

(*b*) *Immunocytochemistry*

The brains from eight animals were frozen and serial 40 μm thick frontal sections were prepared using a Leitz sledge microtome. Free-floating sections were incubated with NO synthase antiserum and processed according to the avidin-biotin peroxidase complex (ABC) procedure (Guesdon *et al.* 1979; Hsu *et al.* 1981; Hsu & Raine 1981) to visualize the immunoreactive sites.

Briefly, free-floating sections were incubated in phosphate-buffered saline (PBS) containing 3% normal goat serum (ICN Biochemicals Ltd) and 0.2% Triton X-100, for 30 min and then in the antiserum against cNOS diluted 1 : 2500 in PBS/Triton X-100, overnight at 4°C. After washing several times in PBS, the sections were incubated in an ABC kit (Vector Laboratories Ltd) and the peroxidase activity was demonstrated following the nickel-enhanced diaminobenzidine procedure (Shu *et al.* 1988).

(*c*) *Immunocytochemical controls*

Controls were performed on two animals. No immunolabelling was observed when the primary antibody was omitted or replaced with an equivalent concentration of preimmune serum, normal rabbit IgG, or when the tissue sections were incubated with primary antiserum preabsorbed (overnight at 4°C) with the antigen extracted from rat brain.

3. ABBREVIATIONS USED IN THE TEXT AND FIGURES

I–VI	cortical layers
6	abducens nucleus
10	dorsal motor nucleus of the vagus nerve
3V	3rd ventricle
4V	4th ventricle
ac	anterior commissure
aca	anterior commissure, anterior
Acb	accumbens nucleus
ACo	anterior cortical amygdaloid nucleus
AHA	anterior hypothalamic area
AI	agranular insular cortex
AMPO	anteromedial preoptic nucleus
AOB	accessory olfactory bulb
AOD	anterior olfactory nucleus, dorsal
AOL	anterior olfactory nucleus, lateral
AOM	anterior olfactory nucleus, medial
AOP	anterior olfactory nucleus, posterior
AOV	anterior olfactory nucleus, ventral
AP	area postrema
Aq	aqueduct
Arc	arcuate hypothalamic nucleus
AV	anteroventral thalamic nucleus
AVPO	anteroventral preoptic nucleus
ax	axon
B	basket cell
b	basket terminal
BAOT	bed nucleus accessory olfactory tract
BMA	basomedial amygdaloid nucleus
bp	brachium pontis
BST	bed nucleus stria terminalis
BSTMPL	posterolateral division of bed nucleus of stria terminalis
BSTV	bed nucleus stria terminalis, pars ventralis
C	circularis nucleus
CA1–3	field CA1–CA3 of Ammon's horn
CC	central canal
cc	corpus callosum
CeL	centrolateral amygdaloid nucleus
CeM	centromedial amygdaloid nucleus
cg	cingulum
Cg	cingulate cortex
CG	central grey
CGD	central grey dorsal
CGPn	central grey of the pons
CI	caudal interstitial nucleus
CL	claustrum
CLi	caudal linear nucleus raphe
CnF	cuneiform nucleus
cp	cerebral peduncle
CPu	caudate putamen
Cu	cuneate nucleus
DA	dorsal hypothalamic area
DC	dorsal cochlear nucleus

DEn	dorsal endopiriform nucleus
DG	dentate gyrus
DI	dysgranular insular cortex
Dk	Darkschewitsch nucleus
Dlg	dorsolateral geniculate nucleus
DM	dorsomedial hypothalamic nucleus
DLL	dorsal nucleus of lateral lemniscus
DP	dorsal peduncular cortex
DpG	deep white layer
DPGi	dorsal paragigantocellular nucleus
DPO	dorsal periolivary region
DR	dorsal raphe nucleus
ec	part ectal of the dentate gyrus
ECIC	external cortex of inferior colliculus
en	part endal of the dentate gyrus
Ent	entorhinal cortex
EP	entopeduncular nucleus
EPL	external plexiform layer olfactory bulb
EW	Edinger-Westphal nucleus
f	fornix
Fr	frontal cortex
fr	fasciculus retroflexus
FStr	fundus striati
G	granule cell
Gi	gigantocellular reticular nucleus
GI	granular insular cortex
GL	glomerular layer
GP	globus pallidus
Gr	gracile nucleus
gr	granular layer
GrA	granular cell layer of accessory olfactory bulb
GrM	granular cell layer of principal olfactory bulb
hbc	habenular commissure
HDB	nucleus horizontal limb diagonal band
IC	inferior colliculus
ic	internal capsule
ICj	island of Calleja
ICjM	island of Calleja, major island
IF	interfascicular nucleus
IG	indusium griseum
IL	infralimbic cortex
ILL	intermediate nucleus lateral lemniscus
IM	intercalated nucleus amygdala
IMG	amygdaloid intramedullary grey
Inf	infundibular stem
InG	intermediate grey layer
IntA	interposed cerebellar nucleus, anterior
IntP	interposed cerebellar nucleus, posterior
InWh	intermediate white layer
IP	interpeduncular nucleus
IRt	intermediate reticular nucleus
LA	lateroanterior hypothalamic nucleus
Lat	lateral cerebellar nucleus
LC	locus coeruleus
LDTg	laterodorsal tegmental nucleus
LDTgV	laterodorsal tegmental nucleus ventral
LDth	laterodorsal thalamic nucleus
LH	lateral hypothalamic nucleus
LHb	lateral habenular nucleus
LL	lateral lemniscus
LM	lateral mamillary nucleus
lm	stratum lacunosum moleculare
lo	lateral olfactory tract
LO	lateral orbital cortex
LPB	lateral parabrachial nucleus
LPGi	lateral paragigantocellular nucleus
LPO	lateral preoptic area
LPth	lateral posterior thalamic nucleus
LRt	lateral reticular nucleus
LSD	lateral septal nucleus, dorsal
LSO	lateral superior olive
LSV	lateral septal nucleus, ventral
LV	lateral ventricle
M	mitral cell
MCPO	magnocellular preoptic nucleus
MdD	medullary reticular field, dorsal
MdV	medullary reticular field, ventral
ME	median eminence
Me	medial amygdaloid nucleus
Me5	mesencephalic trigeminal nucleus
MeA	medial amygdaloid nucleus, anterior
MeP	medial amygdaloid nucleus, posterodorsal
MePV	medial amygdaloid nucleus, posteroventral
mfb	medial forebrain bundle
mfbn	medial forebrain bundle nucleus
MG	medial geniculate nucleus
Mi	mitral cell layer
MiA	mitral cell layer accessory olfactory bulb
MiTg	microcellular tegmental nucleus
ML	medial mamillary nucleus, lateral
MnPO	median preoptic nucleus
MM	medial mamillary nucleus, medial
MO	medial orbital cortex
mol	molecular layer
MPA	medial preoptic area
MPB	medial parabrachial nucleus
MPT	medial pretectal nucleus
MS	medial septal nucleus
MSO	medial superior olive
MVe	medial vestibular nucleus
MVeV	medial vestibular nucleus, ventral area
nBM	nucleus basalis of Meynert
o	stratum oriens
Oc	occipital cortex
ON	olfactory nerve layer
Op	optic nerve layer
OPT	olivary pretectal nucleus
Opt	optical tract
OT	nucleus optic tract
ox	optic chiasm
p	stratum pyramidale
Pa	paraventricular hypothalamic nucleus
Par	parietal cortex
Pas	parasubiculum
PBP	parabrachial pigmented nucleus
pc	posterior commissure
PCRt	parvocellular reticular nucleus
PDTg	posterodorsal tegmental nucleus
Pe	periventricular hypothalamic nucleus
PF	parafascicular thalamic nucleus
Pg	periglomerular cell
PH	posterior hypothalamic area
Pir	piriform cortex
PiRe	pineal recess of third ventricle

PL	paralemniscal nucleus
PLCo	posterolateral cortical amygdaloid nucleus
PMCo	posteromedial cortical amygdaloid nucleus
PMD	paramamillary nucleus, dorsal
PMV	paramamillary nucleus, ventral
Pn	pontine nuclei
PnC	pontine reticular nucleus, caudal
PnO	pontine reticular nucleus, oral
PoDG	polymorph layer of the dentate gyrus
pol	polymorph layer of the olfactory tubercle
PP	peripeduncular nucleus
PPT	posterior pretectal nucleus
PPTg	pedunculopontine tegmental nucleus
Pr5	principal sensory trigeminal nucleus
PRH	perirhinal cortex
PrH	prepositus hypoglossal nucleus
PS	parastrial nucleus
PT	parataenial thalamic nucleus
Pu	Purkinje cell
Pul	Purkinje cell layer
PVA	paraventricular thalamic nucleus, anterior
PVP	paraventricular thalamic nucleus, posterior
Py	pyramidal tract
r	stratum radiatum
Re	reuniens thalamic nucleus
RF	rhinal fissure
Rh	rhomboid thalamic nucleus
RLI	rostral linear nucleus raphe
RMg	raphe magnus nucleus
RS	retrosplenial cortex
Rt	reticular thalamic nucleus
RtTg	reticulotegmental nucleus pons
S	subiculum
SFO	subfornical organ
SHi	septohippocampal nucleus
SHy	septohypothalamic nucleus
SI	substantia innominata
sm	stria medullaris thalamus
SN	substantia nigra
SNC	substantia nigra, compacta
SNL	substantia nigra, lateral
SNR	substantia nigra, reticulata
SO	supraoptic nucleus
Sol	solitary nucleus
SOR	supraoptic nucleus, retrochiasmatic
sp5	spinal trigeminal tract
Sp5C	spinal trigeminal nucleus, caudalis
Sp5I	spinal trigeminal nucleus, interpolaris
Sp5O	spinal trigeminal nucleus, oralis
spc	superior cerebellar peduncle
SpTg	subpeduncular tegmental nucleus
SpVe	spinal vestibular nucleus
St	stellate cell
st	stria terminalis
SuC	superior colliculus
SuG	superficial grey layer
SuM	supramamillary nucleus
SuVe	superior vestibular nucleus
TC	tuber cinereum
Te	temporal cortex
TT	taenia tecta
Tu	olfactory tubercle
Tz	nucleus trapezoid body
VCA	ventral cochlear nucleus, anterior
VDB	nucleus vertical limb diagonal band
VEn	ventral endopiriform nucleus
VG	ventral geniculate nucleus
VL	lateral ventricle
VlG	ventrolateral geniculate nucleus
VLL	ventral nucleus of the lateral lemniscus
VMH	ventromedial hypothalamic nucleus
VN	vomeronasal nerve layer
VO	ventral orbital cortex
VP	ventral pallidum
VTA	ventral tegmental area
ZI	zona incerta

4. RESULTS

The distribution of cNOS immunoreactive (cNOS-IR) structures is graphically represented in diagrams of a series of frontal sections of the telencephalon, diencephalon, mesencephalon, pons, medulla oblongata and cerebellum (figure 1*a–y*).

(*a*) *Telencephalon*

(i) *Cortex*

Immunoreactive neurons were found at all levels of the cerebral cortex from rostral to caudal poles. The morphology of these immunoreactive neurons ranged from fusiform, to triangular and to multipolar, and all were distributed in layers II–III, IV and VI (figure 2*a–d*). The cNOS-IR neurons contained a few, long primary aspiny processes, which showed a small number of long and varicose collaterals. In general, the dendritic arborization was not complicated, being situated around the perikaryon. In some cases the initial portion of the axon was immunoreactive. Some of the immunoreactive cortical neurons showed long processes, which extended to proximal layers. In general, all cortical areas showed immunoreactive varicose fibres, some of which were found crossing all cortical layers. Varicose processes formed a dense plexus in layer I, where punctate immunoreactive fibres were also found (figure 3*a–d*).

In more rostral sections, immunoreactive neurons were found in the deep layer of the infralimbic cortex (figure 4*a*) and occasionally in the ventrolateral and lateral orbital cortices. The cingulate cortex contained few and scattered immunoreactive neurons distributed in layers II and III, closely related to the indusium griseum. In caudal levels of the cingulate cortex, numerous cNOS-IR neurons were mainly located in layer IV and in the border with the cingulum. This latter area always showed immunoreactive neurons.

The frontal cortex contained cNOS-IR neurons distributed in layers II–IV (figure 4*b*), which were immersed in a dense plexus of immunoreactive varicose processes, and in layers V and VI. The parietal (figure 4*c*) and temporal cortices contained immunoreactive neurons in the II–III and VI layers. Occasional immunoreactive neurons were found in layer I. The granular, disgranular and agranular insular cortices showed lightly immunoreactive

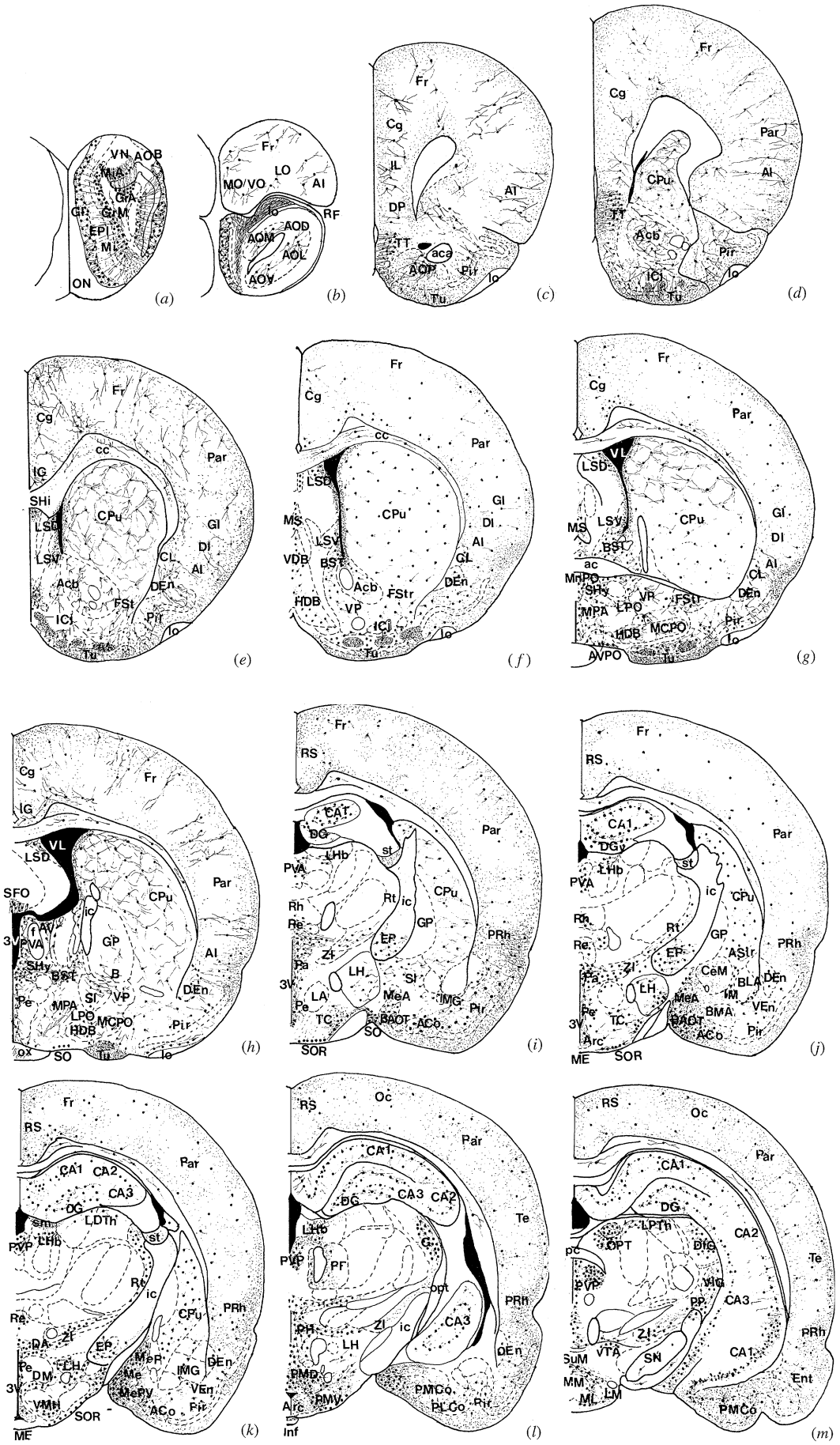

Figure 1. Diagrams showing (*a–y*) cNOS-IR nerve fibres and neurons in the telencephalon, diencephalon, pons, medulla oblongata and cerebellum. Scale bars = 50 μm.

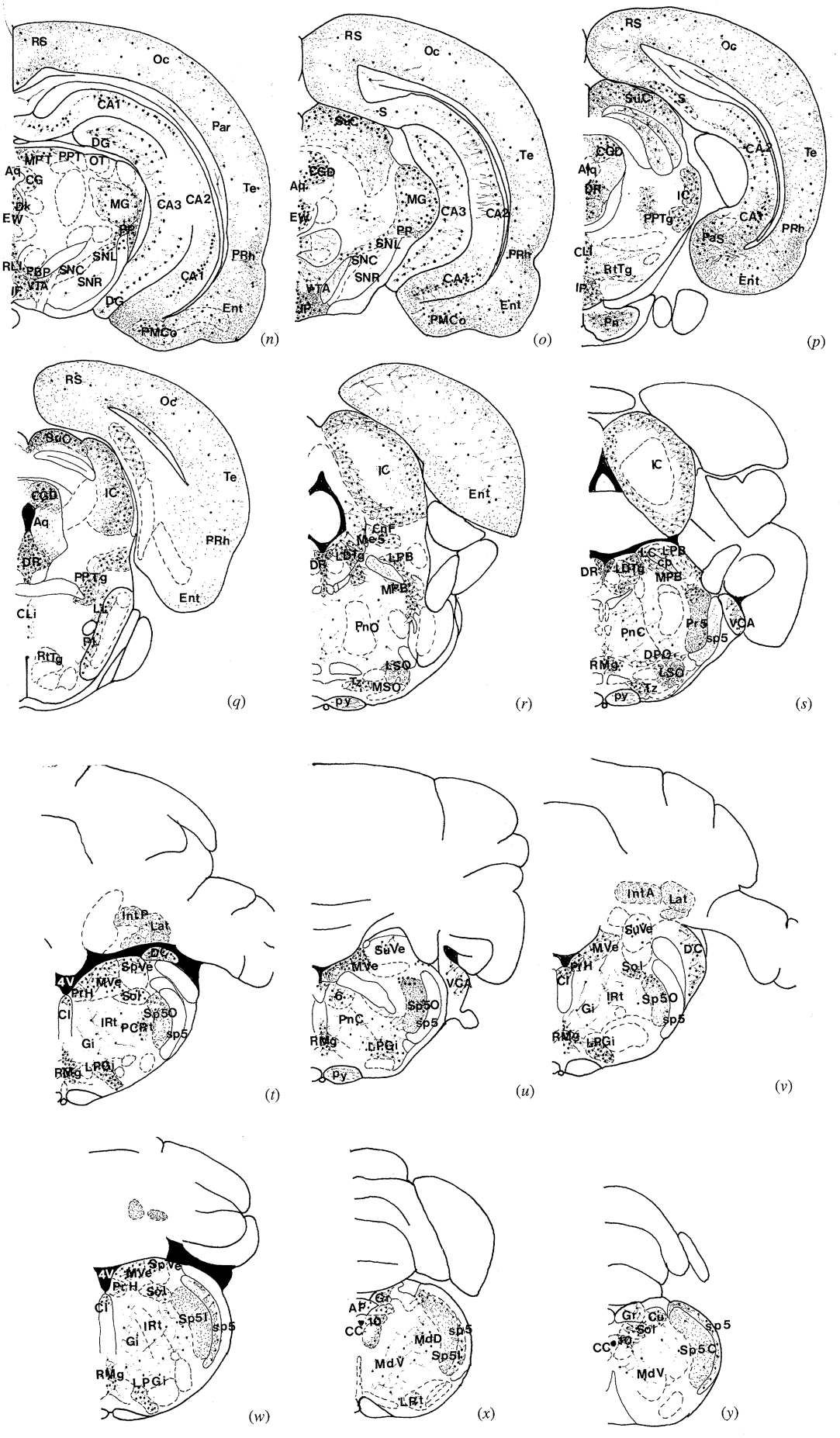

Figure 1 (*Continued*)

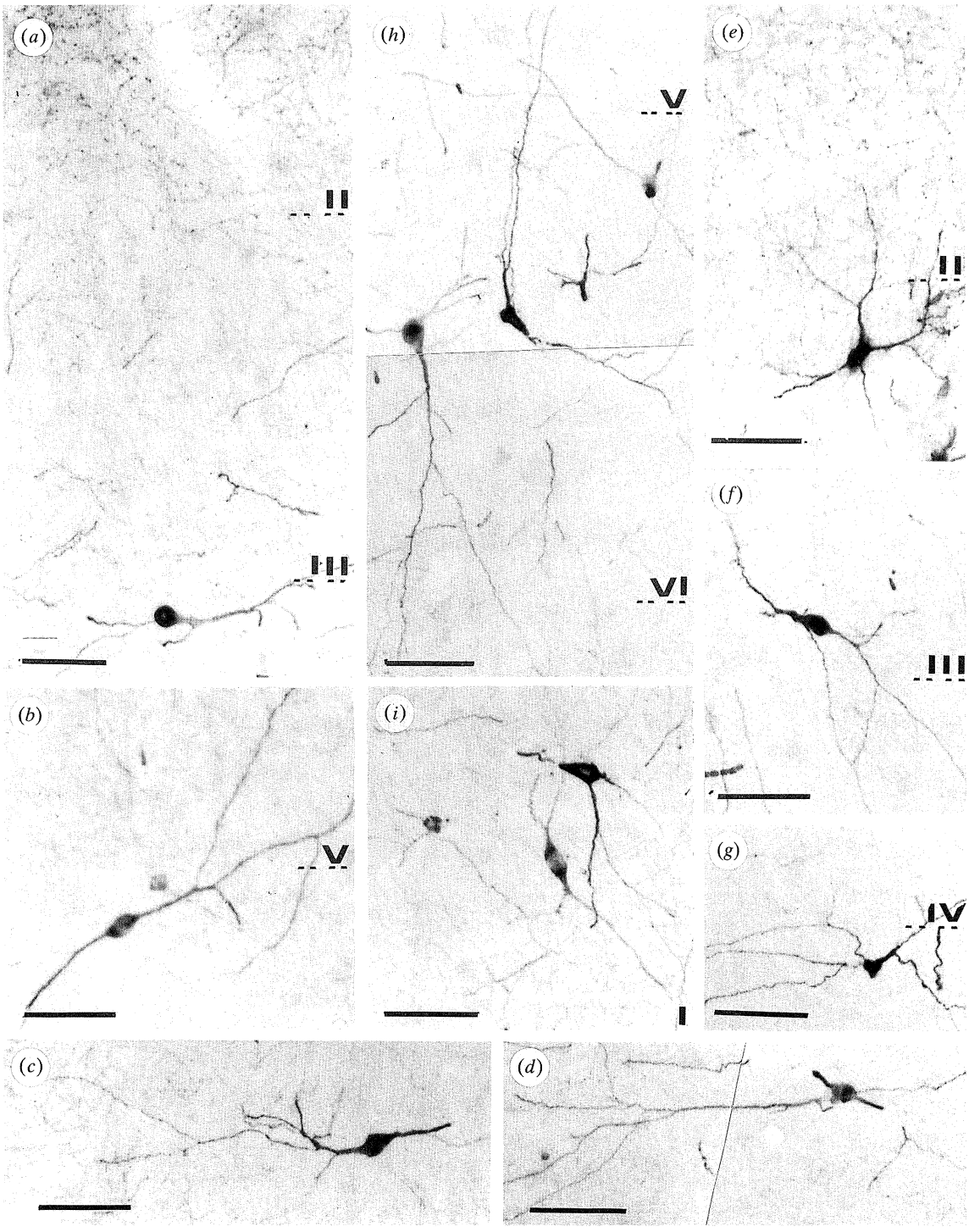

Figure 2. The morphology of immunoreactive neurons in the cingulate and frontal cortices. Aspiny cNOS-IR neurons are distributed in layers III (*a*) and V (*b*) of the cingulate cortex. Immunoreactive neurons situated in the indusium griseum are represented in (*c*) and (*d*). (*e–g*) cNOS-IR neurons in layers II–IV of the frontal cortex. (*h*) Aspects of aspiny neurons located in layers V–VI of the frontal cortex. (*i*) cNOS-IR aspiny multipolar neurons depicted bordering the cingulum. Scale bars = 50 μm.

neurons, which were distributed similarly. A dense immunoreactive plexus was found in layers II and III.

(ii) *Piriform cortex*

The piriform cortex comprises three layers organized radially, namely the superficial plexiform, the pyramidal and the polymorph cell layers. In the plexiform layer, an immunoreactive varicose plexus was found containing some immunoreactive neurons. In the pyramidal cell layer, a few weakly immunoreactive neurons were found in its deepest portion, close to the polymorph layer. The polymorph layer contained cNOS-IR neurons, 20–25 μm in diameter, with fusiform or multipolar morphology. Long aspiny processes were oriented in all directions, particularly

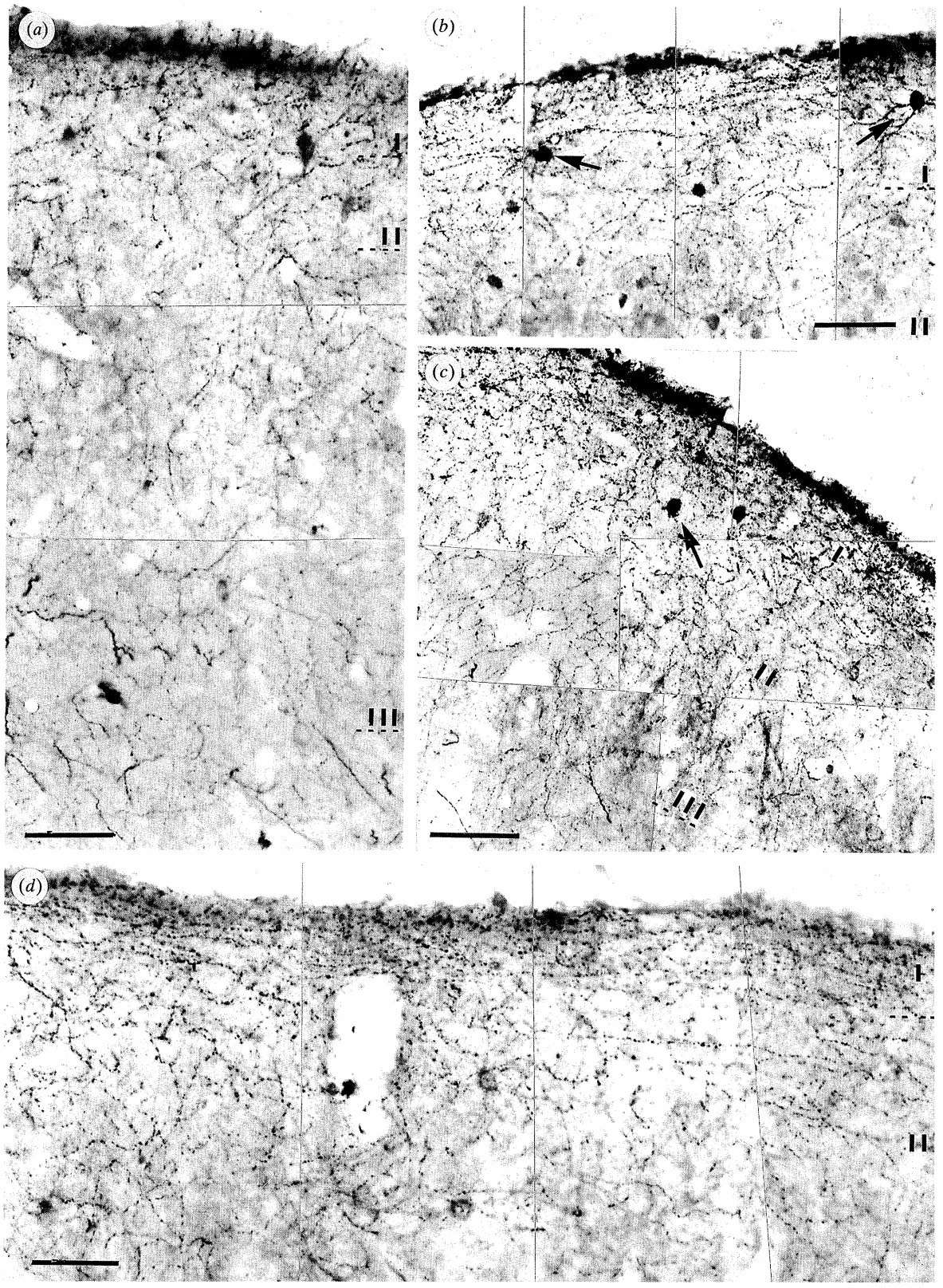

Figure 3. The distribution of varicose immunoreactive plexuses in different cortical areas. (*a*) A dense reactive network in layers I–III of the parietal cortex. Notice the strong density of nerve fibres in layer I, with the number of cNOS-IR fibres decreasing progressively in layers II and III. (*b*) The immunoreactive plexus in layers I and II of the temporal cortex. The long, horizontally orientated immunoreactive nerve fibres in layer I constitute a dense plexus. Notice in (*b*) the presence of a few, weakly immunoreactive neurons among the immunoreactive fibres. (*c*) An immunoreactive plexus made by horizontal nerve fibres in layer I of the dysgranular insular cortex which contains a few small immunoreactive neurons. (*d*) The distribution of immunoreactive nerve fibres in the perirhinal cortex. Notice in (*a*) the presence of some immunoreactive neurons in layer I and a dense plexus in layer II. Scale bars = 50 μm.

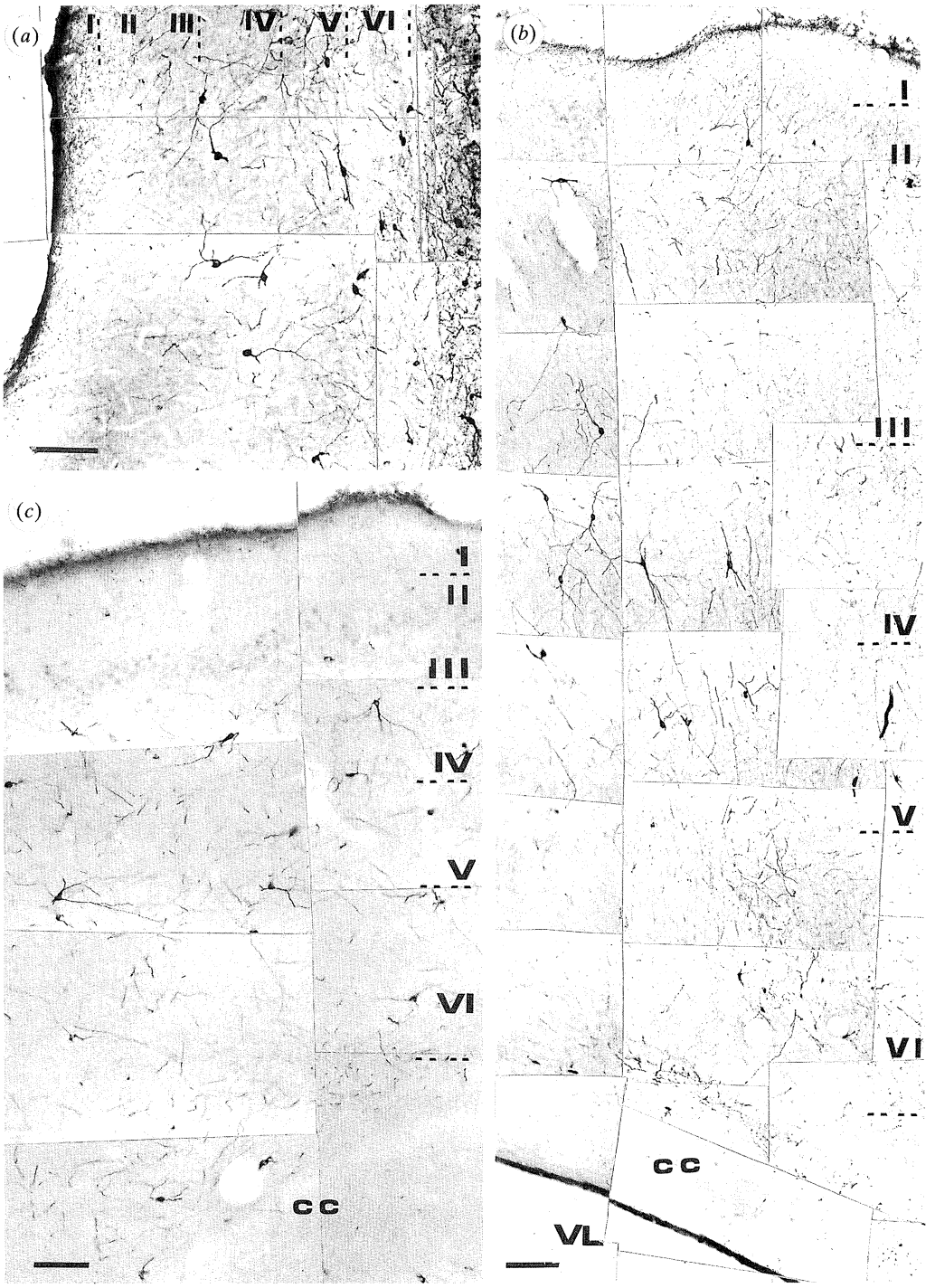

Figure 4. Photomontage showing a general view of the distribution of cNOS-IR in the infralimbic (*a*), frontal (*b*) and parietal (*c*) cortices. Scale bars = 100 μm.

to the pyramidal and plexiform layers where they showed varicose morphology and contributed to the formation of the intrinsic plexus. The density of immunoreactive fibres forming the plexus in the plexiform layers increased close to the rhinal fissure.

(iii) *Entorhinal cortex*

The entorhinal cortex contained a moderate number of cNOS-IR multipolar neurons, which were distributed in the deepest layers and included in a dense immunoreactive plexus formed by thin varicose fibres and thicker processes intensely stained (figure 5). A similar arrangement was also visualized in the amygdalo-piriform transition cortex.

(iv) *Corpus callosum*

The corpus callosum was crossed by immunoreactive fibres and contained a few immunoreactive neurons with elongated or fusiform morphology.

(v) *Dorsal endopiriform nucleus and claustrum*

These structures, both situated deep in the insular

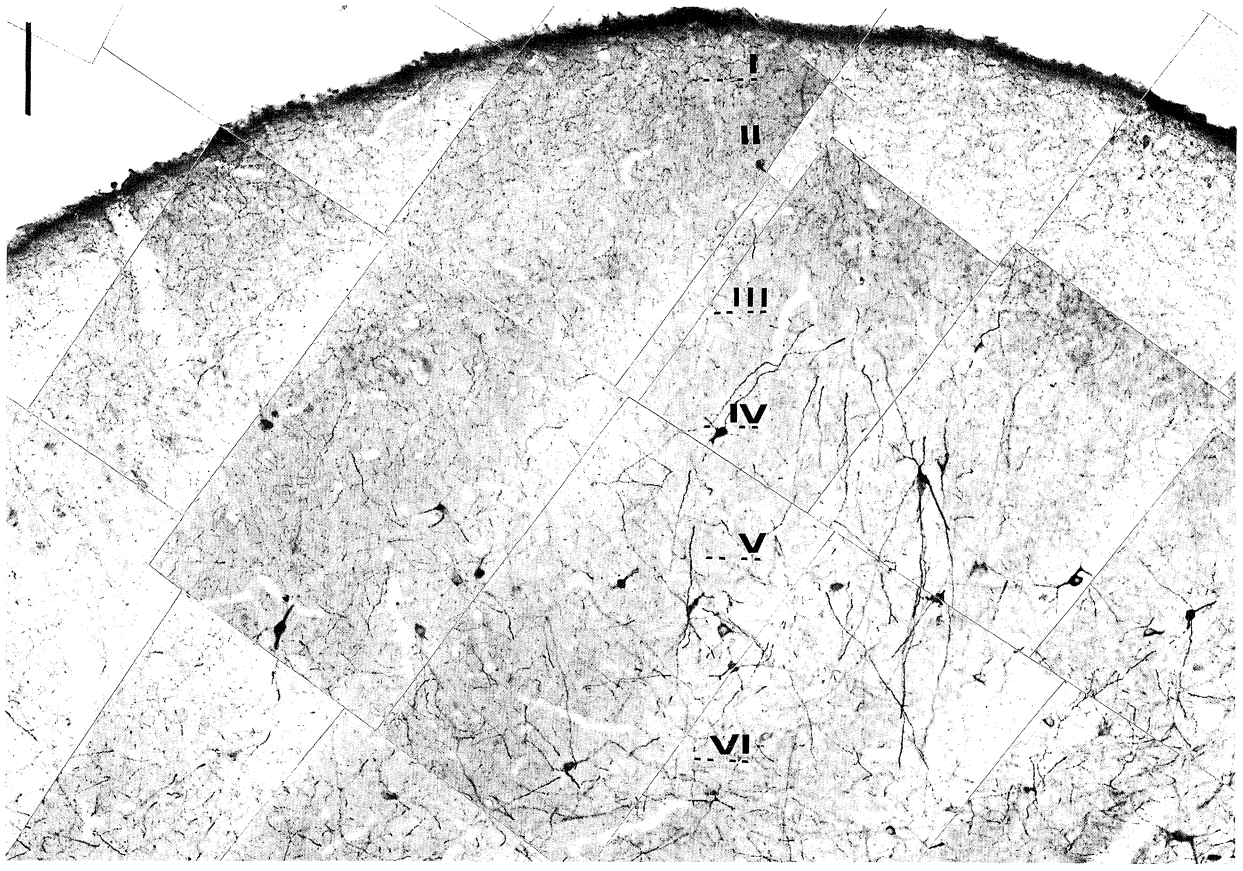

Figure 5. Photomontage illustrating the distribution of cNOS-IR in the entorhinal cortex. Notice that multipolar reactive neurons are located in layers IV and VI. Scale bar = 100 μm.

and primary olfactory cortices, were limited ventromedially by the deepest part of the amygdala and, in rostral coronal sections, by the more ventral portion of the caudate putamen and the fundus striatum. These nuclei contained immunoreactive neurons, 15–20 μm in diameter, which showed long processes that formed a small plexus placed dorsally along the lateral border of both nuclei. cNOS-IR neurons were more numerous in the ventral endopiriform nucleus than in the claustrum, but the number decreased laterally and ventrally in the transitional area with the deep layer of the agranular insular cortex and polymorph layer of the piriform cortex, respectively.

(vi) *The main olfactory bulb*

cNOS-IR neurons were found forming clusters in the granule cell layer (figure 6*a*,*b*). Some of these were intensely stained and were located close to the boundary of the ependymal layer. The cells showed rounded, fusiform, elongated and flattened shapes, with 15–25 μm maximum soma diameter and thick apical dendrites orientated towards upper layers (figure 6*b*). A small number of intensely stained neurons was also found in the deep portion of the granular cell layer, displaying morphological aspects of short-axon type cells (figure 6*c*) whose proximal dendrites were oriented in parallel to the white matter, forming a delicate and varicose plexus. In the upper portions of the granule cell layer, some multipolar cells were seen showing weak immunoreactivity and with varicose processes which were oriented radially to external layers of the main olfactory bulb, crossing the unreactive mitral cell layer and the internal and external plexiform layer.

Numerous cNOS-IR neurons with round or piriform shapes and 10–20 μm soma extent were found in the glomerular layer. These cells resembled periglomerular cells (figure 6*d*,*e*). The primary immunoreactive process gave rise to short collaterals, which contributed to form a dense and varicose plexus at the level of the glomerular layer.

Immunoreactive fibres forming small fascicles crossed all layers and, in the granular cell layer, constituted small fascicular bundles that separated clusters of immunoreactive granular cells.

(vii) *The accessory olfactory bulb*

The immunoreactivity in this region was very intense, which was in striking contrast with that in the main olfactory bulb (figure 7*a*). The granular cell layer contained numerous small, round neurons, 10–15 μm in diameter, which had a stained cytoplasmic ring and an apical process (figure 7*b*,*c*). These processes, forming fascicular bundles, crossed the myelinated axons of the lateral olfactory tract and the mitral cell layer to terminate close to the external plexiform layer in a dense arborization. Some immunoreactive neurons, exhibiting the appearance of mitral cells (figure 7*d*), were found in the deepest portion of the mitral cell layer placed in parallel to the

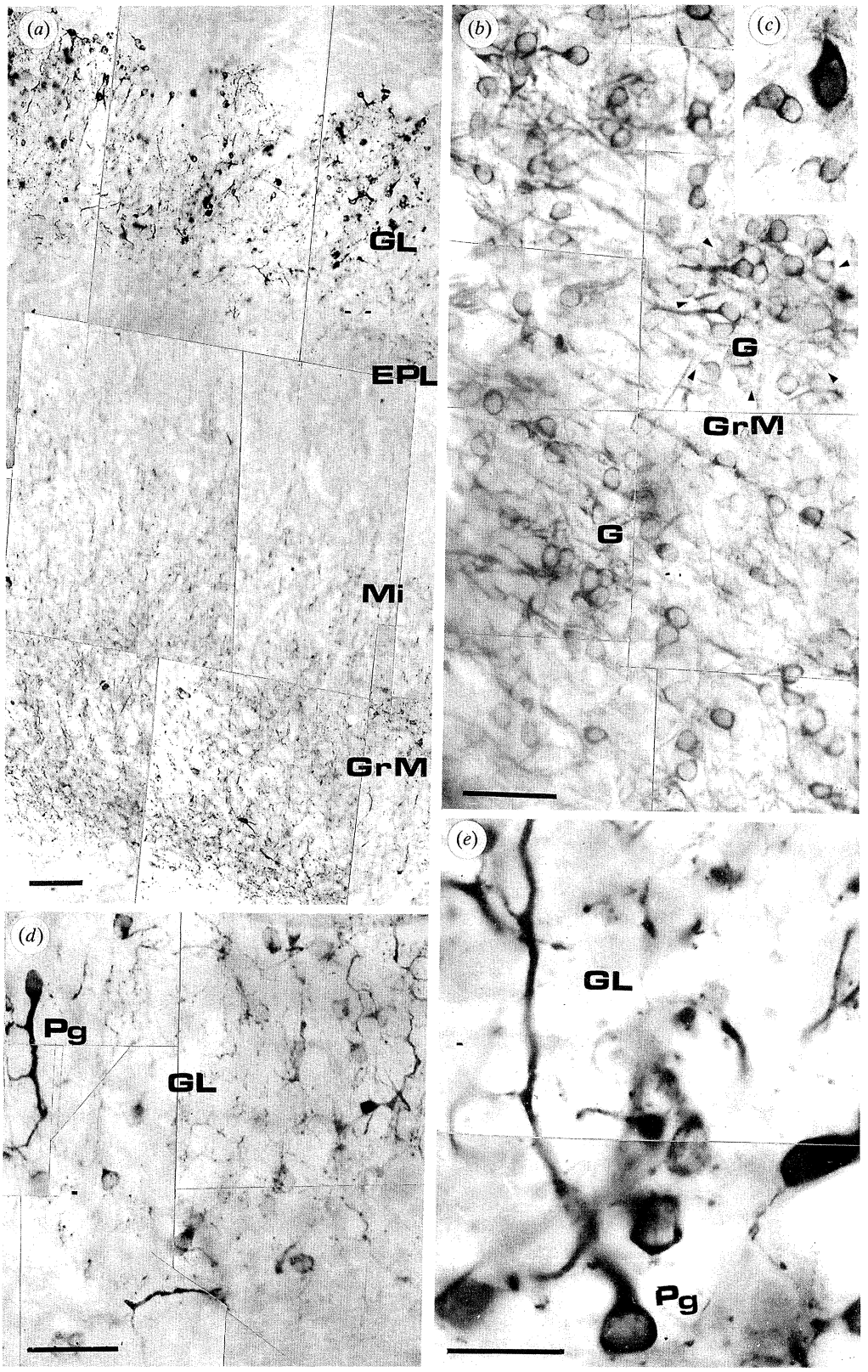

Figure 6. Photographs showing the distribution of cNOS-IR in the main olfactory bulb. (*a*) General view of the immunoreactive structures distributed in different layers of the main olfactory bulb, including the granule cell layer (GrM), mitral layer (Mi), external plexiform layer (EPL) and glomerular cell layer (GL). (*b*) Distribution and morphology of the granule cells (G) that form clusters (arrowheads) in the GrM, illustrated in more detail. (*c*) An immunoreactive neuron of the short-axon cell type. (*d*) Immunoreactive structures in the glomerular cell layer. Notice the periglomerular neurons (Pg) in (*d*). (*e*) A high-power magnification showing details of Pg cNOS-IR neurons. Scale bars: (*a*,*b*,*c*,*d*) = 100 μm; (*e*) = 50 μm.

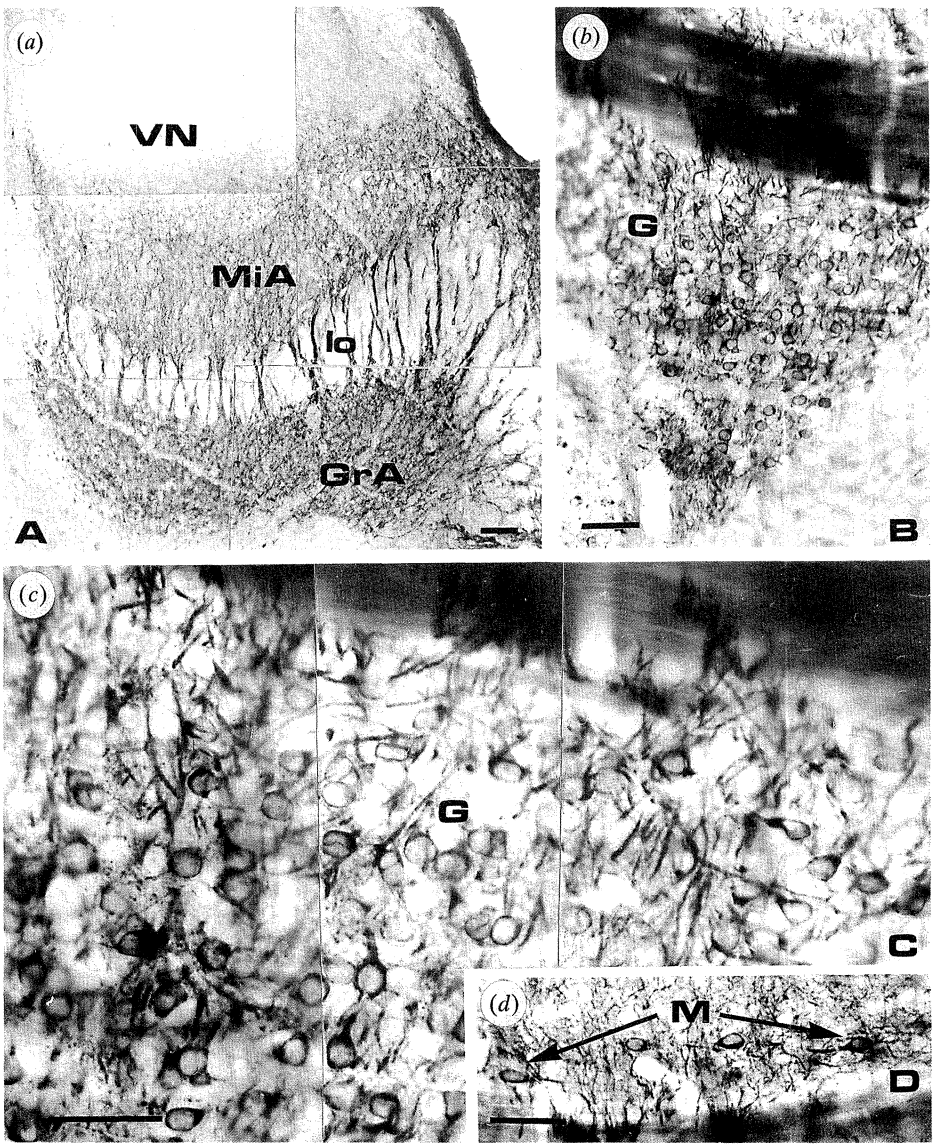

Figure 7. The distribution of cNOS-IR structures in the accessory olfactory bulb. (*a*) General view of the different immunoreactive layers that form the accessory olfactory bulb, including the granule cell layer (GrA), lateral olfactory tract (Io), mitral cell layer (MiA) and vomeronasal nerve layer (VN). (*b*) Details of immunoreactive granule cells (G) that form the granule cell layer. (*c*) A high-power magnification showing aspects of cNOS-IR granule cells. (*d*) Immunoreactive mitral-like cells (M) located in parallel to the olfactory tract. Scale bars = 100 μm.

fascicles of the nerve fibres that formed the olfactory tract. The periglomerular cells and glomerular layer were consistently not stained.

(viii) *Anterior and posterior olfactory nuclei*

A few scattered multipolar cNOS-IR neurons, 15–25 μm in diameter, were found in the external, lateral, ventral, medial and dorsal aspects of the anterior olfactory nuclei (figure 8*a–c*), as well as in the posterior aspect of the anterior olfactory nucleus (figure 8*d,e*). All of these neurons surrounded the anterior bulbar limb of the anterior commissure and showed few, long aspiny processes and a small number of collaterals. In the caudal portion of the posterior part of the anterior olfactory nucleus, the number of immunoreactive neurons was increased. A dense immunoreactive plexus of varicose nerve fibres was found distributed in these nuclei.

(ix) *Precommissural hippocampus (Taenia tecta)*

The taenia tecta showed clusters of cNOS-IR neurons, which were laterally in continuity with a few scattered immunoreactive neurons situated in the transition area that surrounded the olfactory ventricle, the posterior part of the anterior olfactory nucleus and the rostral portion of the accumbens nucleus.

The dorsal part of the taenia tecta contained a small number of neurons, 10–15 μm in diameter, with a triangular or piriform shape, and also some punctate immunoreactive fibres (figure 9*a*).

The ventral part showed numerous immunoreactive neurons and fibres. The neurons situated in the deepest portion of the taenia tecta were 10–15 μm in diameter and pyramidal in form. Some immunoreactive neurons, with fusiform or triangular forms, were found in the upper layers immersed in an immunoreactive varicose plexus.

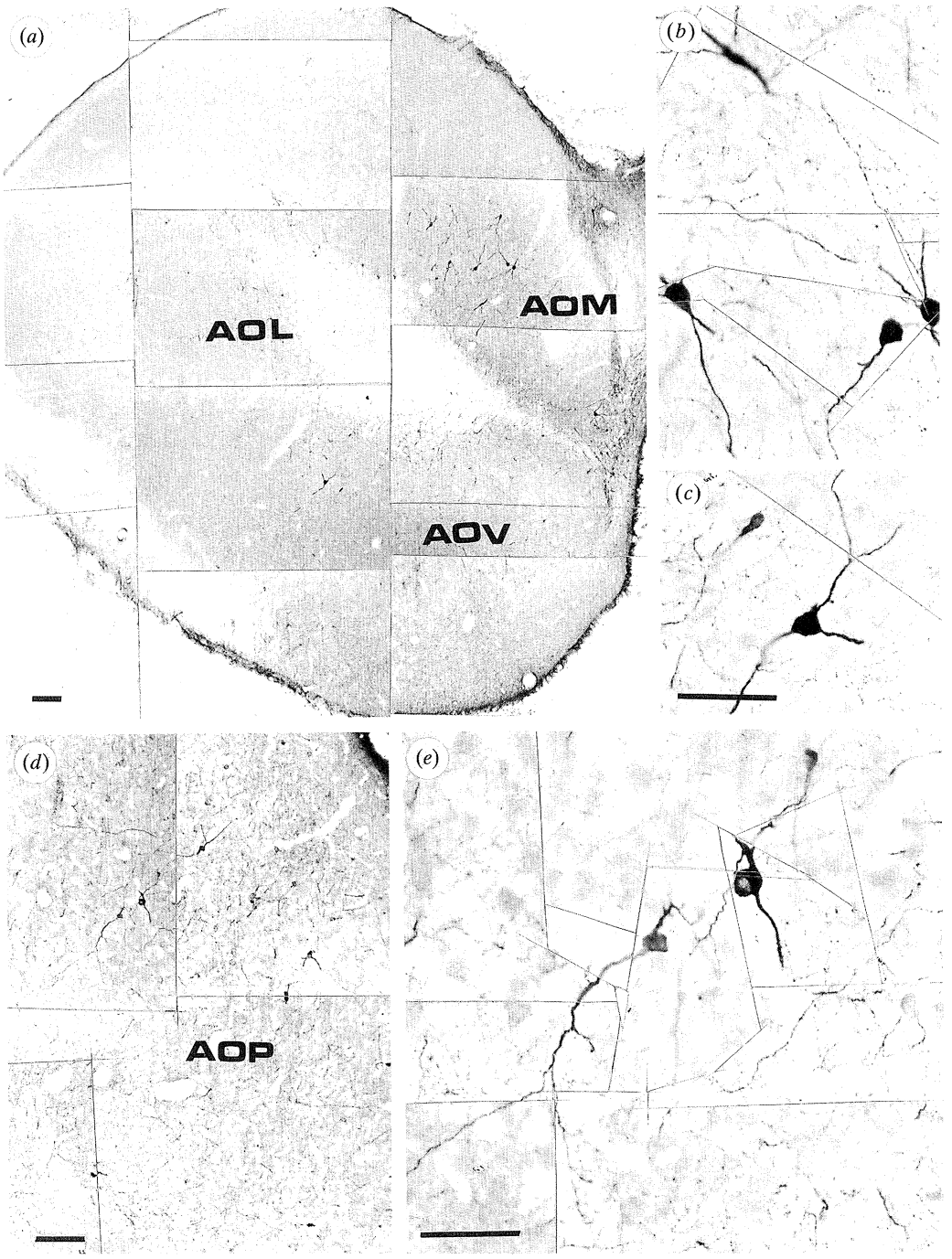

Figure 8. Photographs showing the distribution of cNOS-IR neurons and processes in the anterior olfactory nucleus. (*a*) A low power magnification, showing the medial (AOM), lateral (AOL) and ventral (AOV) groups of the anterior olfactory nucleus. (*b,c*) High-power magnifications showing features of immunoreactive neurons of the AOM and AOV, respectively. (*d*) Details of the localization of cNOS-IR in the posterior division of the anterior olfactory nucleus (AOP). (*e*) A high-power magnification of cNOS-IR neurons of the AOP. Scale bars = 100 μm.

(x) *Nucleus accumbens*

The nucleus accumbens contained cNOS-IR neurons of 15 to 20 μm diameter, with a small number of long processes surrounding the anterior commissure (figure 9*b,c*). These neurons were immersed in a dense, immunoreactive and varicose plexus.

(xi) *Stria terminalis*

Caudally, an extensive group of cNOS-IR neurons was found to be distributed in the intermedial, lateral, medial and ventral divisions of the nucleus of the stria terminalis (figure 10*a*). The neurons had long processes and few collaterals of varicose morphology.

(xii) *Caudate-putamen*

The caudate-putamen contained a large number of cNOS-IR neurons, which were included and also contributed to the formation of the rich, varicose

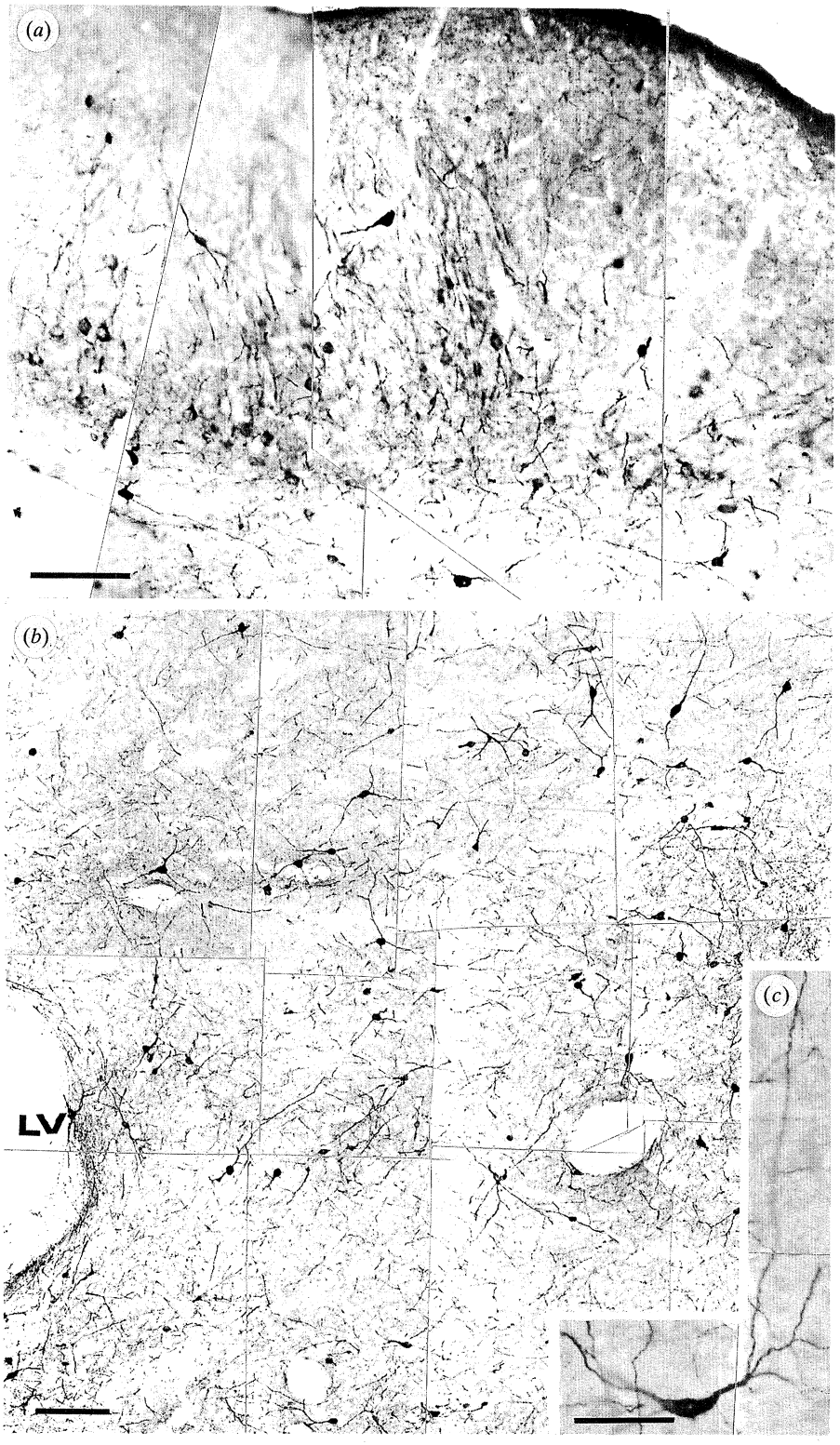

Figure 9. Photomontage of immunoreactive areas of the taenia tecta (*a*) and accumbens nucleus (*b*). (*c*) A high-power magnification of cNOS-IR neurons located in the accumbens nucleus. Notice that reactive neurons possess a few long, aspiny processes with a small number of collaterals. Scale bars: (*a*,*b*) = 100 μm; (*c*) = 50 μm.

interstitial plexus (figure 10*b*), between the unreactive fascicles that crossed the caudate-putamen. The neurons were of medium size (15–20 μm) and showed variable morphology, from fusiform to multipolar shapes, with long, varicose and aspiny processes and few collaterals.

(xiii) *Olfactory tubercle*

The olfactory tubercle contained a dense plexus of cNOS-IR varicose terminal fibres in the molecular layer and processes of neurons located in the polymorph layer (figure 10*c*). The immunoreactive neurons in the polymorph layer were multipolar in

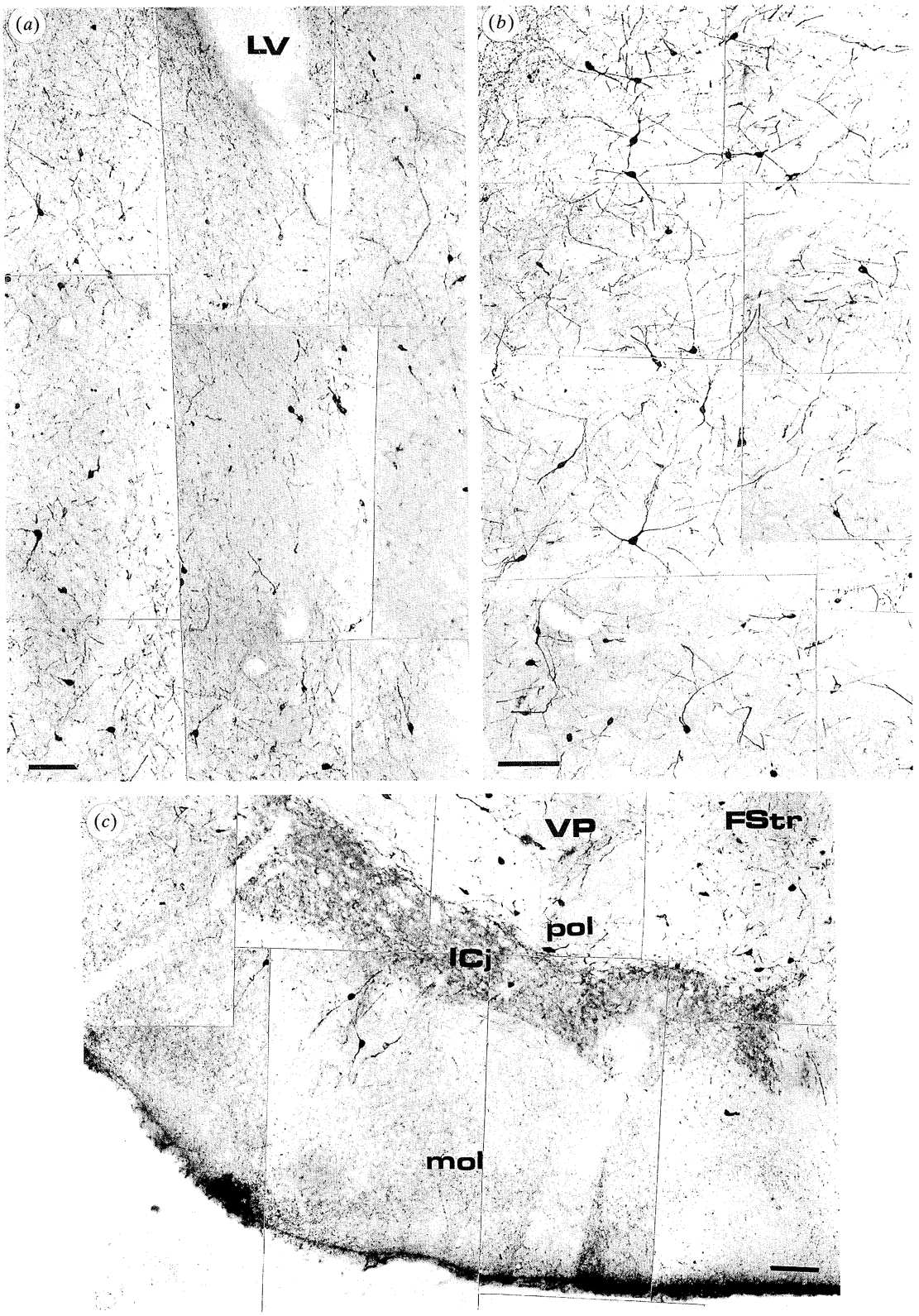

Figure 10. The distribution of cNOS-IR neurons and their long processes in the bed nucleus of the stria terminalis (*a*) and caudate-putamen (*b*). (*c*) Morphology of the island of Calleja located in the deepest portion of the polymorph layer of the olfactory tubercle. Notice that the island of Calleja contains a dense immunoreactive plexus and small immunoreactive neurons. The island of Calleja is surrounded by immunoreactive neurons of the polymorph layer. VP, ventral pallidum. Scale bars = 100 μm.

shape, containing large, intensely stained processes that ended in the molecular layer and short processes surrounding the soma. Dorsally, the immunoreactive neurons situated in the deep portion of the olfactory tubercle were connected, through immunoreactive bridges, with those that formed the ventral portion of the caudate-putamen. These bridges were formed by immunoreactive varicose fibres and also by some large and fusiform neurons.

(xiv) *Islands of Calleja*

The islands of Calleja, situated in the deep portion of the polymorph layer of the olfactory tubercle, comprised a dense plexus of cNOS-IR varicose nerve fibres and small cNOS-IR granular cells (figure 10*c*). The islands of Calleja were surrounded by multipolar cNOS-IR neurons that constituted the polymorph layer and dorsally by the ventral striatum and ventral pallidum.

(xv) *Insula Magna of Calleja*

The insula Magna of Calleja, situated close to the mediodorsal border of the accumbens nucleus, also contained cNOS-IR granular cells (figure 11*a*).

(xvi) *Septum*

Coronal sections from the rostral to the caudal part of the septum contained abundant cNOS-IR neurons, which were mainly distributed in their medial and lateral divisions (figures 11 and 12). Dorsally to the medial division of the septum, in the septo-hippocampal nucleus (figure 12*a*), few cNOS-IR neurons were found, whereas in the ventral portion of the medial septum (figure 11*b*) the number of cNOS-IR neurons increased mainly at the level of the vertical and horizontal limbs of the diagonal band of Broca (figures 11*a* and 12*c*), where clusters of strongly stained magnocellular neurons were present. The cNOS-IR neurons of the horizontal limb were in continuity with cNOS-IR neurons located in the ventral portion of the magnocellular preoptic nucleus (figure 12*d*), in the ventral striatum and in the ventral pallidum.

In the lateral division (figure 12), cNOS-IR neurons were of medium size (15–20 μm), and were situated along and below the wall of the lateral ventricle. These neurons were more numerous in the dorsal (figure 12*a*) and ventral portions of the lateral septum, decreasing in number in the intermediate portion of the lateral septum.

The neurons situated close to the wall of the lateral ventricle were of medium size (15–20 μm) and had immunoreactive varicose processes which contributed to the formation of a dense subependymal plexus (figure 13*a–c*). The nerve fibres in this plexus had collaterals that penetrated into the epithelium just close to the lumen of the lateral ventricle. A similar immunoreactive plexus was found around the wall of the third ventricle, containing nerve fibres that also penetrated into the epithelium; however, the density of the nerve fibres in the wall of the third ventricle was less than those found in the lateral ventricles (figure 13*d*). The intracerebral blood vessels that cross the basal area of the horizontal limb of the diagonal band of Broca showed an intense immunoreactive perivascular plexus (figure 13*e*). The extracerebral blood vessels were also surrounded by a dense immunoreactive varicose plexus. Small cNOS-IR neurons (5–10μm) were also found in the subfornical organ (figure 13*f*).

(xvii) *Globus pallidus and substantia innominata*

cNOS-IR neurons forming clusters were found close to the ventrolateral and ventromedial borders of the globus pallidus and in the interstitial spaces that divided the fascicles of the medial forebrain bundle (figure 14*a*). The number of cNOS-IR neurons decreased towards the dorsal area of the globus pallidus, but increased ventrally in the area of the substantia innominata. These neurons were 20–25 μm in diameter and showed multipolar morphology, with few processes and collaterals. Weakly stained fibres showing a varicose aspect were scattered mainly in the ventrolateral portion of the globus pallidus.

The entopeduncular nucleus showed a large number of cNOS-IR neurons, 20–25 μm in diameter, situated in the interstitial spaces formed by immunoreactive varicose fibres that surrounded non-immunoreactive fascicles.

(xviii) *Hippocampus*

Scattered cNOS-IR neurons were seen distributed in all the areas of the hippocampus studied. The dentate gyrus contained a moderate number of immunoreactive neurons in the ectal and endal limbs of the dentate granular cell layer (figure 14*b*). These neurons were of multipolar form with a scarce number of short processes and few collaterals, which were mainly located in the granular cell layer. Occasionally, immunoreactive neurons were found in the molecular layer of the dentate gyrus. cNOS-IR neurons were found distributed in all areas of Ammon's horn of the hippocampus. The rostral sections of the hippocampus showed some cNOS-IR neurons, distributed in the pyramidal cell layer of CA1 and CA2–CA3 fields of Ammon's horn. These immunoreactive neurons had basal varicose processes distributed into the stratum oriens. The apical dendrite comprised a single process through the stratum radiatum, forming a discrete tuft into the stratum lacunosum moleculare (figure 14*c*). Immunoreactive neurons were more numerous in CA1 than in CA2–CA3 fields of Ammon's horn.

In caudal sections of the hippocampus, the immunoreactive neurons of the dentate gyrus were more numerous (figure 15*a*) and, at the level of CA1 of the parasubiculum, the number of immunoreactive pyramidal cells was increased. These cells, which possessed dense tufts, were distributed in the stratum radiatum and stratum lacunosum moleculare (figure 15*b*). Some small, scattered cells of multipolar form were present in the stratum oriens, radiatum and lacunosum moleculare (figure 15*c–e*). Ventrally, these immunoreactive neurons formed part of the parasubiculum, which extended ventrolaterally to the medial subdivision of the entorhinal cortex.

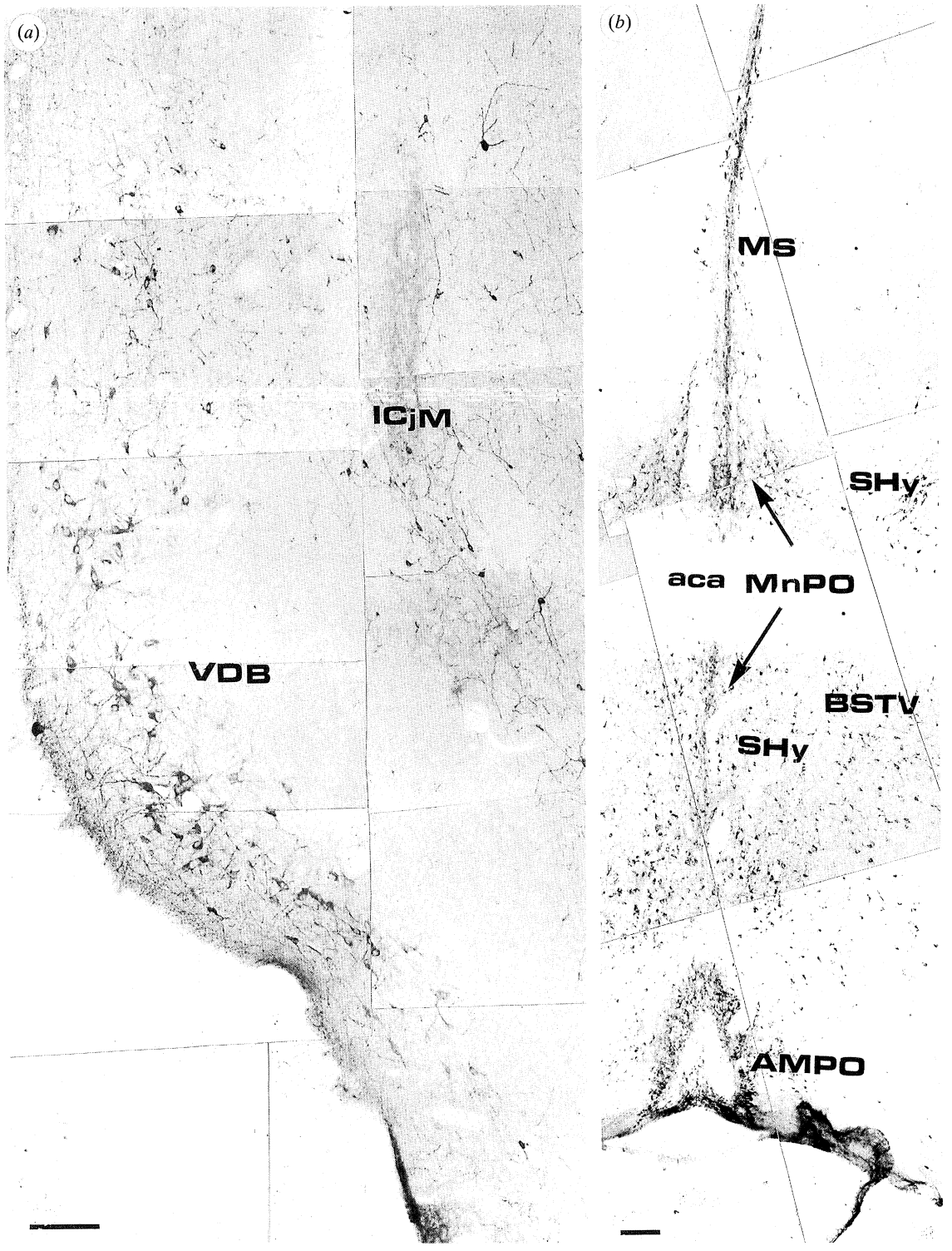

Figure 11. Photomontage showing the distribution of immunoreactivity in the middle line of the septal area. (*a*) Distribution of cNOS-IR neurons in the nucleus of the vertical limb of the diagonal band of Broca (VDB). ICjM is an island of Calleja major which contains many reactive fibres forming a dense immunoreactive plexus containing small immunoreactive neurons. (*b*) Medial septal nucleus (MS) containing cNOS-IR neurons. aca, anterior commissure; SHy, septohypothalamic nucleus; BSTV, ventral division of the nucleus of the stria terminalis; AMPO, anteromedial preoptic nucleus; MnPO, median preoptic nucleus. Scale bars = 100 μm.

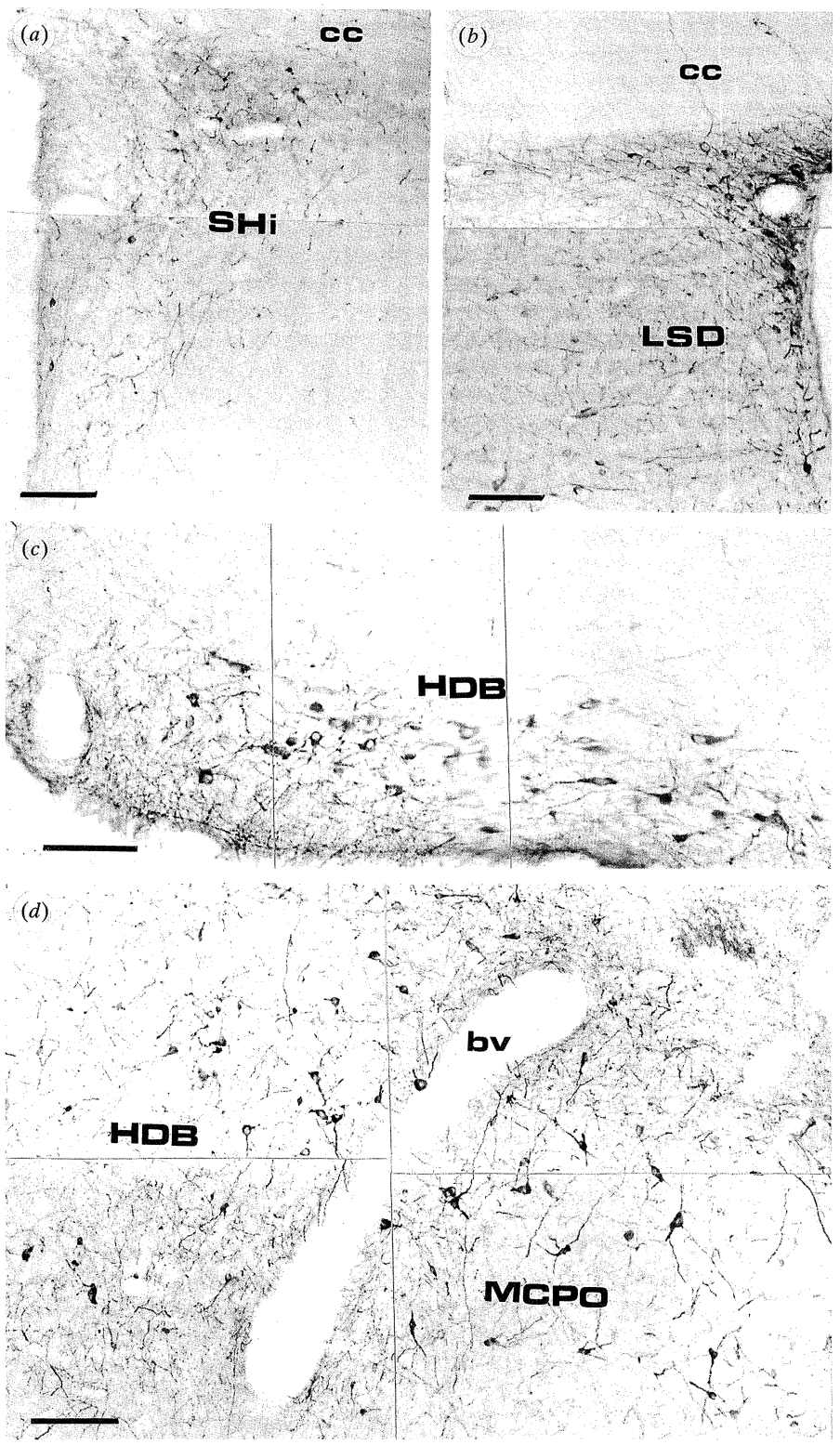

Figure 12. The distribution of cNOS-IR structures in the dorsomedial regions of the septal area and in the nucleus of the horizontal limb of the diagonal band of Broca. (*a*) Few immunoreactive neurons are present in the septohippocampal nucleus (SHi). (*b*) Distribution of immunoreactive neurons in the dorsal region of the lateral septum (LSD). (*c*) Distribution of immunoreactive neurons in the nucleus of the horizontal limb of the diagonal band of Broca (HDB). (*d*) cNOS-IR neurons in the most caudal portion of the nucleus of the HDB. Notice that the pattern of immunoreactivity present in the latter nucleus extends laterally into the magnocellular preoptic nucleus (MCPO). bv, blood vessel. Scale bars = 100 μm.

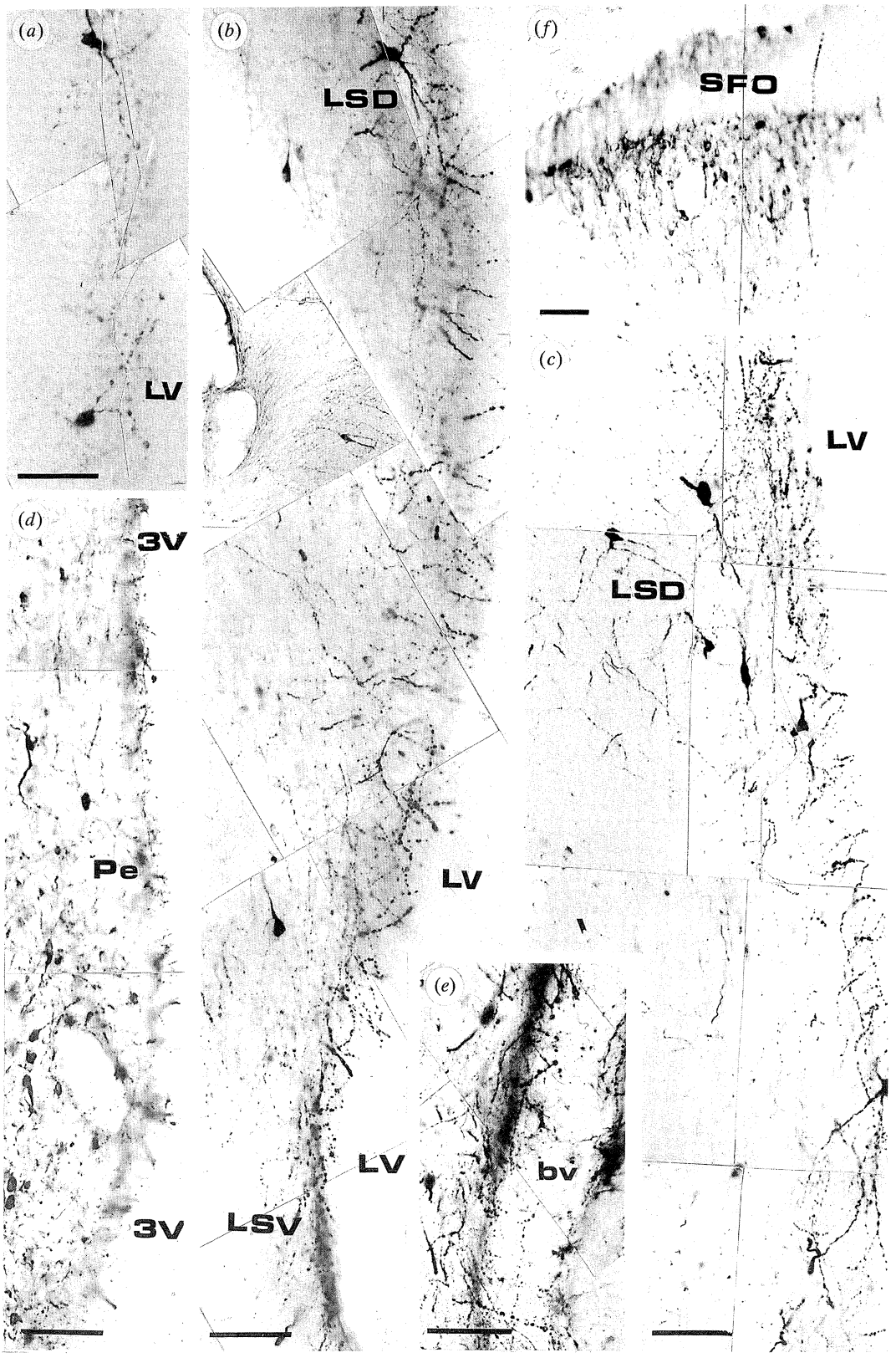

Figure 13. The distribution of cNOS-IR neurons and processes in the wall of the lateral and third ventricles, around blood vessels and in the subfornical organ. (*a–c*) Immunoreactive neurons and fibres penetrating into the wall of the lateral ventricle. Notice in (*a–c*) that some immunoreactive neurons located in the dorsal (LSD) and ventral (LSV) regions of the lateral septum exhibit varicose dendrites that contribute to the formation of a plexus in the subependymal region. (*d*) The dense innervation of the wall of the third ventricle. (*e*) Structure of a perivascular plexus. (*f*) Immunoreactive neurons in the subfornical organ (SFO). bv, blood vessel; LV, lateral ventricle; 3V, third ventricle. Scale bars: (*a–e*) = 50 μm; (*f*) = 100 μm.

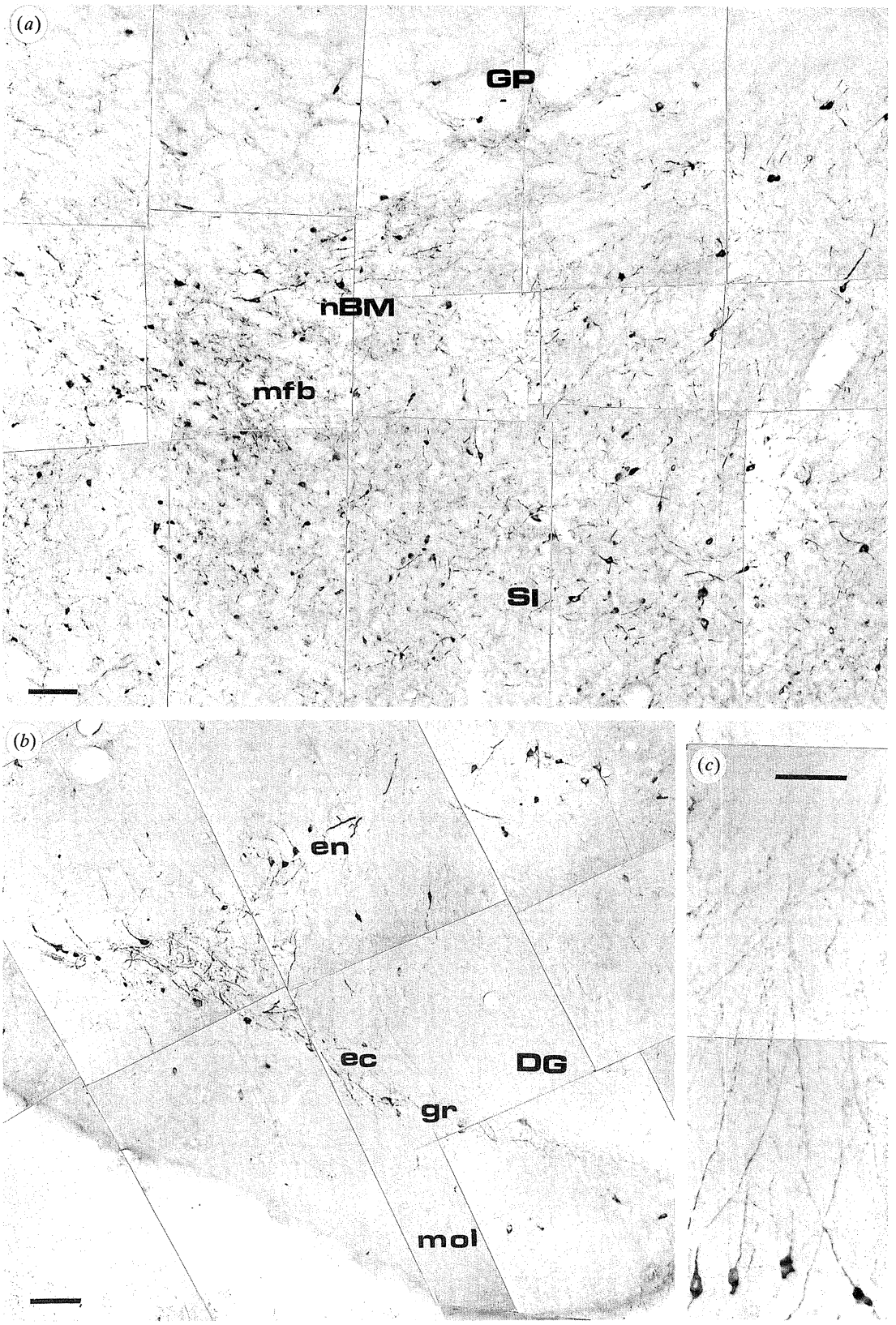

Figure 14. The distribution of cNOS-IR cell bodies and processes in the globus pallidus (GP) and rostral portion of the hippocampus. (*a*) A few immunoreactive neurons are located in the ventral portion of the GP. Notice in (*a*) that these neurons are mainly located in the area of the nucleus basalis magnocellularis (nBM), in the medial forebrain bundle (mbf) and in the substantia innominata (SI). (*b*) Distribution of immunoreactive neurons in the ectal (ec) and endal (en) regions of the dentate gyrus at the level of the granular cell layer. Notice that some small immunoreactive neurons are present in the molecular layer of the dentate gyrus. (*c*) Immunoreactive neurons located in the CA1 field of Ammon's Horn. Notice that the high power magnification used in (*c*) shows the distribution of neurons in the different layers that constitute this field. A large number of these neurons is found in the pyramidal cell layer. These cells have long basal processes distributed in the stratum oriens and their apical processes penetrate the stratum radiatum and lacunosum moleculare. Scale bars: (*a*,*b*) = 100 μm; (*c*) = 50 μm.

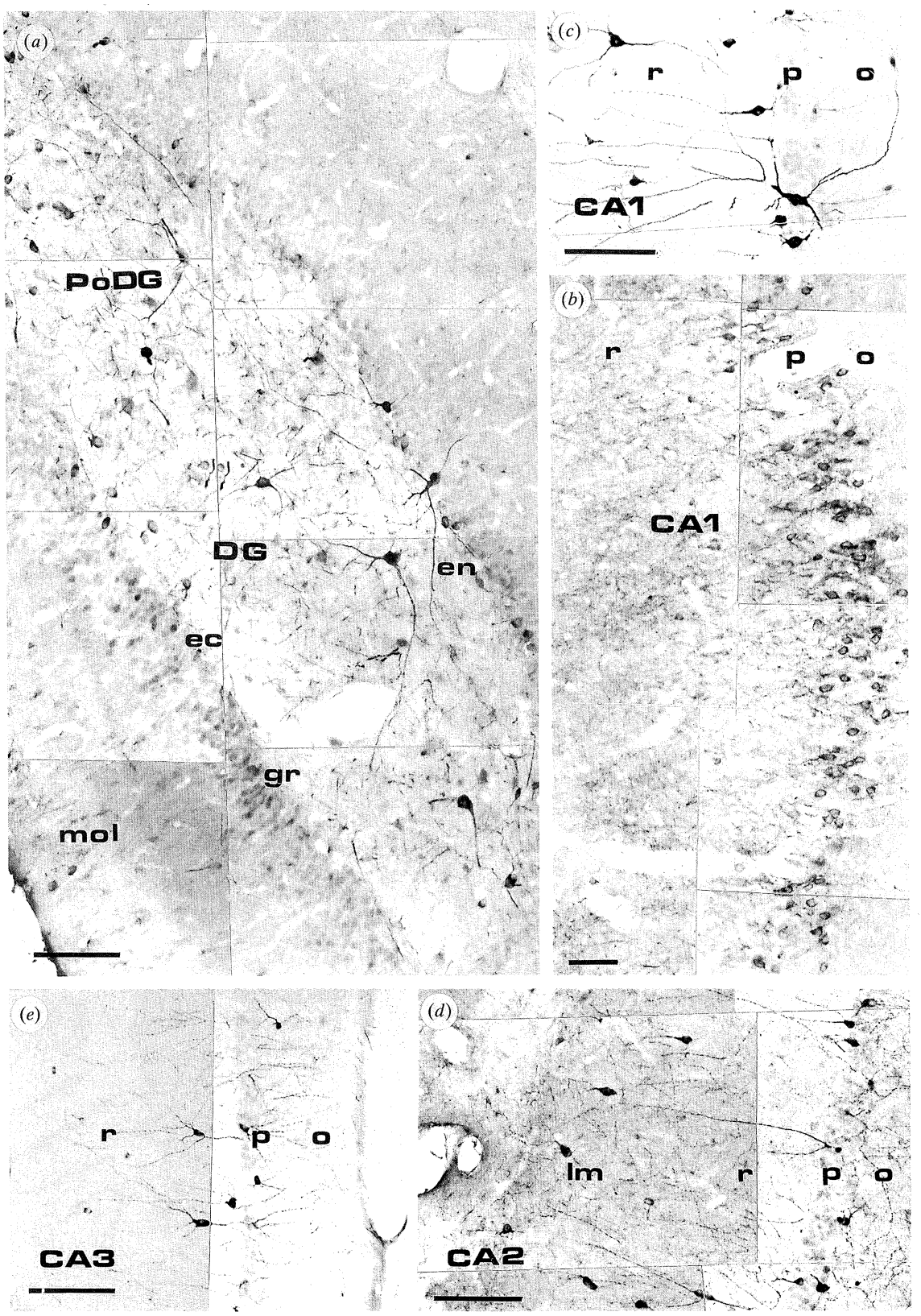

Figure 15. Photomontage of immunoreactive neurons distributed in the caudal hippocampus. (*a*) Immunoreactive neurons in the dentate gyrus. Notice the presence of neurons in the polymorph layer of the dentate gyrus. (*b*) Immunoreactive neurons in CA1 close to the parasubiculum. Notice in (*b*) that a large number of pyramidal cells can be found in the pyramidal cell layer. Details of the morphology of the latter cells can be seen in (*c–e*) taken from CA1–CA3 fields of Ammon's Horn. Scale bars = 100 μm.

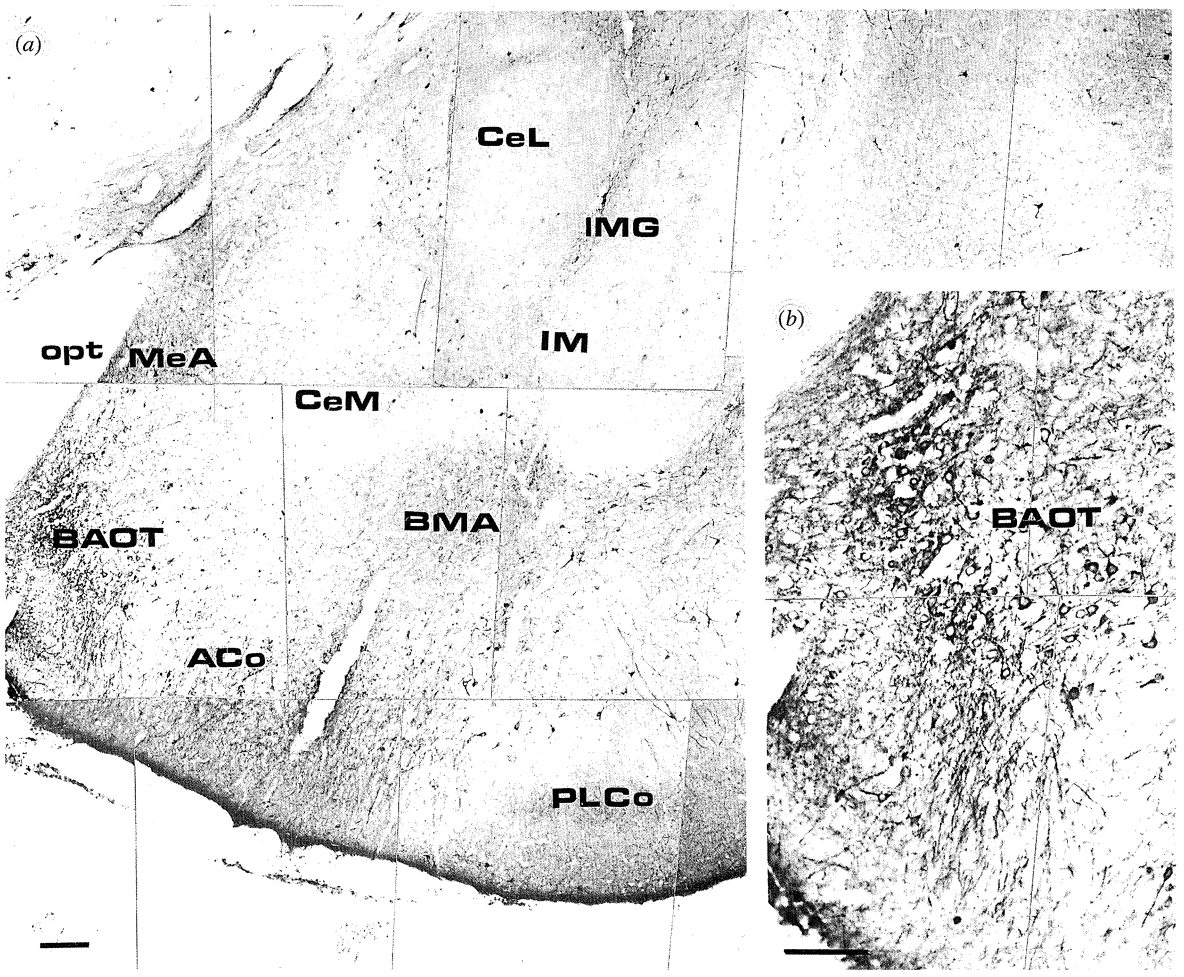

Figure 16. Photographs of cNOS-IR structures in different areas of the amygdala. (*a*) Immunoreactive neurons principally distributed in the medial amygdaloid nucleus as well as in the intercalated (IM) and basomedial amygdaloid (BMA) nuclei. Immunoreactive neurons are also detected in the bed nucleus of the accessory olfactory tract (BAOT), which are continuous with the immunoreactive neurons situated in the anterior cortical amygdaloid nucleus and the posterolateral cortical amygdaloid nucleus (PLCo). (*b*) High-power magnification showing aspects of immunoreactive neurons in the BAOT. Scale bars = 100 μm.

(xix) *Amygdala*

The distribution of cNOS-IR neurons in the amygdaloid complex was heterogeneous (figure 16*a*). The greatest number of cNOS-IR neurons was found in the medial amygdaloid division, mainly distributed in their anteroventral, anterodorsal, posteroventral and posterodorsal areas. A few, scattered immunoreactive neurons were situated in the anterior, posterior and ventral areas of the basolateral amygdaloid nucleus. The basomedial amygdaloid nucleus and the intercalated nucleus of the amygdala also showed cNOS-IR neurons, as did the amygdalostriatal and amygdalopiriform transition areas. A dense plexus of immunoreactive fibres was found surrounding the lateral and ventral boundary of the ventral basolateral and basomedial amygdaloid nuclei. These fibres were in continuity with immunoreactive fibres that constituted the deep layer of the ventral endopiriform nucleus and the deep layer of the piriform cortex, respectively. The bed nucleus of the accessory olfactory tract and the cortical amygdaloid nucleus showed a dense distribution of cNOS-IR neurons and fibres in the posteromedial, posterolateral and anteroposterior areas (figure 16*b*).

(*b*) *Diencephalon*

(i) *Hypothalamus*

The medial division of the hypothalamus contained cNOS-IR neurons in numerous groups. Rostrally, cNOS-IR neurons were principally distributed in the septo-hypothalamic nucleus and some immunoreactive neurons were also found in the anteromedial preoptic nucleus, in the medial preoptic area, in the medial preoptic nucleus and in the anteroventral preoptic nucleus. Scattered immunoreactive neurons were also found distributed laterally, in the lateral preoptic area and in the tail of the horizontal limb of the diagonal band of Broca. These immunoreactive groups of neurons were limited dorsolaterally by the ventral and lateral divisions of the bed nucleus of the stria terminalis and the anterior commissure, by the ventral pallidum and substantia innominata and medially by the third ventricle. Caudally, the hypothalamus showed numerous cNOS-IR neurons

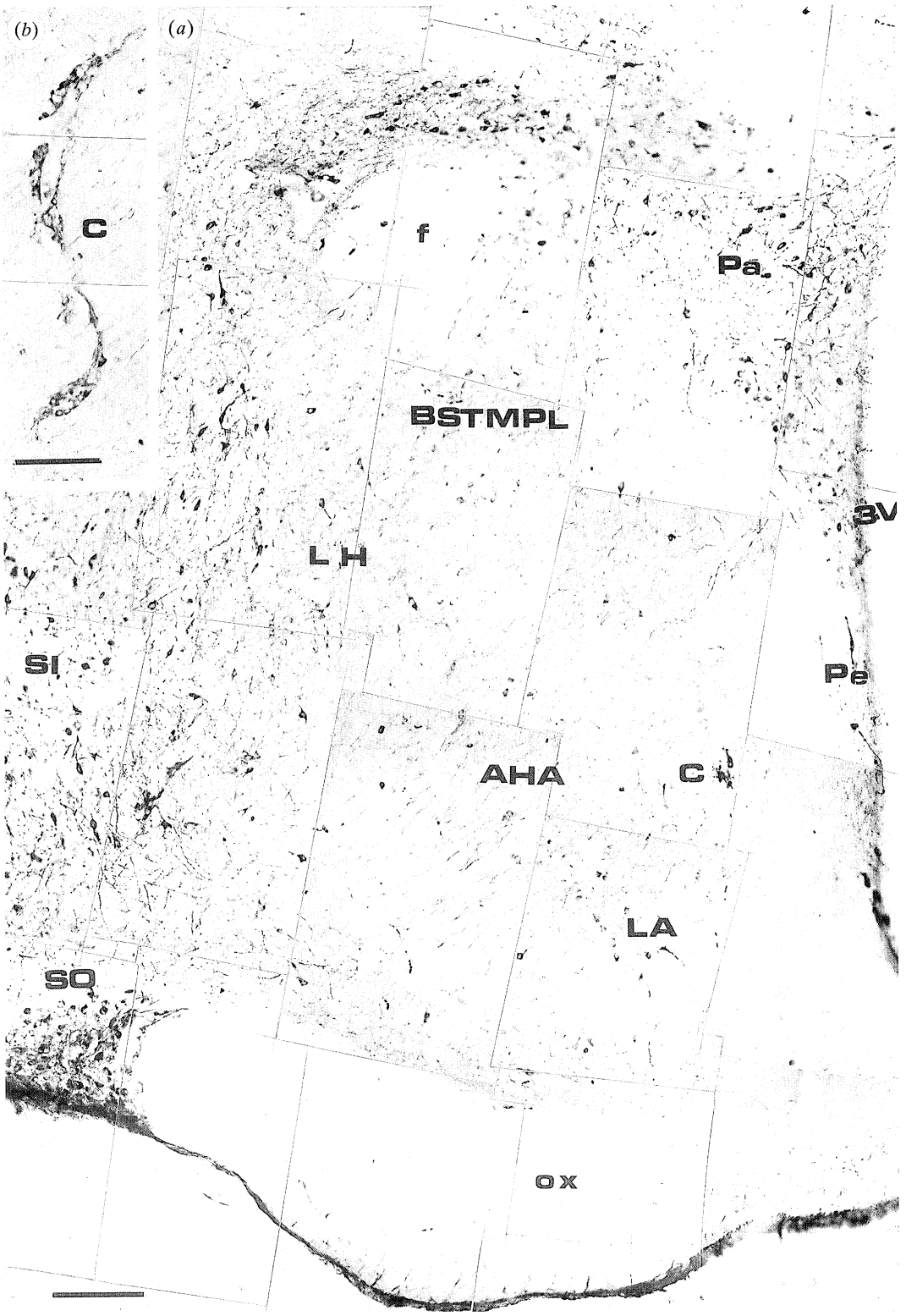

Figure 17. (*a*) Photomontage showing the distribution of immunoreactive neurons and processes in the hypothalamus. Notice that these are more abundant in the paraventricular (Pa) and supraoptic nucleus (SO) nuclei. (*b*) cNOS-IR neurons located around the blood vessels in the circularis nucleus (C). Scale bars: (*a*) = 100 μm; (*b*) = 50 μm.

situated in the anterior, posterior, dorsal, dorsomedial and lateral portions of the magnocellular and parvocellular paraventricular hypothalamic nuclei, with the number of immunoreactive neurons decreasing in the periventricular nucleus (figure 17*a*). The cNOS-IR neurons decreased laterally in the anterior part of the anterior hypothalamic area and medial preoptic area, where some immunoreactive fibres crossed it. Immunoreactive neurons in the medial preoptic area were found surrounding blood vessels,

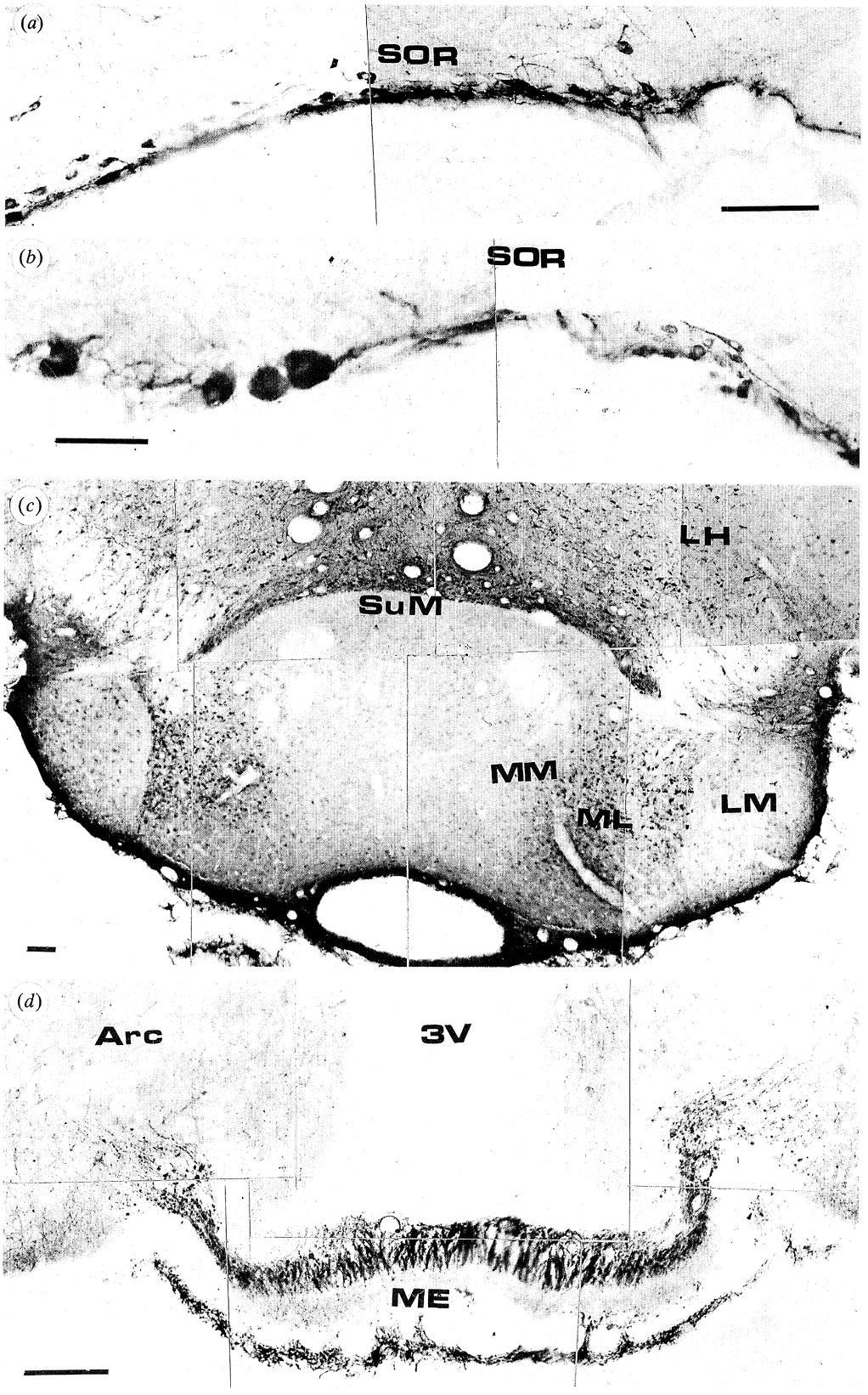

Figure 18. (*a,b*) Immunoreactive neurons forming the supraoptic retrochiasmatic nucleus (SOR) in the caudo-ventral part of the hypothalamus. (*c,d*) Distribution of cNOS-IR neurons in the mamillary nucleus and median eminence (ME), respectively. LH, lateral hypothalamus; SuM, supramamillary nucleus; MM, medial mamillary nucleus, medial division; ML, medial mamillary nucleus, lateral division: LM, lateral mamillary nucleus; Arc, arcuate hypothalamic nucleus. Scale bars = 100 μm.

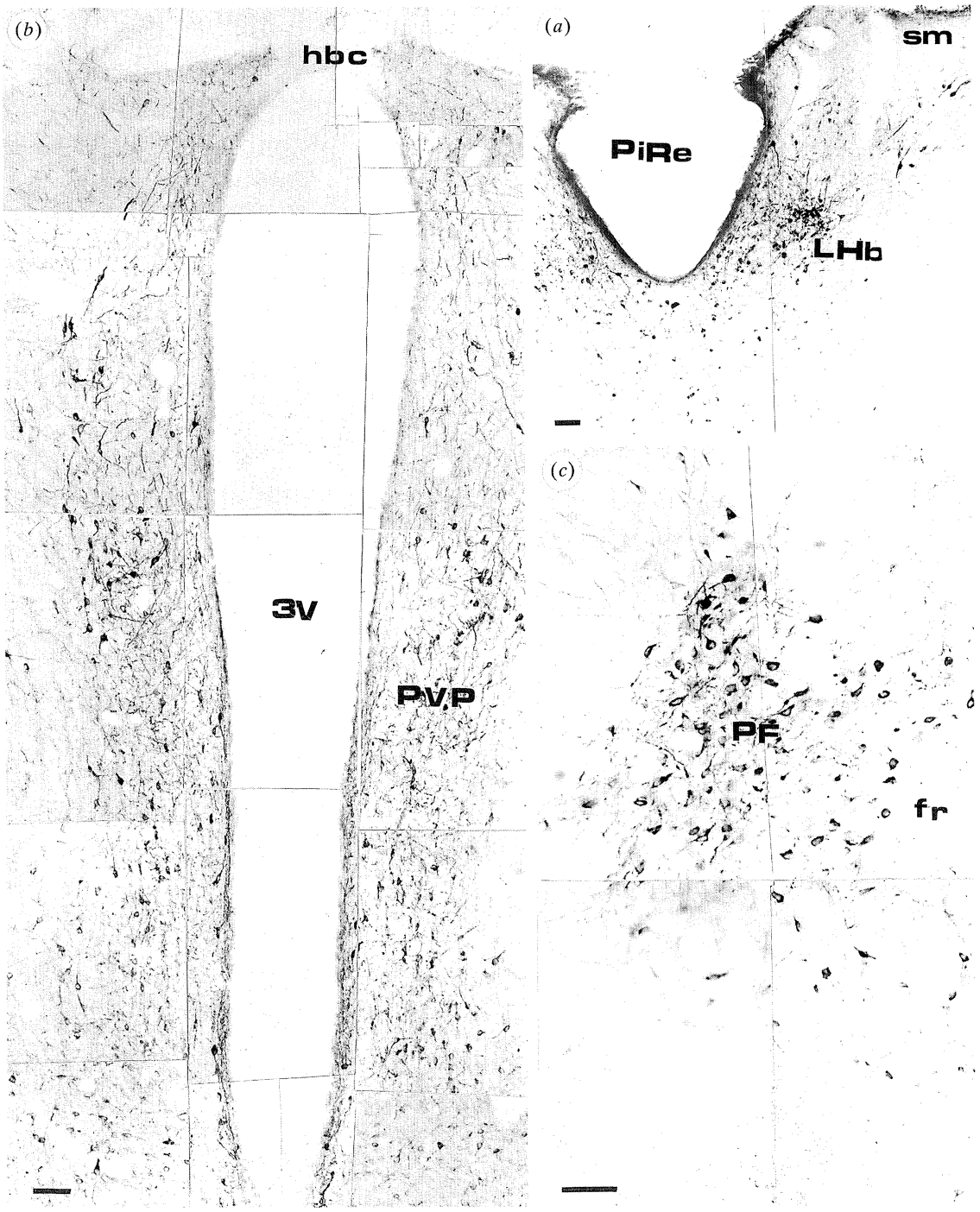

Figure 19. Distribution of cNOS-IR neurons in the mediodorsal thalamic region. (*a*) Immunoreactive neurons located in the lateral habenular nucleus (LHb). (*b*) Positive neurons located along the wall of the third ventricle (3V) forming part of the posterior portion of the paraventricular nucleus (PVP). (*c*) Immunoreactive neurons in the parafascicular nucleus (PF). fr, fasciculus retroflexus. Scale bars = 100 μm.

contributing to the formation of the nucleus circularis (figure 17*b*).

The rostral portion of the lateral hypothalamic area showed a discrete number of cNOS-IR neurons connecting laterally with the globus pallidus, medial forebrain bundle, substantia innominata, the tail of the horizontal limb of the diagonal band of Broca and the magnocellular preoptic nucleus.

The lateral division of the hypothalamus showed the greatest density of immunoreactive neurons, which were situated at the level of the supraoptic nucleus (figure 17*a*), in the accessory neurosecretory nucleus and the retrochiasmatic part of the supraoptic nucleus.

Caudally, the number of immunoreactive neurons decreased and only a few neurons containing cNOS-IR were found in the tuber cinereum. Characteristically, the dorsomedial hypothalamic nucleus, the lateral portions of the magnocellular hypothalamic nucleus and the dorsomedial portion of the ventro-

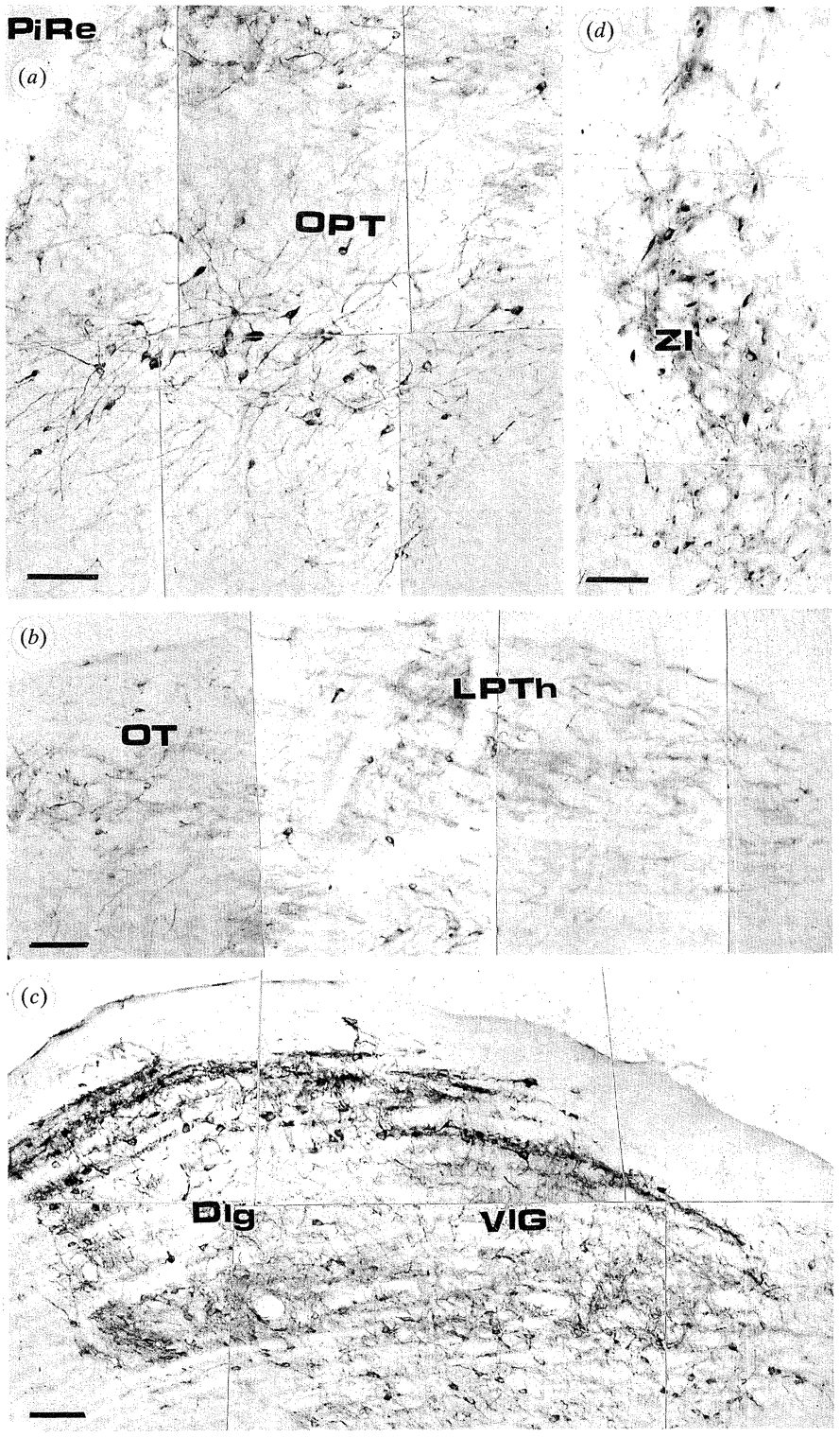

Figure 20. Micrographs illustrating the distribution of cNOS-IR neurons in the dorsolateral region of the thalamus. (*a*) Positive neurons in the olivary pretectal nucleus (OPT). (*b*) Positive neurons in the nucleus of the optic tract (OT) and in the lateroposterior thalamic nucleus (LPTh). (*c*) Distribution of immunoreactive nerve fibres and neurons in the dorsolateral geniculate (Dlg) and ventrolateral geniculate (VlG) nuclei. (*d*) Distribution of reactive nerve fibres and neurons in the zona incerta (ZI). Scale bars = 100 μm.

medial hypothalamic nucleus were consistently unstained. cNOS-IR neurons were also found in the caudal portion of the hypothalamus, constituting the medial tuberal nucleus, the ventrolateral part of the ventromedial hypothalamic nucleus and the retrochiasmatic region of the supraoptic nucleus (figure 18*a*,*b*). Occasional lightly stained neurons were found in the nucleus arcuatus, which also showed a dense immunoreactive varicose plexus.

The mamillary region showed cNOS-IR neurons distributed in the ventral and dorsal portion of the paramamillary nucleus and in the ventral part of the

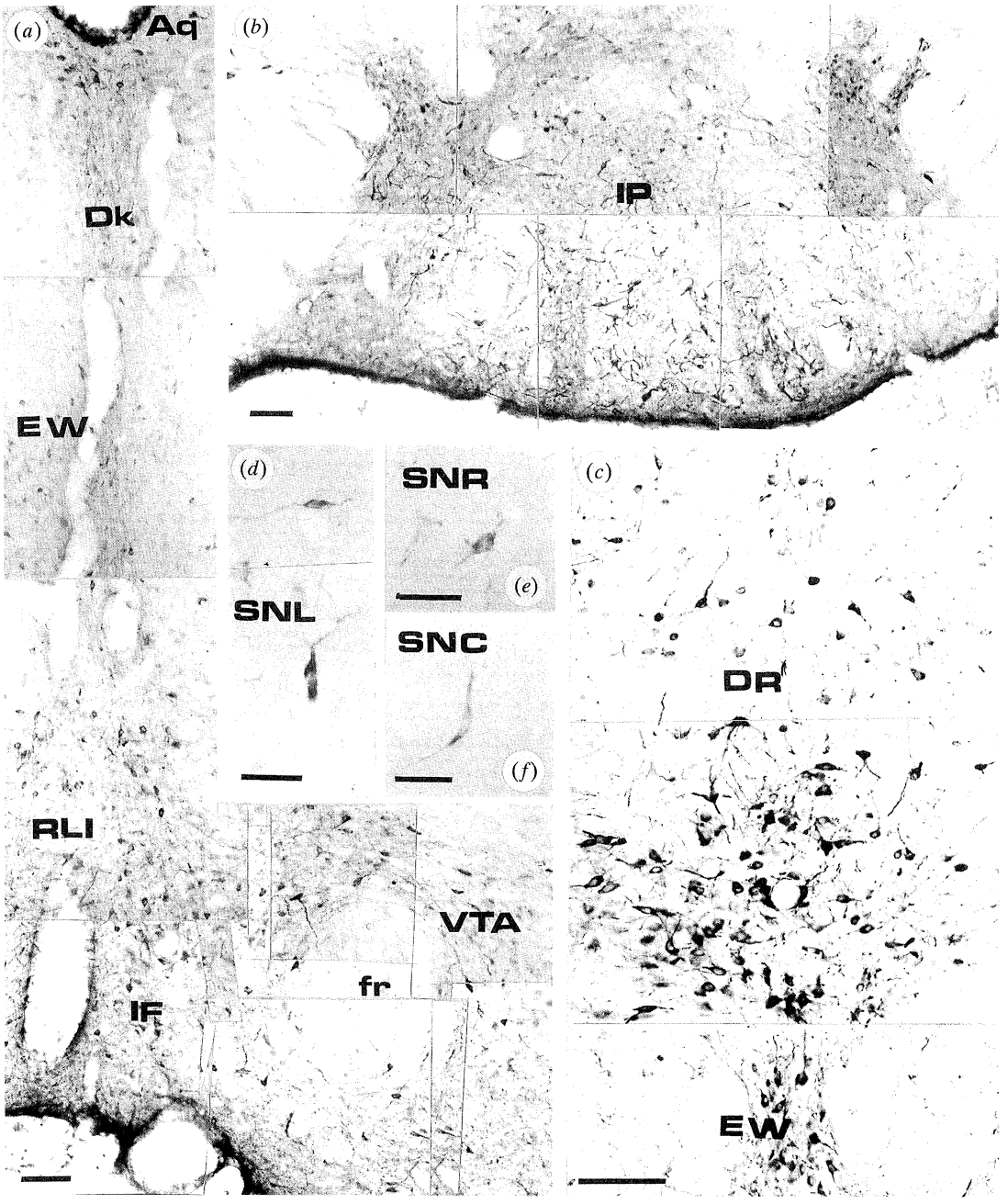

Figure 21. Photomontage showing the distribution of immunoreactive neurons in the mesencephalon. (*a*) Positive neurons in the ventral tegmental area (VTA), interfascicular nucleus (IF), rostral linear nucleus raphe (RLI), Edinger-Westphal nucleus (EW) and nucleus of Darkschewitsch (Dk). (*b*) Immunoreactive neurons in the interpeduncular nucleus (IP). (*c*) Reactive neurons in the dorsal raphe nucleus (DR). (*d–f*) Isolated immunoreactive neurons in the pars lateralis (SNL), pars reticulata (SNR) and pars compacta (SNC) of the substantia nigra. Scale bars: (*a–c*) = 100 μm; (*d–f*) = 50 μm.

medial and lateral mamillary nuclei, which laterally connected with the area of the lateral hypothalamus (figure 18*c*). cNOS-IR neurons were found distributed in the supramamillary nucleus and, dorsally, in the supramamillary decussation.

cNOS-IR nerve fibres were found in the ventral portion of the hypothalamus, crossing the dorsomedial hypothalamic nucleus, the nucleus arcuatus and the lateral and medial parts of the medial mamillary nucleus, to form a dense plexus at the level of the median eminence of the infundibular stem and mamillary recess of the third ventricle (figure 18*d*), mainly in the internal layer.

(ii) *Thalamic area*

cNOS-IR neurons were found in the dorsomedial area of the thalamus, distributed mainly in the anterior portion of the paraventricular thalamic nucleus, stria medularis and anteroventral thalamic nucleus. cNOS-IR neurons were found in the medial and lateral regions of the lateral habenular nucleus (figure 19*a*). The dorsal region of this nucleus

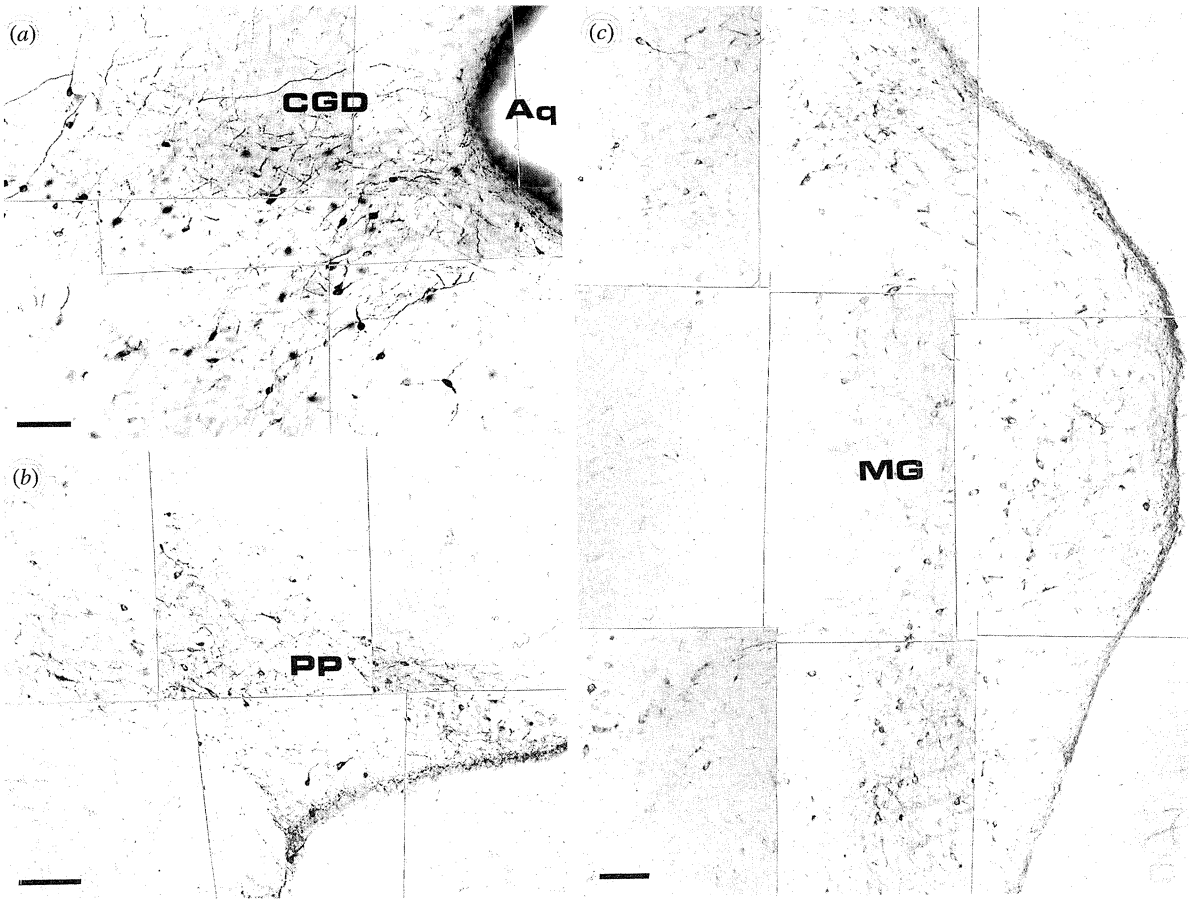

Figure 22. (*a*) Distribution of cNOS-IR neurons in the dorsal portion of the periaqueductal central grey (CGD). (*b*) Positive neurons in the peripeduncular nucleus (PP). (*c*) Positive neurons in the medial geniculate nucleus (MG). Scale bars = 100 μm.

contained a dense cNOS-IR varicose plexus. Scattered immunoreactive neurons were found crossing the ventral boundary of the medial part of the laterodorsal thalamic nucleus. cNOS-IR neurons formed part of the posterior region of the paraventricular thalamic nucleus and, laterally, the parafascicular thalamic nucleus (figure 19*b*). Dorsally and laterally, few cNOS-IR neurons were found in the precommissural nucleus (figure 19*c*). The olivary pretectal nucleus showed large, immunoreactive neurons, displaying long, aspiny processes (figure 20*a*). Few cNOS-IR neurons were found in the dorsal area of the anterior pretectal nucleus and lateral posterior thalamic nucleus. These formed part of a dense immunoreactive plexus of nerve fibres, which was very intense at the level of the nucleus of the optic tract (figure 20*b*). Some immunoreactive neurons were also found in the rhomboid, reuniens and ventral reuniens thalamic nuclei. Laterally, cNOS-IR neurons were found comprising the different regions of the geniculate nucleus (figure 20*c*), where some immunoreactive neurons, showing fusiform morphology, penetrated the reticular thalamic nucleus in a ventromedial direction and contributed to the formation of the zona incerta (figure 20*d*).

Immunoreactive nerve fibres were found in the part ventralis of the zona incerta crossing the internal capsule, the reticular thalamic nucleus and the stria terminalis, penetrating into the ventral posteromedial and posterolateral thalamic nuclei, and caudally into the medial geniculate nucleus.

(*c*) *Mesencephalon*

Medially, numerous cNOS-IR neurons of small to medium size (10–15 μm maximum diameter) were found forming part of the interfascicular nucleus, the parabrachial pigmented nucleus, the paranigral nucleus and the ventral tegmental area (figure 21*a*). Medium-sized immunoreactive neurons (15 μm maximum diameter) were also found in the caudolateral, intermedial and dorsomedial subnuclei of the interpeduncular nucleus (figure 21*b*) and a few immunoreactive neurons occurred in the rostral linear nucleus of the raphe. A few scattered neurons were found in the medial boundary of the parvocellular oculomotor nucleus. Dorsally and in the midline, some cNOS-IR neurons were also distributed in both the Darkschewitsch and Edinger-Westphal nuclei. The dorsal raphe nucleus (figure 21*c*) also showed abundant cNOS-IR neurons (15–20 μm maximum diameter) which were bordered ventrolaterally by the medial longitudinal fasciculus. Few immunoreactive neurons were situated in the pars lateralis of the substantia

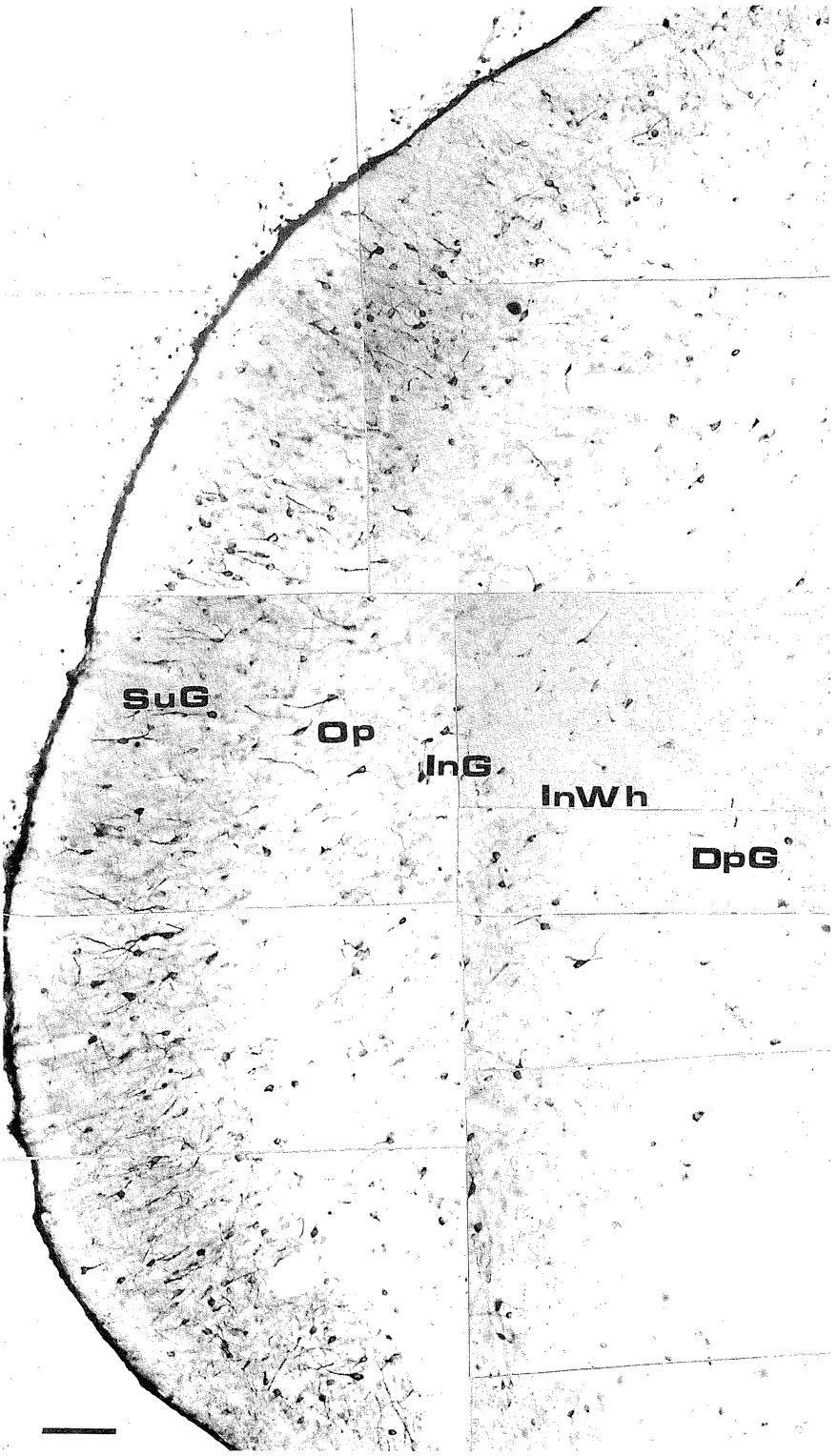

Figure 23. Photomontage showing the distribution of cNOS-IR neurons in the superior colliculus. A large number of positive neurons are present in the superficial grey layer (SuG); these neurons are less abundant in the optic nerve layer (Op), the intermediate grey layer (InG), intermediate white layer (InWh) and in the deep white layer (DpG). Scale bars = 100 μm.

nigra and isolated neurons occurred in the pars compacta and reticulata of the substantia nigra (figure 21*d–f*) and the ventrolateral part of the medial lemniscus. Large and medium sized cNOS-IR neurons (15–20 μm maximum diameter) were mainly distributed in the dorsal and medial area of the central grey; scattered immunoreactive neurons were located along the posterior commissure (figure 22*a*). Dorsolateral to the substantia nigra some immunoreactive neurons were found within the peripeduncular nucleus (figure 22*b*).

Caudally and laterally, immunoreactive neurons were detected in the medial region of the geniculate

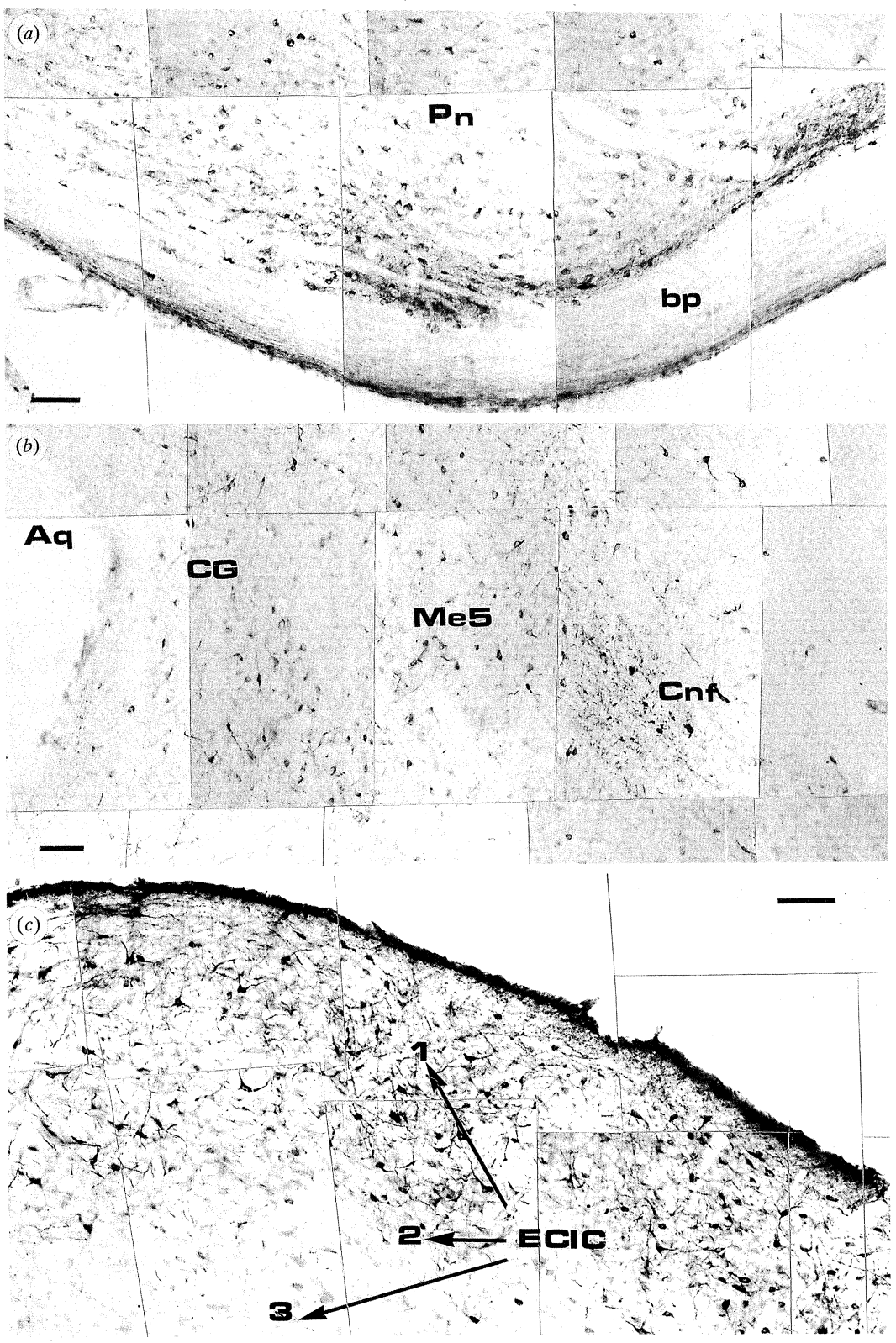

Figure 24. (*a*) Distribution of cNOS-IR neurons in the pontine nucleus (Pn). (*b*) Reactive neurons in the cuneiform (Cnf) nucleus and in the region of the mesencephalic trigeminal (Me5) nucleus. (*c*) Distribution of cNOS-IR neurons in the inferior colliculus. Notice that most reactive neurons in this nucleus are located in layer 1 of the external cortex (ECIC). Aq, aqueduct; CG, central grey; bp, brachium pontis. Scale bars = 100 μm.

nucleus, with the number decreasing in the lateral part of the medial geniculate nucleus (figure 22*c*).

Immunoreactive neurons were found in the anterior part of the superior colliculus, mainly distributed in the superficial grey layer (figure 23). Discrete and scattered cNOS-IR neurons were also found in the optic nerve layer, and occasionally in the medial and lateral portions of the intermediate grey and white

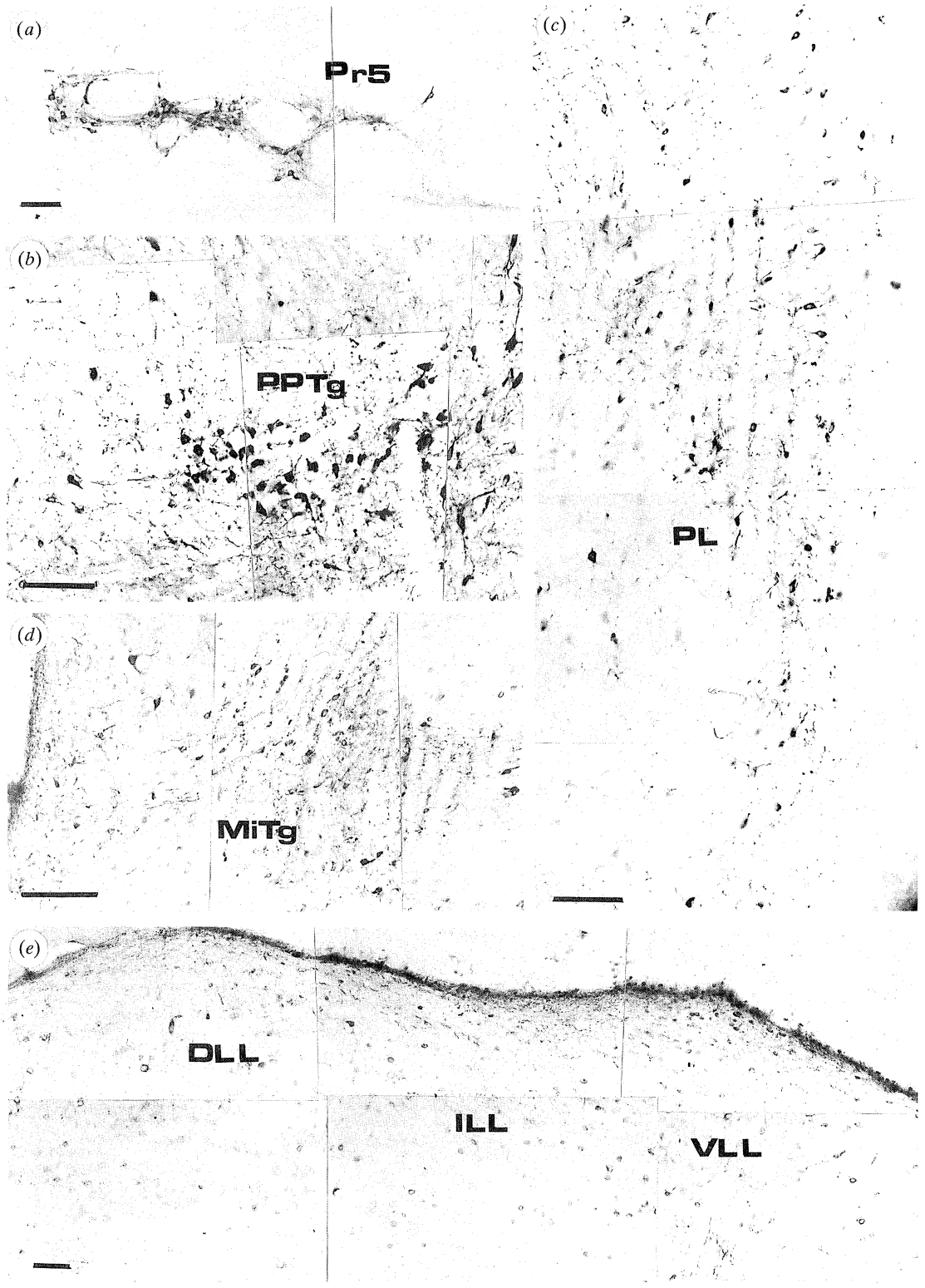

Figure 25. (*a*) Immunoreactive neurons in the principal sensory trigeminal nucleus (Pr5). (*b*) Reactive neurons in the pedunculopontine tegmental nucleus (PPTg). (*c*) Discrete distribution of immunoreactive neurons in the paralemniscal nucleus (PL). (*d*) Immunoreactive neurons distributed in the microcellular tegmental nucleus (MiTg). (*e*) A small number of reactive neurons distributed along the dorsal (DLL), intermediate (ILL) and ventral (VLL) nuclei of the lateral lemniscus. Scale bars = 100 μm.

layers. Immunoreactive nerve fibres that formed part of the brachium of the superior colliculus penetrated laterally into the colliculus and were distributed mainly in the intermediate grey and white layers, including the deep grey and white layers.

A few dispersed nerve fibres containing cNOS-IR were found crossing the parvocellular and magnocellular red nucleus, the retrorubral field, the ventrolateral tegmental area and the deep mesencephalic nucleus.

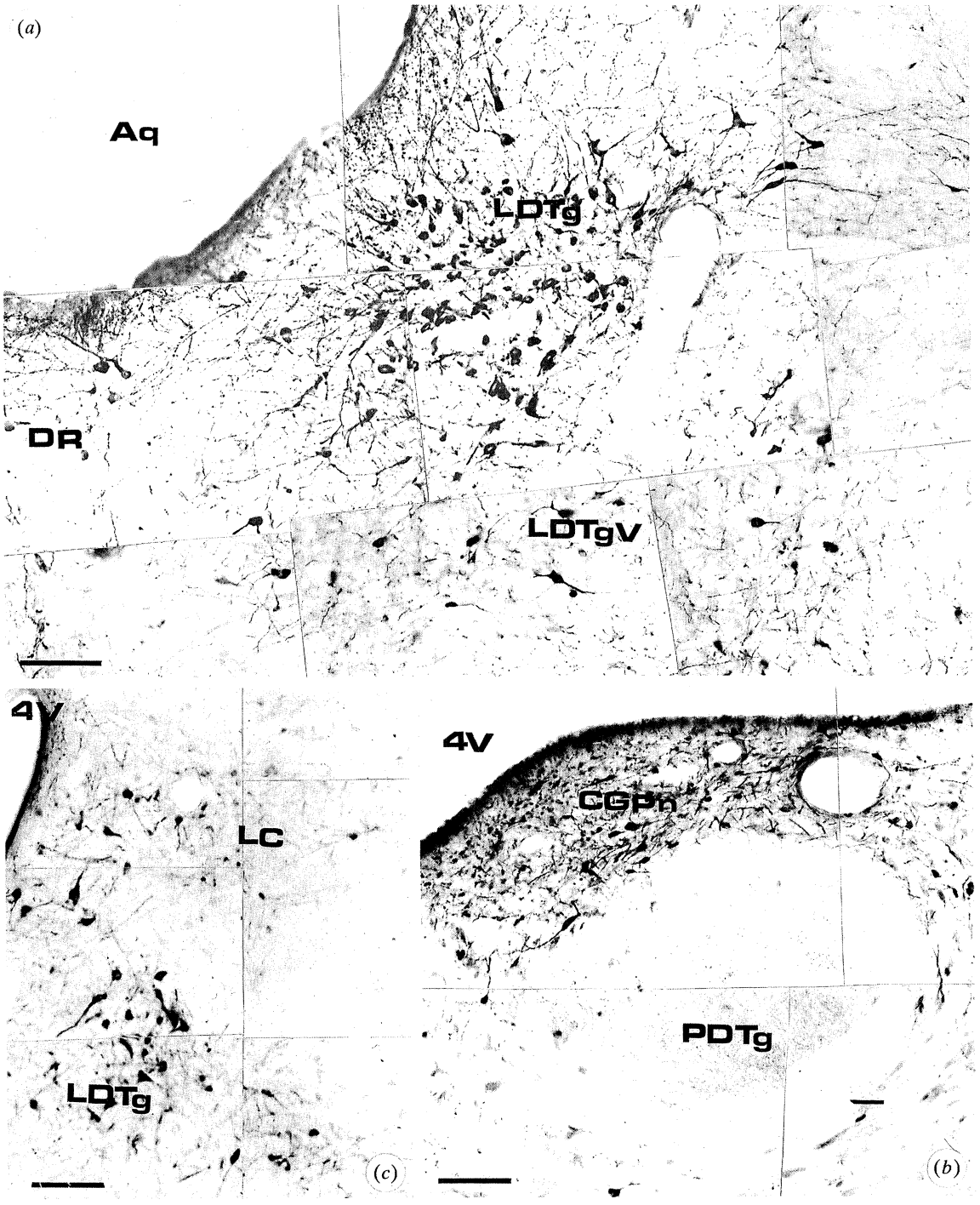

Figure 26. (*a*) Photomontage showing the distribution of cNOS-IR neurons in the rostral area of the laterodorsal tegmental nucleus (LDTg). Notice that reactive neurons are ventrally continuous with the ventral part of the laterodorsal tegmental nucleus (LDTgV). (*b*) Distribution of positive neurons in the central grey of the pons (CGPn) surrounding the posterodorsal tegmental nucleus (PDTg). (*c*) Immunoreactive neurons in the locus coeruleus (LC). 4V, fourth ventricle; DR, dorsal raphe nucleus; Aq, aqueduct. Scale bars = 100 μm.

(*d*) *Pons and medulla oblongata*

Immunoreactive cNOS-IR neurons were found in the medial and lateral areas of the mesencephalic-pons junction, where it was possible to see small immunoreactive neurons situated in the pontine nucleus (figure 24*a*). The central grey showed cNOS-IR neurons distributed around the aqueductus of cerebri, which laterally contained small scattered immunoreactive neurons, which were continuous with the cuneiform nucleus. Between the cuneiform nucleus and the neurons that form the central grey, a few cNOS-IR neurons were situated in the region of the mesencephalic trigeminal nucleus (figure 24*b*). Laterally, in the mesencephalic-pons junction area, cNOS-IR neurons were found in the inferior colliculus (figure 24*c*). The brachium inferior colliculus showed a dense plexus of varicose immunoreactive fibres. Immunoreactive nerve fibres were displayed in the sensory root of the trigeminal nerve (figure 25*a*).

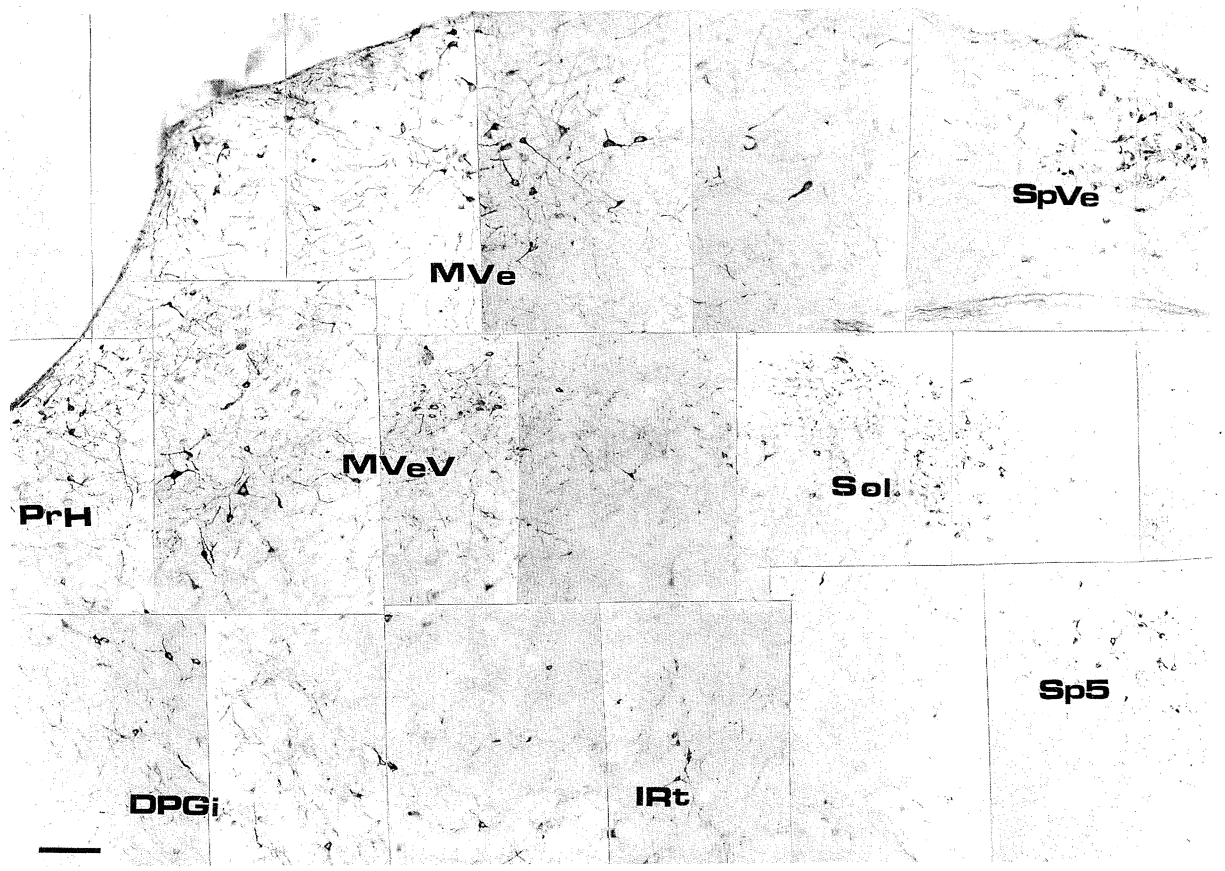

Figure 27. Photomontage illustrating the distribution of immunoreactive neurons of the dorsal area of the medulla oblongata. PrH, prepositus hypoglossal nucleus; MVe, medial vestibular nucleus; MVeV, ventral area of medial vestibular nucleus; SpVe, spinal vestibular nucleus; Sp5, dorsomedial spinal trigeminal nucleus; Sol, nucleus of the solitary tract; DGPi, dorsal paragigantocellular nucleus; IRt, intermediate reticular nucleus. Scale bar = 100 μm.

In the pons, intensely immunoreactive neurons were found, forming the pedunculopontine tegmental and retrorubral nuclei, which were ventrally continuous with immunoreactive neurons that formed the paralemniscal nucleus (figure 25*b*,*c*), and dorsolaterally with the microcellular tegmental nucleus (figure 25*d*). This itself was continuous ventrally with a reduced number of immunoreactive neurons located in the ventrolateral tegmental nucleus, reticulotegmental pontine nucleus and its pericentral area. A few scattered immunoreactive neurons were also found in the dorsal, intermediate and ventral nuclei of the lateral lemniscus (figure 25*e*).

Ventral to the aqueduct and lateral to the dorsal raphe nucleus, there were large, intensely immunoreactive neurons forming the laterodorsal tegmental nucleus (figure 26*a*). Laterally, these neurons were continuous with other immunoreactive neurons that comprised the ventral division of the laterodorsal tegmental nucleus, the subpeduncular tegmental nucleus and the most caudal part of the pedunculopontine tegmental nucleus. Small fascicles of punctate immunoreactive fibres crossed the superior cerebellar peduncle. In the midline a few neurons comprised the more caudal area of the dorsal raphe nucleus and the pericentral area of the dorsal tegmental nucleus (figure 26*b*). The laterodorsal tegmental nucleus was surrounded caudally and dorsolaterally by some immunoreactive neurons and fibres in the locus coeruleus (figure 26*c*), ventromedially by the most caudal area of the central and pericentral regions of the dorsal tegmental nucleus, and dorsomedially by the sphenoid nucleus. Caudally and laterally, the laterodorsal tegmental nucleus was continuous with some immunoreactive neurons that formed the medial and lateral areas of the parabrachial nucleus. The supragenual nucleus showed small immunoreactive neurons, and a dense fibre network, which continued into the prepositus hypoglossal nucleus. Dorsolaterally, cNOS-IR neurons were found in the medial and spinal vestibular nuclei (figure 27).

A few cNOS-IR neurons were found in the dorsomedial region of the principal sensory trigeminal nucleus, immersed in a dense plexus of immunoreactive nerve fibres. A dense plexus of varicose immunoreactive nerve fibres was located in the ventrolateral portion of the principal sensory trigeminal nucleus. Only a few immunoreactive neurons, with stellate morphology surrounded by varicose nerve terminals, were seen between the principal sensory trigeminal nucleus and the sensory root of the trigeminal nucleus. This sensory root also contained a few varicose immunoreactive nerve fibres.

Ventromedially, the nucleus of the trapezoid body contained intensely immunoreactive cell bodies in a palisade arrangement and separated by unreactive

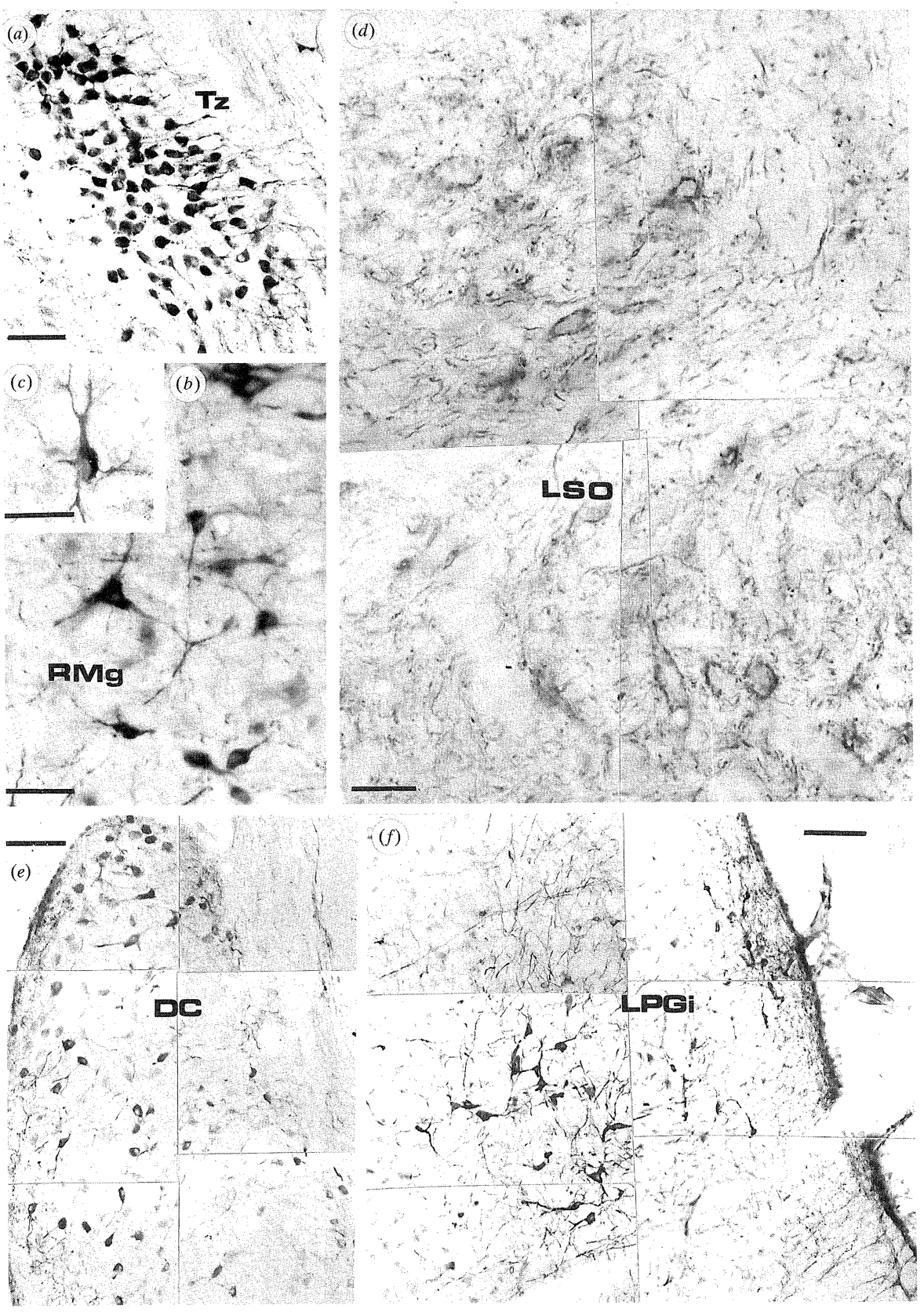

Figure 28. (*a*) Immunoreactive neurons in the trapezoid body (Tz). (*b*) Reactive neurons in the raphe magnus nucleus (RMg). (*c*) Morphological details of immunoreactive neurons of the RMg. (*d*) Distribution of cNOS-IR fibres in the lateral superior olive (LSO). Notice in (*d*) that varicose reactive fibres surround unreactive neurons. (*e*) Immunoreactive neurons distributed in the dorsal cochlear nucleus (DC). (*f*) cNOS-IR neurons forming the lateral paragigantocellular nucleus (LPGi). Scale bars: (*a*, *d–f*) = 100 μm; (*b*,*c*) = 50 μm.

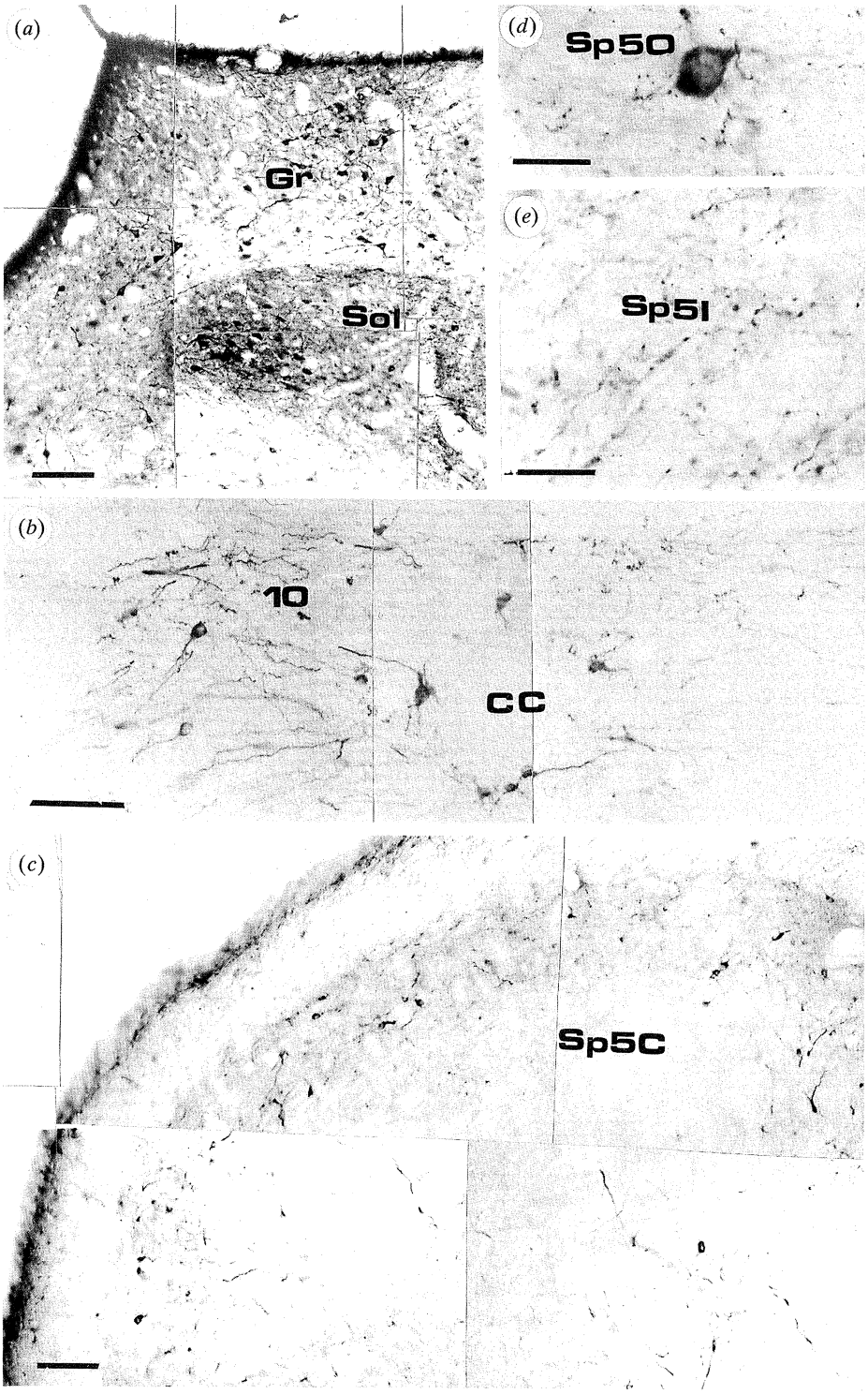

Figure 29. (*a*) Micrograph illustrating the distribution of immunoreactive neurons in the gracile nucleus (Gr) and caudal area of the nucleus of the solitary tract (Sol). (*b*) Immunoreactive neurons in the nucleus of the dorsal motor vagus nerve (10). (*c–e*) Distribution of immunoreactive neurons and processes in the pars oralis (Sp5O), interpolaris (Sp5I) and caudalis (Sp5C) of the spinal trigeminal nucleus. Scale bars: (*a–c*) = 100 μm; (*d,e*) = 25 μm.

fascicles of nerve fibres, which crossed this obliquely (figure 28*a*). In the ventromedial boundary of the trapezoid nucleus, the pyramidal tract contained a small number of immunoreactive fibres crossing it transversally. In the dorsomedial boundary of the trapezoid nucleus and in the midline, large immunoreactive neurons (20–25 μm in diameter) were found forming part of the raphe magnus nucleus (figure 28*b,c*). Dorsolaterally to the trapezoid nucleus an extensive field, made up of the ventral and dorsal areas of the pontine reticular nuclei, contained scattered immunoreactive neurons with large processes. Lateral to the trapezoid nucleus, the lateral superior olive, the superior paraolivary nucleus, the

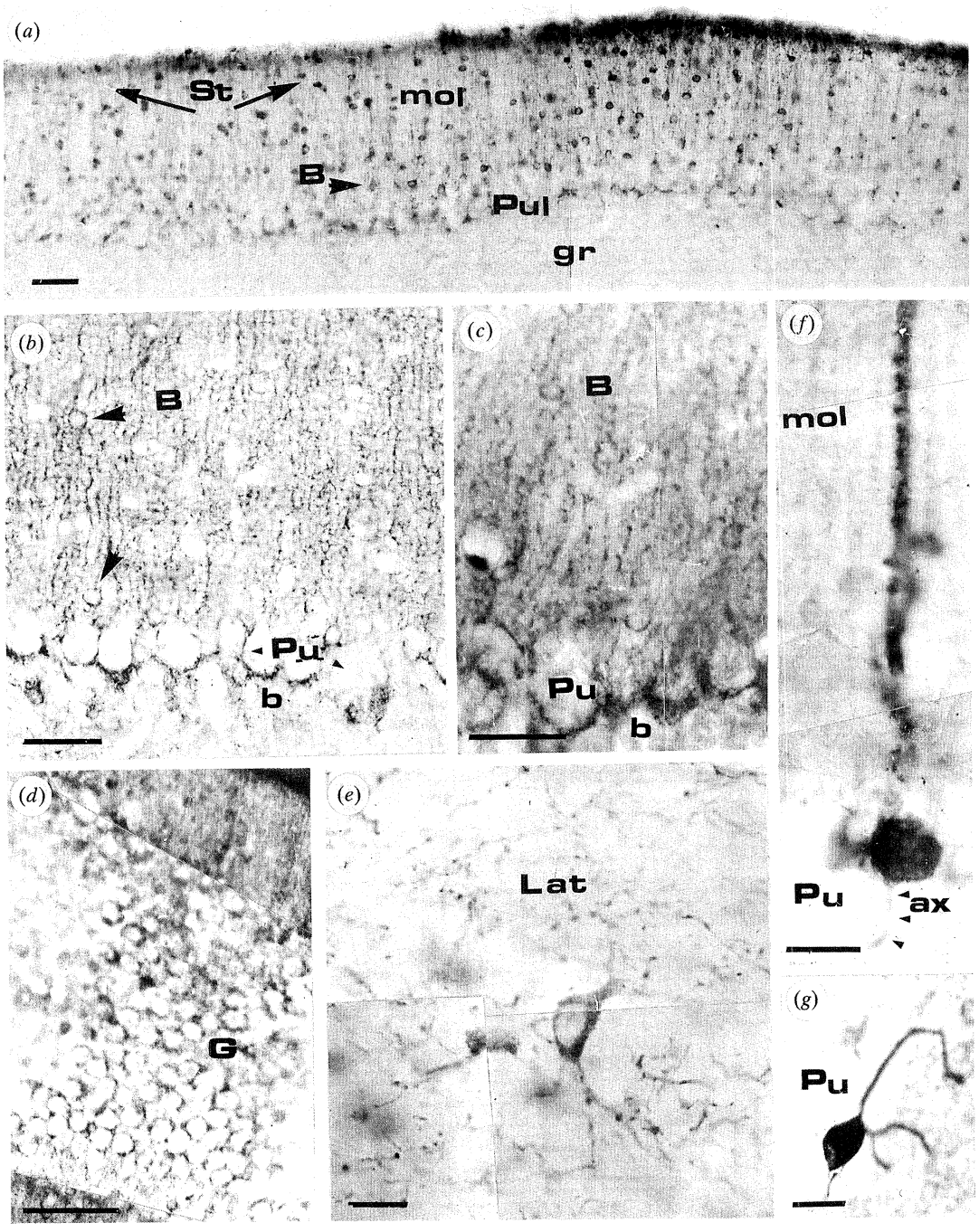

Figure 30. Distribution of cNOS-IR in the cerebellum. (*a*) General view of reactive structures in the different layers of the cerebellar cortex. Stellate cells (St) are located in the upper portion of the molecular layer (mol). Basket cells (B) are situated in the deep regions of the mol (arrow heads). Pul, Purkinje cell layer; gr, granular cell layer. (*b*) Distribution of basket cell bodies (arrowheads) and terminals (b). Pu, Purkinje cells. (*c*) High-power magnification of the molecular and Purkinje cell layers, providing details of the distribution of the basket terminals (b) which characteristically surround the initial portion of the Purkinje cell axons. (*d*) Granule cells exhibiting endogenous cNOS. (*e*) depicts the distribution of immunoreactive varicose nerve fibres and neurons in the lateral cerebellar nucleus (Lat). (*f*,*g*) Isolated immunoreactive Purkinje cells (Pu) located in the vermis and paraflocculus, respectively. ax, initial portion of Purkinje cell axon. Scale bars: (*a*–*d*) = 100 μm; (*e*–*g*) = 25 μm.

lateroventral and the medioventral preolivary nuclei also contained a dense plexus of immunoreactive varicose nerve fibres. Mainly in the superior olive, immunoreactive nerve terminals formed a complicated network surrounding unreactive neurons (figure 28*d*). Lateral to this olivary complex, immunoreactive nerve fibres formed part of the rubrospinal tract. Dorsally, the olivary complex was surrounded by cNOS-IR neurons and fibres that comprised the dorsal preolivary region.

The anterior portion of the ventral cochlear nucleus contained abundant immunoreactive nerve fibres, mainly in the granular layer, which exhibited large varicosities in close relationship with unreactive

neurons. Also found in this area were immunoreactive neurons, showing two intensities of immunoreactivity and exhibiting one principal thick process oriented to the granular cell layer. Round cNOS-IR neurons were found in the dorsal cochlear nucleus (figure 28*e*).

Immunoreactive neurons with long processes, surrounded by immunoreactive nerve fibres that formed a light plexus, were found in the lateral paragigantocellular nucleus (figure 28*f*) and scattered neurons were distributed in the rostral ventrolateral reticular nucleus, where some of them exhibited long processes and collaterals. A few immunoreactive neurons and fibres were also found in the more dorsal part of the caudal interstitial nucleus of the medial longitudinal fasciculus, in the nucleus of the solitary tract and in the intercalated nucleus of the medulla oblongata (figure 29*a*). A few small immunoreactive neurons were also found in the area postrema and in the gracile and cuneatus nuclei. The dorsal motor nucleus of the vagus nerve showed immunoreactive neurons (figure 29*b*), and some immunoreactive fibres and neurons were located in the lateral part of the hypoglossal nucleus and in the ambiguus nucleus.

The oral, interpolar and caudal parts of the spinal trigeminal nucleus showed a discrete number of small immunoreactive neurons situated in the most external layer (figure 29*c*). However, a dense varicose immunoreactive plexus containing few cNOS-IR neurons pervaded all areas of the spinal trigeminal nucleus (figure 29*d*,*e*), which was bordered medially by scattered neurons distributed in the dorsal portion of the medullary reticular field.

(*e*) *Cerebellum*

The molecular layer contained cNOS-IR basket and stellate cells (figure 30*a*). The basket terminal arborizations that the basket cells form around the initial portion of the axon of the non-immunoreactive Purkinje cells were also immunoreactive (figure 30*b*,*c*). The stellate cells were situated near the pial surface and basket cells at the level of the middle and deep portions of the molecular layer. The granular cell layer showed weak immunoreactivity in the granule cells and in their processes that contribute to form the glomeruli (figure 30*d*). The deep cerebellar nuclei, principally the lateral and the anterior interposed nuclei, showed a light plexus of immunoreactive varicose fibres containing some neurons (figure 30*e*). A very small number of cNOS-IR Purkinje cells were found in the middle line of the vermis and in the paraflocculus (figure 30*f*,*g*).

5. DISCUSSION

This study shows a detailed neuroanatomical distribution of the NO synthase enzyme in the rat central nervous system. Most of the results of this study are in agreement with others that have described partial maps of the distribution of NO synthesizing neurons in the rat brain (Bredt *et al.* 1990, 1991*b*; Forstermann *et al.* 1990; Dawson *et al.* 1992; Springall *et al.* 1992).

Some of the discrepancies that do arise might be related to the antibodies used in the different studies. The one used in our study is a very high titre polyclonal antibody raised against the purified, native rat neuronal NO synthase, fully characterized by Springall *et al.* (1992) and Riveros-Moreno *et al.* (1993). The other important difference is the fixation protocol used, as it is well established that brain structures can easily be damaged so that they are not recognized by antibodies. The free floating technique for the immunoreaction allows very efficient penetration of the antibody into the thick sections that were used in this case to obtain an almost three-dimensional picture of each neuron. This immunocytochemical protocol does not involve drying of the tissue, thus its preservation is improved.

The positive staining previously observed in the molecular and granule cell layers of the cerebellum, the granular cell layer of the olfactory bulb, the superior and inferior colliculi, the dentate gyrus of the hippocampus, the bed nucleus of the stria terminalis, the islands of Calleja, the horizontal limb of the diagonal band of Broca and the cerebral cortex (Bredt *et al.* 1990, 1991*b*) were also observed in our study. Our results also confirm those showing that immunoreactivity to NO synthase occurs in a discrete population of medium-to-large aspiny neurons of the corpus striatum and in some neurons of the cerebral cortex, including the corpus callosum, the pedunculopontine tegmental nucleus, the cerebellum, the posterior pituitary, the supraoptic and the paraventricular hypothalamic nuclei (Dawson *et al.* 1991). Our results are also in agreement with those obtained in the human central nervous system (Springall *et al.* 1992). Thus the present work completes previous studies by giving a detailed description, including the morphology and distribution, of NO synthase-containing structures in the entire rat central nervous tissue. Our study should help to clarify discrepancies observed in previous studies as well as facilitating a greater understanding of the distribution of NO synthase and the possible roles of NO in the central nervous system.

In the hippocampus, Bredt *et al.* (1990) described intense immunoreactivity in the dentate gyrus; however, no immunoreactivity was found associated with pyramidal cells in different areas of Ammon's horn. Subsequently, Bredt *et al.* (1991*b*) reported some scattered immunoreactive neurons in CA1 hippocampal formation, which did not correspond to pyramidal cells, confirming their own previous results (Bredt *et al.* 1990). In striking contrast, our results, using paraformaldehyde as a fixative, have shown numerous immunoreactive neurons in the dentate gyrus and in the CA1–CA3 of Ammon's horn, including pyramidal cells, whose number was increased in the pre- and parasubiculum areas.

In the cerebellum, there are also a few differences between our results and those obtained previously (Bredt *et al.* 1990, 1991*b*). In 1990 Bredt and co-workers reported strong labelling of the glomeruli and granule cells in the granule cell layer of the cerebellum. In the molecular layer, staining was

associated with basket cells and their processes. The presence in the granular cell layer of cNOS mRNA has suggested that NO synthase in the molecular cell layer of the cerebellum corresponds largely to cNOS-IR processes arising from the granule cells (Bredt *et al.* 1991*b*). It has also been shown that NO synthase in the cerebellum is present in virtually all basket cells of the molecular layer and in the granule cells and mossy fibre terminals of the glomeruli in the granular cell layer (Dawson *et al.* 1991). In these studies the NADPH diaphorase activity was found to have an identical pattern of distribution.

Our results have demonstrated that immunoreactivity to cNOS is present in the cerebellum in both the molecular and granular cell layers as well as in the lateral and interposed cerebellar nuclei. The cNOS-IR in the molecular layer was present in the stellate cells and basket cells, as well as in their basket terminal processes which surround the initial portions of the Purkinje cell axons. In the granular cell layer, the immunoreactivity was localized in the granule cells and their processes which contribute to the formation of the glomeruli. In striking contrast with the results of Dawson *et al.* (1992), we found that the mossy fibres were consistently non-immunoreactive. Our finding suggests that the reactivity of the glomeruli corresponds to the dendrites of granule cells.

It is noteworthy that the pattern of staining shown by Bredt *et al.* (1990, 1991*b*) was not found by Hope & Vincent (1989), by Mizukawa *et al.* (1988), or by Vincent & Kimura (1992) who, using NADPH diaphorase histochemistry as a cytochemical marker to visualize NO-producing cells, showed that the granule cells exhibited weak reaction, that Purkinje cells were unstained, and that the neuropil of the molecular layer was homogeneously stained. Many cells in the inner third of the molecular layer that showed weak reaction were not morphologically characterized. Dawson *et al.* (1991) showed that the pattern of staining following NADPH diaphorase histochemistry and NO synthase immunoreactivity in the cerebellum was similar after mild fixation with 2% or less of paraformaldehyde.

Our results are similar to those obtained by Schmidt *et al.* (1992) in the cerebellum, olfactory bulb and hippocampus after using acetone as fixative and an antibody against pure rat cerebellar NO synthase. The pattern of distribution of NO synthase that we have found in the rat cerebellum is also comparable to that showed by Southam *et al.* (1992) following NADPH diaphorase histochemistry.

In summary, two main types of interneurons containing NO synthase are present in the cerebellum: the granule cells in the granular cell layer, and stellate and basket cells in the molecular cell layer. Of these, the granule and basket cells are the origin of the parallel fibres and basket terminal arborization, respectively, which were also immunoreactive to cNOS and both connect with the same target neuron, the Purkinje cell.

Southam *et al.* (1992), using an antibody against cGMP, showed that cGMP immunoreactivity was evident in the vicinity of Purkinje cells, in the cytoplasm of Bergman glial cell bodies and in their radial fibres that crossed the molecular layer ascending to the pial surface. Purkinje cell somata were weakly immunoreactive, as also were the basket and stellate interneurons. The staining in the granule cell layer was generally light, although when the sensitivity of the procedure was increased by concentrating the primary antibody, the basal cGMP immunoreactivity appeared in astrocytes and glomeruli.

The cerebellum has been reported to be the area of the brain that has the highest NO synthase activity (Bredt *et al.* 1990, 1991*b*) and where the activation of glutamate receptors and/or other stimuli can trigger the enzymic formation of NO from the amino acid L-arginine (Garthwaite *et al.* 1988). Among the glutamate receptors, the *N*-methyl-D-aspartate (NMDA) subtype appears to be of particular relevance in this regard. The major function of NO is to activate soluble guanylate cyclase and thereby raise cGMP concentrations. In the cerebellum, there are two excitatory inputs to Purkinje cells, the climbing fibres and parallel fibres, which emanate from the inferior olivary complex (Brodal 1940) and the granule cells, respectively. The occurrence of NO synthase in granule cells (Southam *et al.* 1992) suggests that parallel fibres in the molecular layer contain NO. However, the fact that we have found cells in the olivary complex to be cNOS-negative and no cNOS-IR fibres in the white matter of the cerebellum suggests that climbing and mossy fibres lack NO.

Glutamate is thought to be the neurotransmitter of the parallel fibres, which influence Purkinje cells by opening ion channels (Ito & Kane 1982) or stimulating phosphatidyl inositol turnover (Blackstone *et al.* 1989; Rodrigo *et al.* 1993). Activity in these fibres may also lead to NO release and thence to the formation of cGMP in nearby structures.

The highest concentrations of cGMP occur in the cerebellum (Ferrendelli 1978) where glutamate or aspartate, the major excitatory neurotransmitters in the brain, may rapidly increase cGMP levels via the NMDA subtype of the glutamate receptor (Garthwaite 1982). There is a substantial body of evidence suggesting that Purkinje cells are the site where cGMP levels may be regulated, although other evidence also points to the involvement of granule and glial cells (Garthwaite & Garthwaite 1987).

Nitric oxide synthase may regulate cGMP levels in granule cells and basket cells which also possess guanylate cyclase (Zwiller *et al.* 1981; Novelli *et al.* 1987), but much less abundantly than in Purkinje cells (Ariano *et al.* 1982). The presence of NO synthase in basket arborizations surrounding Purkinje cells is also consistent with a role of these fibres in enhancing cGMP formation in Purkinje cells (Ferrendelli 1978). Ultrastructural studies will be needed to identify the immunoreactive neuronal structures containing NO synthase in the cerebellum and their relationship with each other. The functional significance of cNOS in isolated Purkinje cells in the vermis and paraflocculars regions of the cerebellum is, as yet, unknown.

The identification of varicose nerve fibres showing strong immunoreactivity in the proximity of the wall of the lateral and third ventricles is one of the most striking differences we have observed from previous studies. It was impossible to establish in this study the specific relations between these varicose immunoreactive nerve fibres and neighbouring structures. These fibres penetrated the epithelium to end in the proximity of the ventricular lumen in apparent close relationship with the ependymal cells. These nerve fibres may arise from the medial subnuclei of the dorsal raphe nucleus (Richards *et al.* 1973; Parent *et al.* 1984). We have found that neurons in the dorsal raphe nucleus display cNOS immunoreactivity, and Johnson & Ma (1993) have shown that approximately 70% of the serotoninergic neurons in the medial subnuclei of the dorsal raphe also display NADPH diaphorase activity.

Whether or not NO plays a role in the wall of the ventricles is unknown. The proximity of those cNOS-IR fibres to the wall of the ventricles and the presence of immunoreactive neurons in the subfornical organ and the area postrema, suggest that NO synthase and its product, NO, may be involved in the regulation of cerebrospinal fluid. In this context, a role for NO in the production of aqueous humor in the rabbit eye has previously been proposed (Osborne *et al.* 1993). Future electron microscopic studies will provide detailed information about the morphological characteristics of these immunoreactive fibres in the wall of ventricles.

Both large and small blood vessels in the rat brain contain a perivascular cNOS similar to the NADPH diaphorase-positive perivascular plexus described previously by De Felipe (1993) in small blood vessels of the human temporal cortex. This cNOS innervation may participate in the control of the microcirculation in different regions of the brain. As has recently been reported, NO participates in the functional activity of the blood vessel and its blood flow (Goadsby *et al.* 1992). The perivascular cNOS-IR plexus may represent the anatomical site of production of NO for this purpose (Iadecola 1992).

The presence of cNOS-IR non-pyramidal neurons and varicose nerve fibres in all regions and layers of the cortex suggests that cNOS participates in cortical activity. Our results agree with those of De Felipe (1993) who showed that NADPH diaphorase and cNOS are present only in interneurons and that no pyramidal cells were labelled. Different results have been shown by Valtschanoff *et al.* (1993*a*), using NADPH diaphorase histochemistry, who described some pyramidal shaped neurons with ascending axons that were stained in layer VI. In relation to the question of whether or not pyramidal cells contain NADPH diaphorase activity, Sandell (1986), using NADPH diaphorase histochemistry, found labelled cells in layers II and III and some in layers IV and V, but did not find labelled pyramidal or spiny cells. The general distribution of labelled interneurons in different layers of the cortical areas of human brain previously reported using NADPH diaphorase histochemistry (De Felipe 1993) is similar to our results in rat brain. These labelled cells were present in all cortical layers, particularly in layers II and III, but numerous immunoreactive neurons were also found in layers V and VI. These immunoreactive neurons were scarce relative to the total number of neurons that constitute all the cortical layers, suggesting that these immunoreactive plexuses may be developed for intrinsic and extrinsic afferent fibres. We have observed that the density of cNOS-IR nerve fibres is greatest in layers I and II, decreases in layers III and IV and increases in layers V and VI. The presence of NADPH diaphorase and cNOS-IR interneurons in all cortical areas suggests the possible coexistence of NO with γ-aminobutyric acid (GABA) (Hedlich *et al.* 1990; Valtschanoff *et al.* 1993*a*). Valtschanoff *et al.* (1993*a*), using NADPH diaphorase histochemistry, and cNOS and GABA immunohistochemistry, showed that one small fraction of GABA-positive neurons, principally the largest GABA-positive cells, contained all the three markers investigated. Furthermore, all intracortical cNOS-IR neurons also contain GABA. NADPH diaphorase activity has been shown to co-localize with GABA immunoreactivity in horizontal cells of the carp retina (Weiler & Kewitz 1993) and all NADPH diaphorase-positive neurons in the hippocampus also contain GABA (Valtschanoff *et al.* 1993*b*).

A close relationship between some immunoreactive neurons and the small blood vessels within the so-called magnocellular accessory group (Peterson 1966) have been identified in this study. This group of neurons includes the nuclei of the anterior commissure, the anterior and posterior fornical nuclei, the circularis nucleus, the nucleus of the medial forebrain bundle and the retrochiasmatic nucleus. These groups of neurons, located around the blood vessels in the anterior hypothalamus, have been described by Diepen (1962) and Martinez-Rodriguez *et al.* (1979). The latter authors described these neurons as forming a hypothalamo-chiasmatic-perivascular-neurosecretory system. These neurons showed particular characteristics only observable in the neurosecretory neurons, including common sizes and shapes, intense metachromatic staining, intense colloidal iron reactivity, chrome-alum haematoxylin-phloxine staining and histochemical reaction to acetylcholinesterase, thiaminopyrophosphatase and nucleoside-diphosphatase activities (Martinez-Rodriguez *et al.* 1979).

The localization of NO synthase to neuronal projections in the posterior pituitary and adrenal medulla may reflect a functional role. This possibility is supported by findings that NO and sodium nitroprusside, which generates NO, release catecholamines in adrenal medullary preparations (Dohi *et al.* 1983; Bredt *et al.* 1990; O'Sullivan & Burgoyne 1990). Furthermore, an NO-generating mechanism has been linked to the inhibition of insulin secretion by cytokines (Southern *et al.* 1990).

It is well known that cNOS-IR neurons in the hypothalamic nuclei contain other neuroactive substances, including insulin-like growth factor I (Aguado *et al.* 1992), which regulates or modulates

the release of somatostatin and luteinizing hormone-releasing hormone in the hypothalamus and of growth hormone and gonadotropic hormone release in the pituitary (Berelowitz *et al.* 1981; Tannenbaum *et al.* 1983; Yamashita & Melmed 1986; Silverman *et al.* 1989; Hiney *et al.* 1991; Kanematsu *et al.* 1991), an area in which L-arginine is also a potent secretagogue (Barbul 1990). The wide distribution of NO synthase in the hypothalamus, specifically in the so-called magnocellular accessory group, could explain the participation of NO in some aspects of hormonal control. In this regard, changes in NADPH diaphorase activity have been noted following salt intake (Sagar & Ferreiro 1987). Although the role of NO in neurosecretion has not yet been clearly defined, it is possible that NO modifies the properties of storage vesicles, as NO donors partly inhibit catecholamine uptake, and simultaneously affect the electrochemical gradient involved in this uptake (Gronberg *et al.* 1990).

Nitric oxide may also be involved in the regulation of secretion (Pow 1992). NO synthase has been identified in several neural populations, including the hypothalamic paraventricular nucleus, which play a major role in regulating milk ejection via the hypothalamus-neurohypophyseal axis (Ceccatelli & Eriksson 1993).

Our results also show a wide distribution of NO synthase in numerous nuclei and neuronal systems throughout the brain, where NO synthase may be co-localized with other neuroactive substances. It is already known that expression of NO synthase, as visualized by NADPH diaphorase, is co-localized with somatostatin and neuropeptide Y in the corpus striatum and the cerebral cortex (Vincent *et al.* 1983; Mellander *et al.* 1985; Mancillas *et al.* 1986; Kowall *et al.* 1987, 1991; Kowall & Beal 1988; Villalba *et al.* 1988; Bredt *et al.* 1990, 1991*b*; Dawson *et al.* 1991) and olfactory bulb (Villalba *et al.* 1989), with choline acetyltransferase in the pedunculopontine nucleus and lateral tegmental nucleus (Dawson *et al.* 1991) and ascending cholinergic reticular system (Vincent *et al.* 1986), with galanin in the substantia innominata (Mellander *et al.* 1985; Ellison *et al.* 1987; Mesulam *et al.* 1989; Pasqualotto and Vincent 1991) and with calbindin-D28K in the rat olfactory bulb (Alonso *et al.* 1993). These co-localizations, and the possibility that coexistence with other neuroactive substances may occur, confer interesting new possibilities on the functions that NO may play in the regulation and/or modulation of many neurotransmitter-specific systems.

Recent evidence has indicated that NO induces the release of classical neurotransmitters such as acetylcholine from cholinergic neurons (Prast & Philippu 1992), and also that NADPH diaphorase coexists with choline acetyltransferase in the substantia innominata of man (Ellison *et al.* 1987).

In the rat (Martinez-Murillo & Rodrigo 1994), the basal forebrain cholinergic complex, Ch1–Ch4 of Mesulam *et al.* (1983), occupies the medial septum, the vertical and horizontal limb of the diagonal band of Broca, the substantia innominata, the ventromedial region of the globus pallidus and adjacent portions of the internal capsule and the so-called nucleus of the ansa lenticularis. Characteristically, between 20–30% of these cholinergic neurons were found to contain NADPH diaphorase activity (Vincent & Kimura 1992; Geula *et al.* 1993). We found that a considerable number of cNOS-IR neurons in these regions have the same distribution and exhibit the same morphology as the cholinergic neurons, suggesting that a fraction of the cholinergic neurons in the basal forebrain also contain NO synthase. It is well known that cholinergic neurons in the basal forebrain provide the major cholinergic input to the entire neocortex, hippocampus, amygdala and olfactory bulb (Shute & Lewis 1967; Lehmann *et al.* 1980; Divac 1981; Johnston *et al.* 1981; Bigl *et al.* 1982; Fibiger 1982; McKinney *et al.* 1983; Mesulam *et al.* 1983; Struble *et al.* 1986; Senut *et al.* 1989). This suggests a putative role for NO in regulating the cholinergic innervation and activity of these telencephalic areas.

The neurons of the Ch5 and Ch6 cholinergic projection form a continuous column through the caudal aspect of the substantia nigra to rostral domains of the locus coeruleus (Mesulam *et al.* 1983, 1984, 1989; Hallanger *et al.* 1987). Cholinergic neurons of the Ch5 group are within the limits of the pedunculopontine nucleus, and in the cuneiform and parabrachial nuclei. The Ch6 group remains within the periaqueductal grey, with most of these cells lying within the boundaries of the laterodorsal tegmental nucleus. The fact that both cell groups contain NADPH diaphorase (Vincent & Kimura 1992), and that we have found that cNOS-IR neurons in these regions show the same morphology as cholinergic neurons, allow us to suggest that cholinergic neurons in those nuclei also contain NO synthase. These cholinergic neurons are located in close association with several fibre tracts, including the superior cerebellar peduncle, lateral lemniscus, dorsotegmental tract and medial longitudinal fasciculus (Woolf & Butcher 1989). The Ch5 and Ch6 neuron groups provide direct ascending projections that terminate in a number of target structures in the midbrain, diencephalon and telencephalon, including the superior colliculus, anterior pretectal area, interstitial magnocellular nucleus of the posterior commissure, lateral habenular nucleus, magnocellular preoptic nucleus, lateral mamillary nucleus, basal forebrain, olfactory bulb and medial prefrontal cortex (Mesulam *et al.* 1983; Sugimoto and Hattori 1984; Sofroniew *et al.* 1985; Satoh and Fibiger 1986; Jourdain *et al.* 1989). These cholinergic projections constitute a major component of the ascending reticular activating system to the thalamus. Taking into account the above-mentioned connections of the Ch5 and Ch6 cholinergic cell groups, it has been proposed (Martinez-Murillo *et al.* 1990) that the mesopontine tegmental cholinergic system may influence cortical activity through direct and indirect pathways. These neurons appear to be mainly involved in wakefulness and sleep (Jones 1991). The projections towards the pontine nuclei may serve to modulate the neurotransmission of cerebellar afferent

information in accordance with the behavioural state of the animal (Semba *et al.* 1990). On these grounds, it is possible that NO may participate in regulating those functions in which cholinergic neurons are involved.

The distribution of NO synthase and its co-localization with other neuroactive substances as well as its role in different neuropathological disorders in the brain have been established in many previous studies, using the histochemical reaction to demonstrate NADPH diaphorase activity (Ferrante *et al.* 1985; Kowall *et al.* 1987; Ferreiro *et al.* 1988; Halliwell 1989; Uemura *et al.* 1990; Karson *et al.* 1991). Hope *et al.* (1991) demonstrated co-localization of NO synthase and NADPH diaphorase. This was later confirmed by Bredt *et al.* (1991b). However, some doubts do still exist as to whether NO synthase and NADPH diaphorase are the same entity, at least in tissue preparations. Our results, using the immunocytochemical procedure to demonstrate NO synthase in the central nervous system, show some differences when compared with those obtained by Vincent & Kimura (1992). These differences, in spite of the overwhelming similarities between the immunocytochemical and histochemical results, are related to the main olfactory bulb, where we have found large periglomerular cells, in the glomerular layer, to exhibit NO synthase. In contrast, Vincent & Kimura (1992) showed that only a few of these neurons exhibited NADPH diaphorase activity. The differences also occurred in the accessory olfactory bulb, which characteristically contains immunoreactive mitral cells to NO synthase, but were found to be NADPH diaphorase-negative.

Another discrepancy was found in the globus pallidus, substantia nigra, ventral pallidum entopeduncular nucleus, taenia tectae and hippocampus. In these regions, neurons exhibiting cNOS-IR were more numerous than those reported by Vincent & Kimura (1992) to show NADPH diaphorase activity. In the circularis nucleus, the medial tuberal nucleus and arcuate nucleus of the hypothalamus, the parafascicular and medial habenular nuclei of the thalamus, the pars reticulata and lateralis of the substantia nigra, the locus coeruleus, the ventral tegmental nucleus of the pons and area postrema of the medulla oblongata showed cNOS-IR neurons but NADPH diaphorase activity was only found in some nerve fibres (Vincent & Kimura 1992).

These differences may depend on the fixative solutions used, their concentration and the procedures employed for immunohistochemistry and histochemistry. Using paraformaldehyde as a fixative, most NADPH diaphorase activity is inactivated, especially the particulate fraction, but the cytosolic fraction of this enzyme, which is associated with the soluble NO synthase, remains intact (Matsumoto *et al.* 1993). This could explain certain controversial results. Previous reports have shown that the CA1 pyramidal cell layer was largely unstained following NADPH diaphorase histochemistry (Vincent & Kimura 1992; Valtschanoff *et al.* 1993*b*). Following NO synthase immunoreactivity, pyramidal cells either lacked immunostaining (Bredt *et al.* 1991*b*) or only a few were stained (Schmidt *et al.* 1992). Most of the NADPH diaphorase- and NO synthase-positive neurons were generally found outside the pyramidal layer. We have found NADPH diaphorase activity in neurons of the pars lateralis, compacta and reticulata of the substantia nigra and the locus coeruleus in the rat (Martinez-Murillo *et al.* 1989). In contrast, Vincent & Kimura (1992) reported nerve fibres containing NADPH diaphorase activity, but not cell bodies in these areas.

Lack of correlation between NADPH diaphorase staining and NO synthase immunocytochemical staining in the rat spinal cord has recently been reported (Dun *et al.* 1992), as has the fact that the majority of NADPH diaphorase is not NO synthase in fresh brain tissue (Matsumoto *et al.* 1993). The different results obtained in the spinal cord by Dun *et al.* (1993) and by Terenghi *et al.* (1993) may be related to the concentration of paraformaldehyde used as fixative. The evidence from Hope *et al.* (1991) suggests that all neurons that contain NADPH diaphorase activity also contain NO synthase. However, it is possible NADPH diaphorase activity might be positive only in neurons actively synthesizing NO, while the immunohistochemical detection would reveal all neurons containing NO synthase.

The biological function of NO in the brain is of major importance. In the hippocampus, NO is responsible for the initiation of hippocampal long-term potentiation (Bohme *et al.* 1991; Schuman & Madison 1991; Gribkoff & Lum-Ragan 1992; Schmidt *et al.* 1992). It is possible that NO plays an important role in the short-term effects of excitatory amino acids as well as in their long-term effects on brain development, learning and memory (Bohme *et al.* 1991). As mentioned above, NO may mediate the biological effects of other neurotransmitters whose actions are associated with an increase in cGMP (Drummond 1984).

Nitric oxide may also contribute to some aspects of the pathology of the central nervous system (Moncada *et al.* 1989). Excessive production of NO appears to play a role in neurodegenerative disorders, through the influx of Ca^{2+} that accompanies prolonged NMDA receptor activation. It is likely that excessive NMDA receptor activation and the consequent increase in Ca^{2+} contribute to glutamate neurotoxicity by enhanced production of NO. High levels of cGMP also cause destruction of photoreceptor cells in the retina (Lolley *et al.* 1977), where NO synthase has been demonstrated by immunocytochemistry (Ross *et al.* 1990). Superfusion of cGMP analogues onto grafts of hippocampus triggers prolonged epileptiform activity in the pyramidal neurons (Freedman *et al.* 1979). Recently, it has been demonstrated that, in the hippocampus, NO synthase mediates acute CA1 neuronal injury during hypoxia and that inhibition of NO synthase may be a useful neuroprotective strategy (Wallis *et al.* 1992). In this regard, the neurons that contain NO synthase are more resistant to the noxious effects of excitatory amino acids (Beal *et al.* 1986; Koh *et al.* 1986) and hypoxia (Uemura *et al.*

1990) and were also found to survive the degenerative processes which occur in Huntington's and Alzheimer's disease in select areas of the brain (Ferrante *et al.* 1985; Kowall *et al.* 1987; Kowall & Beal 1988).

Future studies at the electron microscope level and investigations of the co-localization of NO synthase with other neuroactive substances will explain the precise distribution of this enzyme in the neurons and processes described in this work and will facilitate our understanding of the different functional implications of NO synthase, and its product NO, in the normal and pathological activity of the brain.

This work was supported by the Dirección General de Investigación Científica y Técnica of Spain (Grant DGICYT PB92–0106), the Royal Society of U.K., the Fondo de Investigaciones Sanitarias (FIS) (Grant 92/0269) and the Grant Charity of Freemasons. We thank Mrs D. Guinea and Ms E. Simon for expert technical assistance and Mrs A. Higgs for help in preparation of the manuscript.

REFERENCES

Aguado, F., Fernandez, T., Martinez-Murillo, R., Rodrigo, J., Cacicedo, L. & Sanchez-Franco, F. 1992 Immunocytochemical localization of insulin-like growth factor I in the hypothalamo-hypophyseal system of the adult rat. *Neuroendocrinology* **56**, 856–863.

Alonso, J.R., Arevalo, R., Porteros, A., Brinon, J.G., Lara, J. & Aijon, J. 1993 Calbindin D-28K and NADPH-diaphorase activity are localized in different populations of periglomerular cells in the rat olfactory bulb. *J. chem. Neuroanat.* **6**, 1–6.

Ariano, M.A., Lewicki, J.A., Brandwein, J.H. & Murad, F. 1982 Immunohistochemical localization of guanylate cyclase within neurons of rat brain. *Proc. natn. Acad. Sci. U.S.A.* **79**, 1316–1320.

Barbul, A. 1990 Physiology and pharmacology of arginine. In *Nitric oxide from L-arginine: a bioregulatory system* (ed. S. Moncada and E. A. Higgs) pp. 317–329. Amsterdam: Excerpta Medica.

Beal, M.F., Kowall, N.W., Ellison, D.W.M., Mazurek, M.F., Swartz, K.J. & Martin, J.B. 1986 Replication of the neurochemical characteristics of Huntington's disease by quinolinic acid. *Nature, Lond.* **321**, 168–171.

Berelowitz, M., Szabo, M., Frohman, L.A., Firestone, S., Chu, L. & Hintz, R.L. 1981 Somatomedin-C mediates growth hormone negative feedback by effects on both the hypothalamus and the pituitary. *Science, Wash.* **212**, 1279–1281.

Bigl, V., Woolf, N.J. & Butcher, L.L. 1982 Cholinergic projections from the basal forebrain to frontal, parietal, temporal, occipital and cingulate cortices. A combined fluorescent tracer and acetylcholinesterase analysis. *Brain Res. Bull.* **8**, 727–749.

Blackstone, C.D., Supattapone, S. & Snyder, S.H. 1989 Inositolphospholipid-linked glutamate receptors mediate cerebellar parallel-fiber-Purkinje-cell synaptic transmission. *Proc. natn. Acad. Sci. U.S.A.* **86**, 4316–4320.

Bohme, G.A., Bou, Ch., Stutzman, J., Doble, A. & Blanchard, J.-Ch. 1991 Possible involvement of nitric oxide in long-term potentiation. *Eur. J. Pharmacol.* **199**, 379–381.

Bredt, D.S. & Snyder, S.H. 1989 Nitric oxide mediates glutamate-linked enhancement of cGMP levels in the cerebellum. *Proc. natn. Acad. Sci. U.S.A.* **86**, 9030–9033.

Bredt, D.S. & Snyder, S.H. 1990 Isolation of nitric oxide synthase, a calmodulin requiring enzyme. *Proc. natn. Acad. Sci. U.S.A.* **87**, 682–685.

Bredt, D.S. & Snyder, S.H. 1992 Nitric oxide: a novel neuronal messenger. *Neuron* **8**, 3–11.

Bredt, D.S., Hwang, P.M. & Snyder, S.H. 1990 Localization of nitric oxide synthase indicating a neural role for nitric oxide. *Nature, Lond.* **347**, 768–770.

Bredt, D.S., Hwang, P.M., Glatt, C.E., Lowenstein, C., Reed, R.R. & Snyder, S.H. 1991*a* Cloned and expressed nitric oxide synthase structurally resembles cytochrome P-450. *Nature, Lond.* **351**, 714–718.

Bredt, D.S., Glatt, C.E., Hwang, P.M., Dawson, T.M. & Snyder, S.H. 1991*b* Nitric oxide synthase protein and mRNA are discretely localized in neuronal populations of the mammalian CNS together with NADPH-diaphorase. *Neuron* **7**, 615–624.

Brodal, A. 1940 Modification of Sudden's method for study of cerebral localization. *Arch. Neurol. Psychiat.* **43**, 46–58.

Busse, R. & Mulsch, A. 1990 Induction of nitric oxide synthase by cytokines in vascular smooth muscle cells. *FEBS Lett.* **275**, 87–90.

Ceccatelli, S. & Eriksson, M. 1993 The effect of lactation on nitric oxide synthase gene expression. *Brain Res.* **625**, 177–179.

Charles, I.G., Palmer, R.M.J., Hickery, M.S., Bayliss, M.T., Chubb, A.P., Hall, V.S., Moss, D.W. & Moncada, S. 1993 Cloning, characterization and expression of a cDNA encoding an inducible nitric oxide synthase from the human chondrocyte. *Proc. natn. Acad. Sci. U.S.A.* **90**, 11 419–11 423.

Dawson, T.M., Bredt, D.S., Fotuhi, M., Hwang, P.M. & Snyder, S.H. 1991 Nitric oxide synthase and neuronal NADPH-diaphorase are identical in brain and peripheral tissues. *Proc. natn. Acad. Sci. U.S.A.* **88**, 7797–7801.

Dawson, T.M., Dawson, V.L. & Snyder, S.H. 1992 A novel neuronal messenger molecule in brain: the free radical nitric oxide. *Ann. Neurol.* **32**, 297–311.

DeFelipe, J. 1993 A study of NADPH-diaphorase-positive axonal plexuses in the human temporal cortex. *Brain Res.* **615**, 342–346.

Diepen, R. 1962 *Handbuch der mikroskopischen Anatomie des Menschen. Nervensystem der Hypothalamus*, p. 82. Berlin: Springer Verlag.

Divac, I. 1981 Cortical projections of the magnocellular nuclei of the basal forebrain. A reinvestigation. *Neuroscience* **6**, 983–984.

Dohi, T., Morita, K. & Tsujimoto, A. 1983 Effect of sodium azide on catecholamine release from isolated adrenal gland and on guanylate cyclase. *Eur. J. Pharmacol.* **94**, 331–335.

Drummond, G.I. 1984 Cyclic GMP. In *Cyclic nucleotides in the nervous system* (ed. P. Greengard & G. A. Robinson), pp. 373–494. New York: Raven press.

Dun, N.J., Dun, S.L., Forstermann, V. & Tseng, L.F. 1992 Nitric oxide synthase immunoreactivity in rat spinal cord. *Neurosci. Lett.* **147**, 217–220.

East, S.J. & Garthwaite, J. 1991 NADPH receptor activation in rat hippocampus induces cyclic GMP formation through the L-arginine-nitric oxide pathway. *Neurosci. Lett.* **123**, 17–19.

Ellison, D.W., Kowall, N.W. & Martin, J.B. 1987 Subset of neurons characterized by the presence of NADPH-diaphorase in human substantia innominata. *J. comp. Neurol.* **260**, 233–245.

Elphick, M.R., Riveros-Moreno, V., Moncada, S. & O'Shea, M. 1993 Identification of nitrergic neurons in invertebrates. *Endothelium* **1**(Suppl.), 57S, abstract 223.

Ferrante, R.J., Kowall, N.W., Beal, M.F., Richardson, E.P. Jr., Bird, E.D. & Martin, J.B. 1985 Selective sparing of a

class of striatal neurons in Huntington's disease. *Science, Wash.* **230**, 561–563.

Ferreiro, D.M., Arcavi, L.J., Sagar, S.M., McIntosh, T.K. & Simon, R.P. 1988 Selective sparing of NADPH-diaphorase neurons in neonatal hypoxia-ischemia. *Ann. Neurol.* **24**, 670–676.

Ferrendelli, J.A. 1978 Distribution and regulation of cyclic GMP in the central nervous system. *Adv. Cyclic Nucleotide Res.* **9**, 453–464.

Fibiger, H.C. 1982 The organization and some projections of cholinergic neurons of the mammalian forebrain. *Brain Res. Revs.* **4**, 327–388.

Forstermann, U., Gorsky, L.D., Pollock, I.S., Schmidt, H.H.H., Heller, M. & Murad, F. 1990 Regional distribution of EDRF-NO synthesizing enzyme(s) in the rat brain. *Biochem. biophys. Res. Commun.* **168**, 727–732.

Forstermann, U., Schmidt, H.H.H., Pollock, J.S., Sheng, H., Mitchell, J.A., Warner, T.D., Nakane, M. & Murad, F. 1991 Isoforms of nitric oxide synthase. Characterization and purification from different cell types. *Biochem. Pharmacol.* **42**, 1849–1857.

Freedman, R., Taylor, D., Seiger, A., Olson, L. & Hoffer, B. 1979 Seizure and related epileptiform activity in hippocampus transplanted to interior chamber in the eye. II. Modulation of cholinergic input. *Ann. Neurol.* **6**, 281–293.

Garthwaite, J. 1982 Excitatory amino acid receptors and guanosine 3′,5′-cyclic monophosphate in incubated slices of immature and adult rat cerebellum. *Neuroscience* **7**, 2491–2497.

Garthwaite, J. 1991 Glutamate, nitric oxide and cell–cell signalling in the nervous system. *Trends Neurosci.* **14**, 60–67.

Garthwaite, J. & Garthwaite, G. 1987 Cellular origins of cyclic GMP responses to excitatory amino acid receptor agonists in rat cerebellum in vitro. *J. Neurochem.* **48**, 29–39.

Garthwaite, J., Charles, S.L. & Chess-Williams, R. 1988 Endothelium-derived relaxing factor release on activation of NMDA receptors suggests role as intercellular messenger in the brain. *Nature, Lond.* **336**, 385–388.

Geller, D.A., Lowenstein, C.J., Shapiro, R.A., Nussler, A.K., Di Silvio, M., Wang, S.C., Nakayama, D.K., Simmons, R.L., Snyder, S.H. & Billiar, T.M. 1993 Molecular cloning and expression of inducible nitric oxide synthase from human hepatocytes. *Proc. natn. Acad. Sci. U.S.A.* **90**, 3491–3495.

Geula, C., Schatz, C.R. & Mesulam, M.-M. 1993 Differential localization of NADPH-diaphorase and calbindin-D 28K within the cholinergic neurons of the basal forebrain, striatum and brainstem in the rat, monkey, baboon and human. *Neuroscience* **54**, 461–473.

Goadsby, P.J., Kaube, H. & Hoskin, K. 1992 Nitric oxide synthesis couples cerebral blood flow and metabolism. *Brain Res.* **595**, 167–170.

Gribkoff, V.K. & Lum-Ragan, J.T. 1992 Evidence for nitric oxide synthase inhibitor-sensitive and insensitive hippocampal synaptic potentiation. *J. Neurophysiol.* **68**, 639–642.

Gronberg, M., Terland, O., Husebye, E.S. & Flatmark, T. 1990 The effect of prenylamine and organic nitrates on the bioenergetics of bovine catecholamine storage vesicles. *Biochem. Pharmacol.* **40**, 351–355.

Gross, S.S., Jaffe, E.A., Levi, R. & Kilbourn, R.G. 1991 Cytokine-activated endothelial cells express an isotope of nitric oxide synthase which is tetrahydrobiopterin-dependent, calmodulin-independent and inhibited by arginine analogs with a rank-order of potency characteristic of activated macrophages. *Biochem. biophys. Res. Commun.* **178**, 823–829.

Guesdon, J.L., Ternyck, T. & Avrameas, S. 1979 The use of avidin-biotin interaction in immunoenzymatic techniques. *J. Histochem. Cytochem.* **27**, 1131–1139.

Hallanger, A.E., Levey, A.Y., Lee, H.J., Rye, D.B. & Wainer, B.H. 1987 The origin of cholinergic and other subcortical afferents to the thalamus in the rat. *J. comp. Neurol.* **262**, 105–124.

Halliwell, B. 1989 Oxidants and the central nervous system: some fundamental questions. Is oxidant damage relevant to Parkinson's disease, Alzheimer's disease, traumatic injury or stroke? *Acta Neurol. Scand.* (Suppl.) **126**, 23–33.

Hedlich, A., Luth, H.-J., Werner, L., Bar, B., Hanish, U. & Winkelmann, E. 1990 GABAergic NADPH-diaphorase positive Martinottizellen im visualencortex der ratte. *J. Hischforsch.* **31**, 618–687.

Hevel, J.M., White, K.A. & Marletta, M.A. 1991 Purification of the inducible murine macrophage nitric oxide synthase. *J. biol. Chem.* **266**, 22 789–22 791.

Hibbs, J.B. Jr, Taintor, R.R., Vavrin, Z. & Rachlin, E.M. 1988 Nitric oxide: a cytotoxic activated macrophage effector molecule. *Biochem. biophys. Res. Commun.* **157**, 87–94.

Hiney, J.K., Ojeda, S.R. & Dees, L.W. 1991 Insulin-like growth factor I: A possible metabolic signal involved in the regulation of female puberty. *Neuroendocrinology* **54**, 420–423.

Hope, B.T. & Vincent, S.R. 1989 Histochemical characterization of neuronal NADPH-diaphorase. *J. Histochem. Cytochem.* **37**, 653–661.

Hope, B.T., Michael, G.J., Knigge, K.M. & Vincent, S.R. 1991 Neuronal NADPH-diaphorase is a nitric oxide synthase. *Proc. natn. Acad. Sci. U.S.A.* **88**, 2811–2814.

Hsu, S.M. & Raine, L. 1981 Protein A, avidin and biotin in immunocytochemistry. *J. Histochem. Cytochem.* **29**, 1349–1353.

Hsu, S.M., Raine, L. & Fanfer, H. 1981 Use of avidin-biotin complex (ABC) in immunoperoxidase technique. *J. Histochem. Cytochem.* **29**, 577–580.

Hyman, B.T., Marzloff, K., Wenniger, J.J., Dawson, T.M., Bredt, D.S. & Snyder, S.H. 1992 Relative sparing of nitric oxide synthase-containing neurons in the hippocampal formation in Alzheimer's disease. *Ann. Neurol.* **32**, 818–820.

Iadecola, C. 1992 Does nitric oxide mediate the increases in cerebral blood flow elicited by hypercapnia? *Proc. natn. Acad. Sci. U.S.A.* **89**, 3913–3916.

Ito, M. & Kane, M. 1982 Long-lasting depression of parallel fiber-Purkinje cell transmission induced by conjunctive stimulation of parallel fibers and climbing fibers in the cerebellar cortex. *Neurosci. Lett.* **33**, 253–258.

Johnson, M.D. & Ma, P.M. 1993 Localization of NADPH diaphorase activity in monoaminergic neurons of the rat brain. *J. comp. Neurol.* **332**, 391–406.

Johnston, M.V., McKinney, M. & Coyle, J.T. 1981 Neocortical cholinergic innervation: a description of extrinsic and intrinsic components in the rat. *Expl Brain Res.* **43**, 159–172.

Jones, B.E. 1991 The role of noradrenergic locus coeruleus neurons and neighbouring cholinergic neurons of the pontomesencephalic tegmentum in sleep-wake states. *Prog. Brain Res.* **88**, 533–543.

Jourdain, A., Semba, K. & Fibiger, H.C. 1989 Basal forebrain and mesopontine tegmental projections to the reticular thalamic nucleus, an axonal collateralization and immunohistochemical study in the rat. *Brain Res.* **505**, 55–65.

Kanematsu, T., Hirahara, M., Miyake, T., Shitsukawa, K. & Aono, T. 1991 Effect of insulin-like growth factor-I on gonadotropin release from the hypothalamus-pituitary axis in vitro. *Acta Endocrinol. Copenh.* **125**, 227–233.

Karson, C.N., Garcia Rill, E., Beidermann, J., Mrak, R.E., Husain, M.M. & Skinner, R.D. 1991 The brain stem reticular formation in schizophrenia. *Psychiatry Res.* **40**, 31–48.

Knowles, R.G., Palacios, M., Palmer, R.M.J. & Moncada, S. 1989 Formation of nitric oxide from L-arginine in the central nervous system: a transduction mechanism for stimulation of the soluble guanylate cyclase. *Proc. natn. Acad. Sci. U.S.A.* **86**, 5159–5162.

Knowles, R.G., Palacios, M., Palmer, R.M.J. & Moncada, S. 1990 Characteristics of nitric oxide synthase from rat brain. *Biochem. J.* **269**, 207–210.

Koh, J.-Y., Peters, S. & Choi, D.W. 1986 Neurons containing NADPH-diaphorase are selectively resistant to quinolinate toxicity. *Science, Wash.* **234**, 73–76.

Kowall, N.W. & Beal, M.F. 1988 Cortical somatostatin, neuropeptide Y and NADPH-diaphorase neurons: normal anatomy and alterations in Alzheimer's disease. *Ann. Neurol.* **23**, 105–114.

Kowall, N.W., Ferrante, R.J. & Martin, J.B. 1987 Patterns of loss in Huntington's disease. *Trends Neurosci.* **10**, 24–29.

Kowall, N.W., Ferrante, R.J., Beal, M.F., Richardson, E.P. Jr., Sofroniew, M.V., Cuello, A.C. & Martin, J.B. 1991 Neuropeptide Y, somatostatin and reduced nicotinamide adenine dinucleotide phosphate diaphorase in the human striatum: a combined immunocytochemical and enzyme histochemical study. *Neuroscience* **20**, 817–828.

Lehmann, J., Nagy, J.I., Atmadja, S. & Fibiger, H.C. 1980 The nucleus basalis magnocellularis: the origin of a cholinergic projection to the neocortex of the rat, *Neuroscience* **5**, 1161–1174.

Lolley, R.N., Farber, D.B., Rayborn, M.E. & Hollyfield, J.G. 1977 Cyclic GMP accumulation causes degeneration of photoreceptor cells: simulation of an inherited disease. *Science, Wash.* **196**, 664–666.

Lowenstein, C.J., Alley, E.W., Raval, P., Snowman, A.M., Snyder, S.H., Russell, S.W. & Murphy, W.J. 1993 Macrophage nitric oxide synthase gene: two upstream regions mediate induction by interferon γ and lipopolysaccharide. *Proc. natn. Acad. Sci. U.S.A.* **90**, 9730–9734.

Lyons, C.R., Orloff, G.J. & Cunningham, J.M. 1992 Molecular cloning and functional expression of an inducible nitric oxide synthase from a murine macrophage cell line. *J. biol. Chem.* **267**, 6370–6374.

Mancillas, J.R., Siggins, G.R. & Bloom, F.E. 1986 Somatostatin selectively enhances acetylcholine-induced excitations in rat hippocampus and cortex. *Proc. natn. Acad. Sci. U.S.A.* **83**, 7518–7521.

Marletta, M.A., Yoon, P.S., Iyengar, R., Leaf, C.D. & Wishnok, J.S. 1988 Macrophage oxidation of L-arginine to nitrite and nitrate: nitric oxide is an intermediate. *Biochemistry* **27**, 8706–8711.

Marsden, P.A. & Ballermann, B.J. 1990 Tumor necrosis factor α activates soluble guanylate cyclase in bovine glomerular mesangial cells via an L-arginine-dependent mechanism. *J. exp. Med.* **172**, 1843–1852.

Martínez, A., Riveros-Moreno, V., Polak, J.M., Moncada, S. & Sesma, P. 1994 Nitric oxide (NO) synthase-immunoreactivity in the starfish *Marthasterias glacialis*. *Cell Tiss. Res.* **275**, 599–603.

Martínez-Murillo, R. & Rodrigo, J. 1994 Cholinergic neurons in the central nervous system. In *Central nervous system neurotransmitters and neuromodulators: acetylcholine* (ed. T. Stone). CRC Press. (In the press.)

Martínez-Murillo, R., Villalba, R., Montero-Caballero, M.I. & Rodrigo, J. 1989 Cholinergic somata and terminals in the rat substantia nigra: an immunocytochemical study with optical and electron microscopic techniques. *J. comp. Neurol.* **281**, 397–414.

Martínez-Murillo, R., Villalba, R.M. & Rodrigo, J. 1990 Immunocytochemical localization of cholinergic terminals in the region of the rat nucleus basalis magnocellularis: a correlated light and electron microscopic study. *Neuroscience* **36**, 361–376.

Martínez-Rodríguez, R., Martínez-Murillo, R., Toledano, A., García-Segura, L.M. & Rovira, M. 1979 Morphological and cytochemical study of a hypothalamo-chiasmatic perivascular neuronal system. *J. Anat.* **128**, 563–570.

Matsumoto, T., Nakane, M., Pollock, J.S., Kuk, J.E. & Forstermann, U. 1993 A correlation between soluble brain nitric oxide synthase and NADPH-diaphorase activity is only seen after exposure of the tissue to fixative. *Neurosci. Lett.* **155**, 61–64.

McKinney, M., Coyle, J.T. & Hedreen, J.C. 1983 Topographic analysis of the innervation of the rat neocortex and hippocampus by the basal forebrain cholinergic system. *J. comp. Neurol.* **217**, 103–121.

Mellander, T., Staines, W.A., Hokfelt, T., Rokaeus, A., Eckenstein, F., Salvaterra, P.M. & Wainer, B.J. 1985 Galanin-like immunoreactivity in cholinergic neurons of the septum-basal forebrain projecting to the hippocampus in the rat. *Brain Res.* **360**, 130–138.

Mesulam, M.-M., Mufson, E.J., Wainer, B.H. & Levey, A.I. 1983 Central cholinergic pathways in the rat, an overview based on an alternative nomenclature, Ch1–Ch6. *Neuroscience* **10**, 1185–1201.

Mesulam, M.-M., Mufson, E.J., Levey, A.I. & Wainer, B.H. 1984 Atlas of cholinergic neurons in the forebrain and upper brainstem of the macaque based on monoclonal choline acetyltransferase immunohistochemistry and acetylcholinesterase histochemistry. *Neuroscience* **12**, 669–690.

Mesulam, M.M., Geula, C., Bothwell, M.A. & Hersh, L.B. 1989 Human reticular formation: cholinergic neurons of the pedunculopontine and laterodorsal tegmental nuclei and some cytochemical comparisons to forebrain cholinergic neurons. *J. comp. Neurol.* **281**, 611–633.

Miki, N., Kawabe, Y. & Kuriyama, K. 1977 Activation of cerebral guanylate cyclase by nitric oxide. *Biochem. biophys. Res. Commun.* **75**, 851–856.

Mizukawa, K., Vincent, S.R., McGeer, P.L. & McGeer, E.G. 1988 Reduced nicotinamide adenine dinucleotide-phosphate (NADPH)-diaphorase-positive neurons in cat cerebral white matter. *Brain Res.* **461**, 274–281.

Moncada, S. & Higgs, A. 1993 The L-arginine-nitric oxide pathway. *N. Engl. J. Med.* **329**, 2002–2012.

Moncada, S., Palmer, R.M.J. & Higgs, E.A. 1989 Biosynthesis of nitric oxide from L-arginine. A pathway for the regulation of cell function and communication. *Biochem. Pharmacol.* **38**, 1709–1715.

Moncada, S., Palmer, R.M.J. & Higgs, E.A. 1991 Nitric oxide: physiology, pathophysiology and pharmacology. *Pharm. Rev.* **43**, 109–142.

Nakane, M., Schmidt, H.H.H.W., Pollock, J.S., Forstermann, U. & Murad, F. 1993 Cloned human brain nitric oxide synthase is highly expressed in skeletal muscle. *FEBS Lett.* **316**, 175–180.

Novelli, A., Nicoletti, F., Wroblewski, J.T., Alho, H., Costa, E. & Giudotti, A. 1987 Excitatory amino acid receptors coupled with guanylate cyclase in primary cultures of cerebellar granule cells. *J. Neurosci.* **7**, 40–47.

Osborne, N.N., Barnett, N.L. & Herrera, A.J. 1993 NADPH diaphorase localization and nitric oxide synthase activity in the retina and anterior uvea of the rabbit eye. *Brain Res.* **610**, 194–198.

O'Sullivan, A.J. & Burgoyne, R.D. 1990 Cyclic GMP regulates nicotine-induced secretion from cultured bovine adrenal chromaffin cells: effects of 8-bromo-cyclic GMP,

atrial natriuretic peptide, and nitroprusside (nitric oxide). *J. Neurochem.* **54**, 1805–1808.

Parent, A., Poitras, D. & Dube, L. 1984 Comparative anatomy of central monoaminergic system. In *Handbook of chemical neuroanatomy*, vol. 2 (*Classical transmitters in the CNS*) (ed. A. Bjorklund & T. Hokfelt), pp. 409–439. Elsevier.

Pasqualotto, B.A. & Vincent, S.R. 1991 Galanin and NADPH-diaphorase coexistence in cholinergic neurons of the rat basal forebrain. *Brain Res.* **551**, 78–86.

Pauwels, P.J. & Leysen, J.E. 1992 Blockade of nitric oxide formation does not prevent glutamate-induced neurotoxicity in neuronal cultures from rat hippocampus. *Neurosci. Lett.* **143**, 27–30.

Peterson, R.P. 1966 Magnocellular neurosecretory centers in the rat hypothalamus. *J. Comp. Neurol.* **128**, 181–190.

Pow, D.V. 1992 NADPH-diaphorase (nitric oxide synthase) staining in the rat supraoptic nucleus is activity-dependent: possible functional implications. *J. Neuroendocrinol.* **4**, 377–380.

Prast, H. & Philippu, A. 1992 Nitric oxide releases acetylcholine in the basal forebrain. *Eur. J. Pharmacol.* **216**, 139–140.

Richards, J.G., Lorez, H.P. and Tranzer, J.P. 1973 Indolealkylamine nerve terminals in cerebral ventricles: identification by electron microscopy and fluorescence histochemistry. *Brain Res.* **57**, 277–288.

Riveros-Moreno, V., Beddell, C. & Moncada, S. 1993 Nitric oxide synthase. Structural studies using autopeptide antibodies. *Eur. J. Biochem.* **215**, 801–808.

Rodrigo, J., Suburo, A.M., Bentura, M.L., Fernandez, T., Nakade, S., Mikoshiba, K., Martínez-Murillo, R. & Polak, J.M. 1993 Distribution of the inositol 1,4,5-triphosphate receptor, P400, in adult rat brain. *J. comp. Neurol.* **337**, 493–517.

Ross, C.A., Bredt, D. & Snyder, S.H. 1990 Messenger molecules in cerebellum. *Trends Neurosci.* **13**, 216–222.

Sagar, S.M. & Ferreiro, D.M. 1987 NADPH diaphorase activity in the posterior pituitary: relation to neuronal function. *Brain Res.* **400**, 348–352.

Salvemini, D., Masini, E., Anggard, E., Mannaioni, P.F. & Vane, J.R. 1990 Synthesis of a nitric oxide-like factor from L-arginine by rat serosal mast cells: stimulation of guanylate cyclase and inhibition of platelet aggregation. *Biochem. biophys. Res. Commun.* **169**, 596–601.

Sandell, J.H. 1986 NADPH-diaphorase histochemistry in the macaque striate cortex. *J. comp. Neurol.* **251**, 388–397.

Satoh, K. & Fibiger, H.C. 1986 Cholinergic neurons of the laterodorsal tegmental nucleus: efferent and afferent connections. *J. comp. Neurol.* **253**, 277–302.

Schmidt, H.H.H.W. & Murad, F. 1991 Purification and characterization of a human NO synthase. *Biochem. biophys. Res. Commun.* **181**, 1372–1377.

Schmidt, H.H.H.W., Gagne, G.D., Nakane, M., Pollock, J.S., Miller, M.F. & Murad, F. 1992 Mapping of neural nitric oxide synthase in rat suggests frequent co-localization with NADPH-diaphorase but not with soluble guanylyl cyclase, and novel paraneural functions for nitrergic signal transduction. *J. Histochem. Cytochem.* **40**, 1439–1456.

Schuman, E.M. & Madison, D.V. 1991 A requirement for the intracellular messenger nitric oxide in long term potentiation. *Science, Wash.* **254**, 1503–1506.

Semba, K., Reinier, P.B. & Fibiger, H.C. 1990 Single mesopontine neurons project to both the pontine reticular formation and the thalamus in the rat. *Neuroscience* **38**, 643–645.

Senut, M.C., Menetrey, D. & Lamour Y. 1989 Cholinergic and peptidergic projections from the medial septum and the nucleus of the diagonal band of Broca to dorsal hippocampus, cingulate cortex and olfactory bulb: a combined wheat germ agglutinin-apohorseradish peroxidase-gold immunohistochemical study. *Neuroscience* **30**, 385–403.

Shu, S., Ju, G. & Fan, L. 1988 The glucose oxidase-DAB-nickel method in peroxidase histochemistry of the nervous system. *Neurosci. Lett.* **85**, 169–171.

Shute, C.C.D. & Lewis, P.R. 1967 The ascending cholinergic reticular system, neocortical, olfactory and subcortical projections. *Brain* **90**, 497–520.

Silverman, B.L., Bettendorf, M., Kaplan, S.l., Grumbach, M.M. & Miller, W.L. 1989 Regulation of growth hormone (GH) secretion by GH-releasing factor, somatostatin and insulin-like growth factor I in ovine fetal and neonatal pituitary cells in vitro. *Endocrinology* **124**, 84–89.

Snyder, S.H. 1992 Nitric oxide: first in a new class of neurotransmitters. *Science, Wash.* **257**, 494–496.

Sofroniew, M.W., Priestley, J.V., Consolazione, A., Eckenstein, F. & Cuello, A.C. 1985 Cholinergic projections from midbrain and pons to the thalamus in the rat, identified by combined retrograde tracing and choline acetyltransferase immunohistochemistry. *Brain Res.* **329**, 213–223.

Southern, C., Schulster, D. & Green, I.C. 1990 Inhibition of insulin secretion by interleukin-I beta and tumour necrosis factor-alpha via an L-arginine-dependent nitric oxide generating mechanism. *FEBS Lett.* **276**, 42–44.

Southam, E., Morris, R. & Garthwaite, J. 1992 Sources and targets of nitric oxide in rat cerebellum. *Neurosci. Lett.* **137**, 241–244.

Springall, D.R., Riveros-Moreno, V., Buttery, L., Suburo, A., Bishop, A.E., Merrett, M., Moncada, S. & Polak, J.M. 1992 Immunological detection of nitric oxide synthase(s) in human tissues using heterologous antibodies suggesting different isoforms. *Histochemistry* **98**, 259–266.

Struble, R.G., Lehmann, J., Mitchell, S.J., McKinney, M., Price, D.L., Coyle, J.T. & DeLong, M.R. 1986 Basal forebrain neurons provide major cholinergic innervation of primate neocortex. *Neuroscience Lett.* **66**, 215–220.

Stuehr, D.J., Kwon, N.S. & Nathan, C.F. 1990 FAD and GSH participate in macrophage synthesis of nitric oxide. *Biochem. biophys. Res. Commun.* **168**, 558–565.

Sugimoto, T. & Hattori, T. 1984 Organization and afferent projections of nucleus tegmenti pedunculopontinus pars compacta with special reference to its cholinergic aspects. *Neuroscience* **11**, 931–946.

Tannenbaum, G.S., Guyda, H.J. & Posner, B.I. 1983 Insulin-like growth factor: a role in growth hormone negative feedback and body weight regulation via brain. *Science, Wash.* **220**, 77–79.

Terenghi, G., Riveros-Moreno, V., Hudson, L.D., Ibrahim, N.B.N. & Polak, J.M. 1993 Immunohistochemistry of nitric oxide synthase demonstrates immunoreactive neurons in spinal cord and dorsal root ganglia of man and rat. *J. Neurol. Sci.* **118**, 34–37.

Uemura, Y., Kowall, N.W. & Beal, M.F. 1990 Selective sparing of NADPH-diaphorase-somatostatin-neuropeptide Y neurons in ischemic gerbil striatum. *Ann. Neurol.* **27**, 620–625.

Valtschanoff, J.I.G., Weinberg, R.J., Kharazia, V.N., Schmidt, H.H.H.W., Nakane, M. & Rustioni, A. 1993*a* Neurons in rat cerebral cortex that synthesize nitric oxide: NADPH-diaphorase histochemistry, NOS immunocytochemistry, and colocalization with GABA. *Neurosci. Lett.* **157**, 157–161.

Valtschanoff, J.I.G., Weinberg, R.J., Kharazia, V.N., Nakane, M. & Schmidt, H.H.H.W. 1993*b* Neurons in

rat hippocampus that synthesize nitric oxide. *J. comp. Neurol.* **33**, 111–121.

Villalba, R.M., Martínez-Murillo, R., Blasco, I., Alvarez, F.J. & Rodrigo, J. 1988 C-Pon containing neurons in the rat striatum are also positive for NADPH-diaphorase activity. A light microscopic study. *Brain Res.* **462**, 359–362.

Villalba, R.M., Rodrigo, J., Alvarez, F.J., Achaval, M. & Martínez-Murillo, R. 1989 Localization of C-Pon immunoreactivity in the rat main olfactory bulb; demonstration that the population of neurons containing endogenous C-Pon display NADPH-diaphorase activity. *Neuroscience* **33**, 373–382.

Vincent, S.R. & Kimura, H. 1992 Histochemical mapping of nitric oxide synthase in the rat brain. *Neuroscience* **46**, 755–784.

Vincent, S.R., Johanson, O., Hokfelt, T., Skirboll, L., Elde, R.P., Terenius, L., Kimmel, J. & Goldstein, M. 1983 NADPH-diaphorase: a selective histochemical marker for striatal neurons containing both somatostatin and avian pancreatic polypeptide (APP)-like immunoreactivities. *J. comp. Neurol.* **217**, 252–263.

Vincent, S.R., Satoh, K., Armstrong, D.M., Panula, P., Vale, W. & Fibiger, H.C. 1986 Neuropeptides and NADPH-diaphorase activity in the ascending cholinergic reticular system of the rat. *Neuroscience* **17**, 167–182.

Wallis, R.A., Panizzon, K. & Wasterlain, C.G. 1992 Inhibition of nitric oxide synthase protects against hypoxic neuronal injury. *Neuroreport* **3**, 645–648.

Weiler, R. & Kewitz, B. 1993 The marker for nitric oxide synthase, NADPH diaphorase, co-localizes with GABA in horizontal cells and cells of the inner retina in the carp retina. *Neurosci. Lett.* **158**, 151–154.

Woolf, N.J. & Butcher, L.L. 1989 Cholinergic systems in the rat brain: IV. Descending projections of the pontomesencephalic tegmentum. *Brain Res. Bull.* **23**, 519–540.

Wright, C.D., Mulsch, A., Busse, R. & Osswald, H. 1989 Generation of nitric oxide by human neutrophils. *Biochem. biophys. Res. Commun.* **160**, 813–819.

Xie, Q.-W., Cho, H.J., Calaycay, J., Mumford, R.A., Swiderek, K.M., Lee, T.D., Ding, A., Troso, T. & Nathan, C. 1992 Cloning and characterization of inducible nitric oxide synthase from mouse macrophages. *Science, Wash.* **256**, 225–228.

Yamashita, S. & Melmed, S. 1986 Insulin-like growth factor I action on rat anterior pituitary cells: suppression of growth hormone secretion and messenger ribonucleic acid levels. *Endocrinology* **120**, 1658–1662.

Yoshikawa, K. & Kuriyama, K. 1980 Characterization of cerebellar guanylate cyclase using N-methyl-N nitro-N-nitrosoguanidine. Presence of two types of guanylate cyclase in soluble and particulate fractions. *Biochim. biophys. Acta* **628**, 377–387.

Yui, Y., Hattori, R., Kosuga, K., Eizawa, H., Hiki, K. & Kawai, C. 1991 Purification of nitric oxide synthase from rat macrophages. *J. biol. Chem.* **266**, 12 544–12 547.

Zwiller, J., Ghandour, M.S., Revel, M.O. & Basset, P. 1981 Immunohistochemical localization of guanylate cyclase in rat cerebellum. *Neurosci. Lett.* **23**, 31–36.

Received 26 January 1994; revised and accepted 15 March 1994

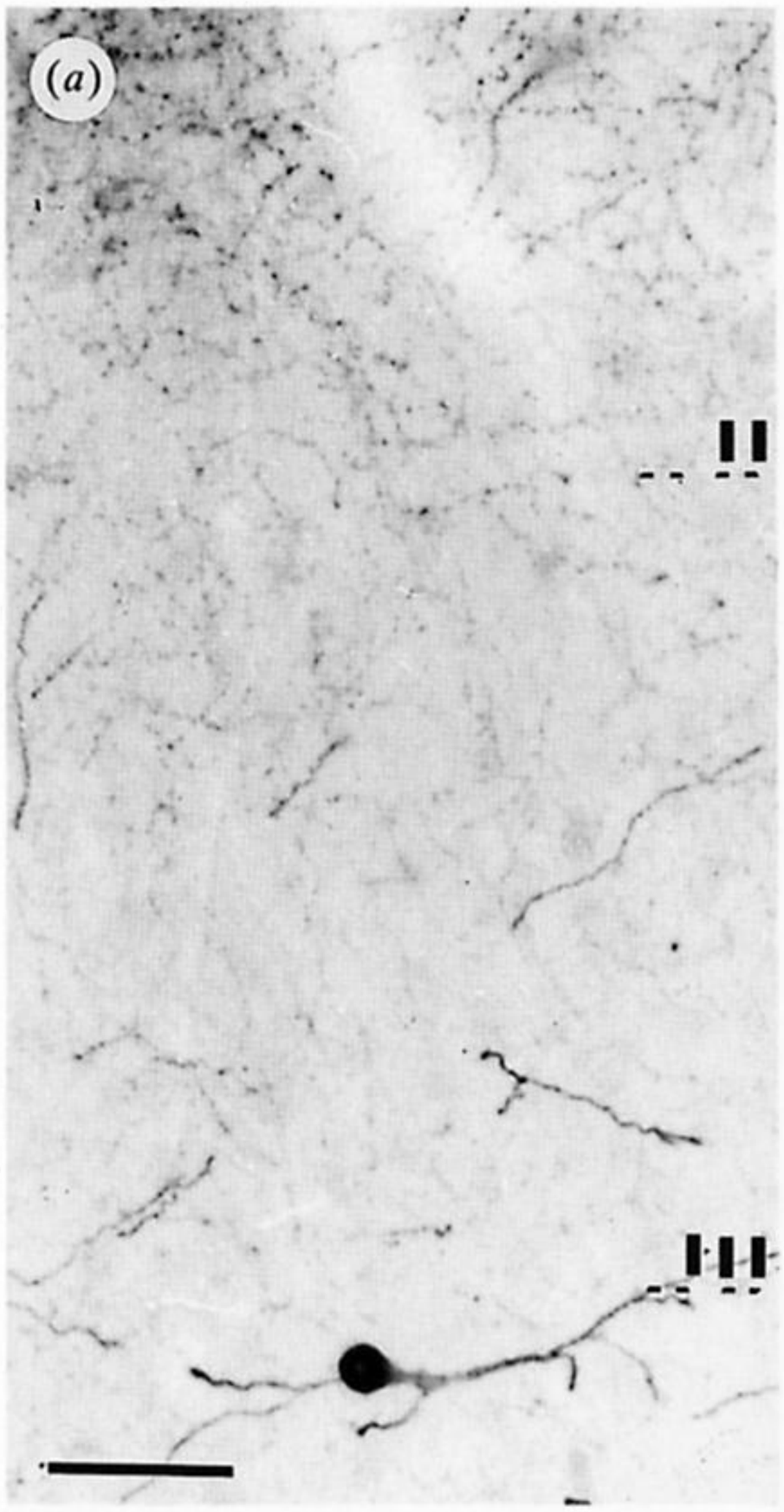

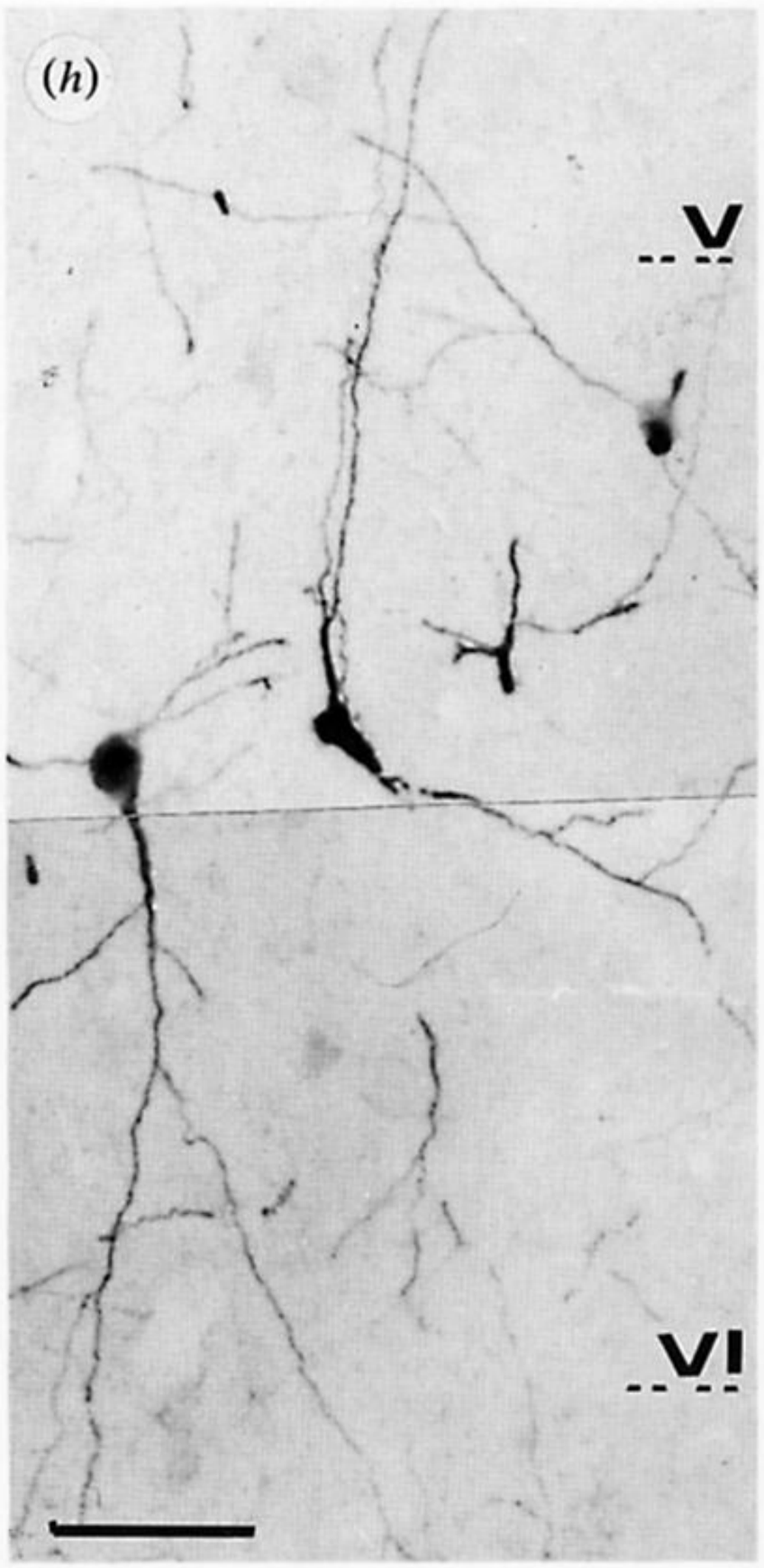

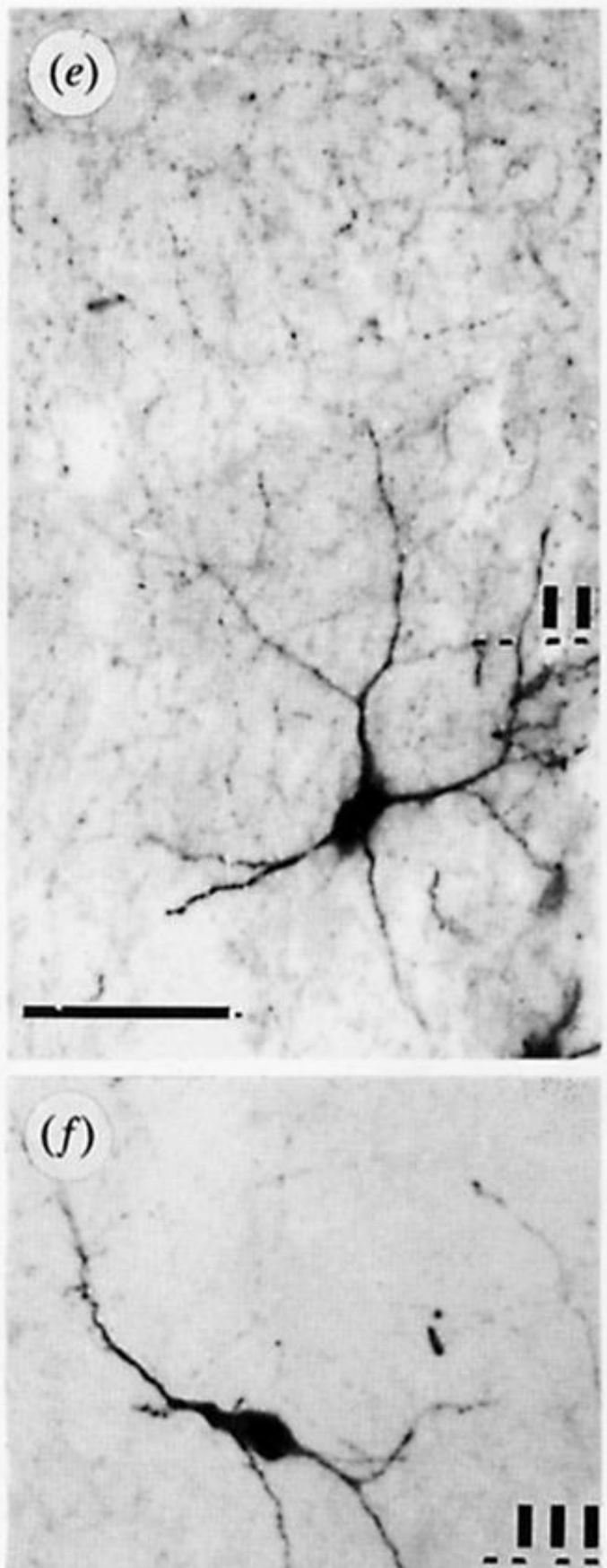

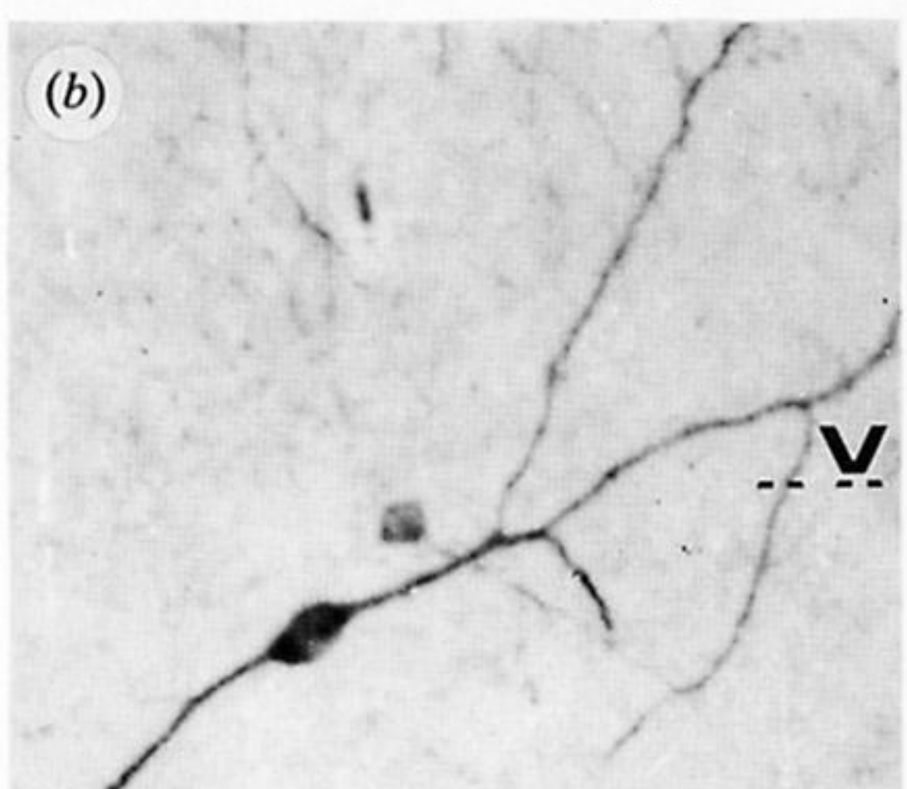

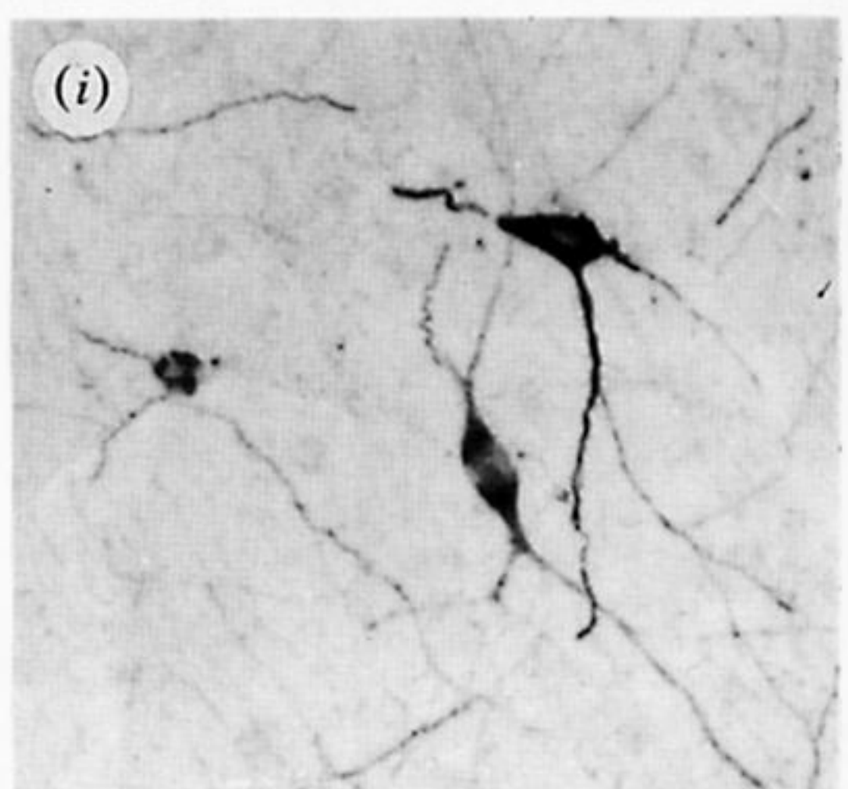

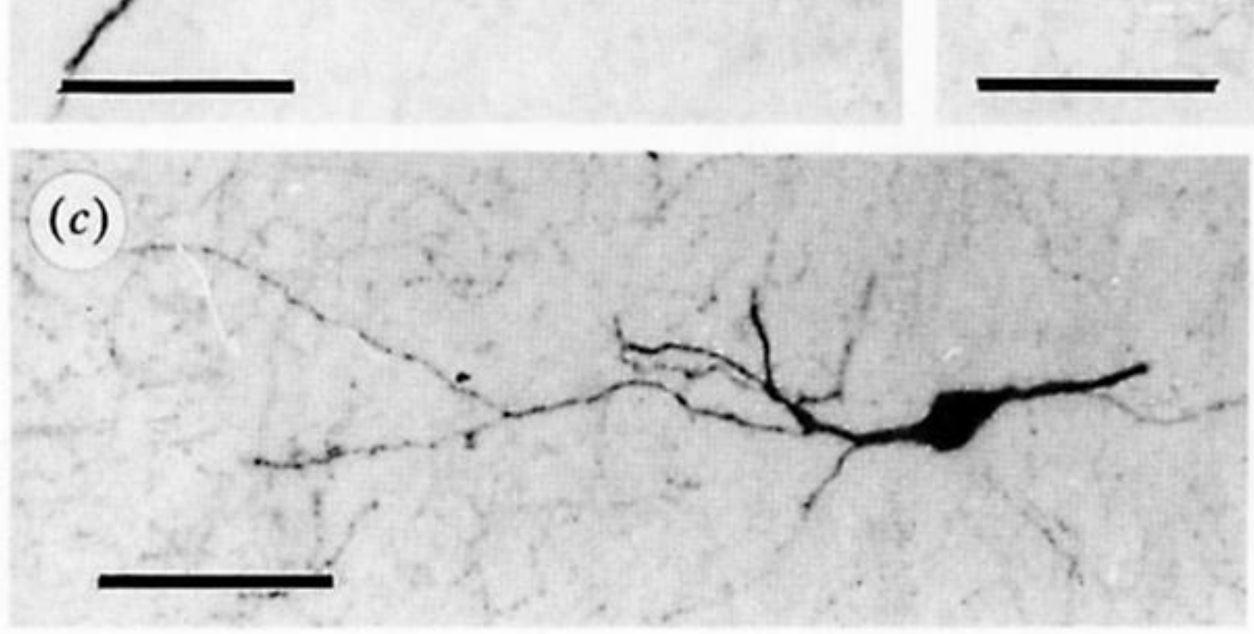

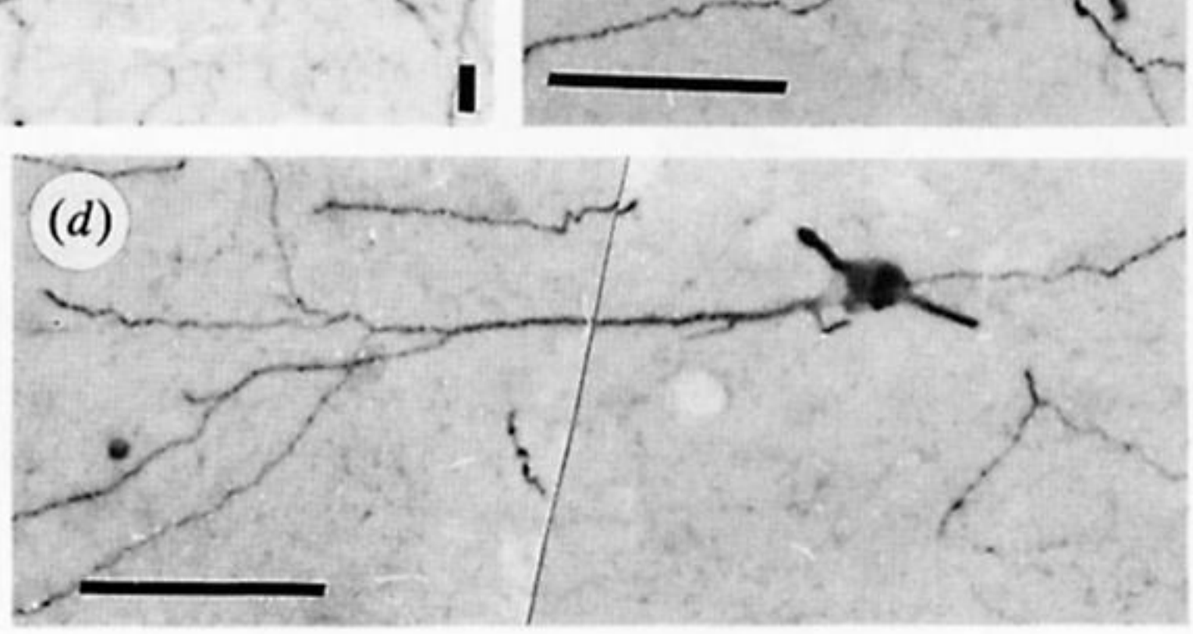

Figure 2. The morphology of immunoreactive neurons in the cingulate and frontal cortices. Aspiny cNOS-IR neurons are distributed in layers III (*a*) and V (*b*) of the cingulate cortex. Immunoreactive neurons situated in the indusium griseum are represented in (*c*) and (*d*). (*e–g*) cNOS-IR neurons in layers II–IV of the frontal cortex. (*h*) Aspects of aspiny neurons located in layers V–VI of the frontal cortex. (*i*) cNOS-IR aspiny multipolar neurons depicted bordering the cingulum. Scale bars = 50 μm.

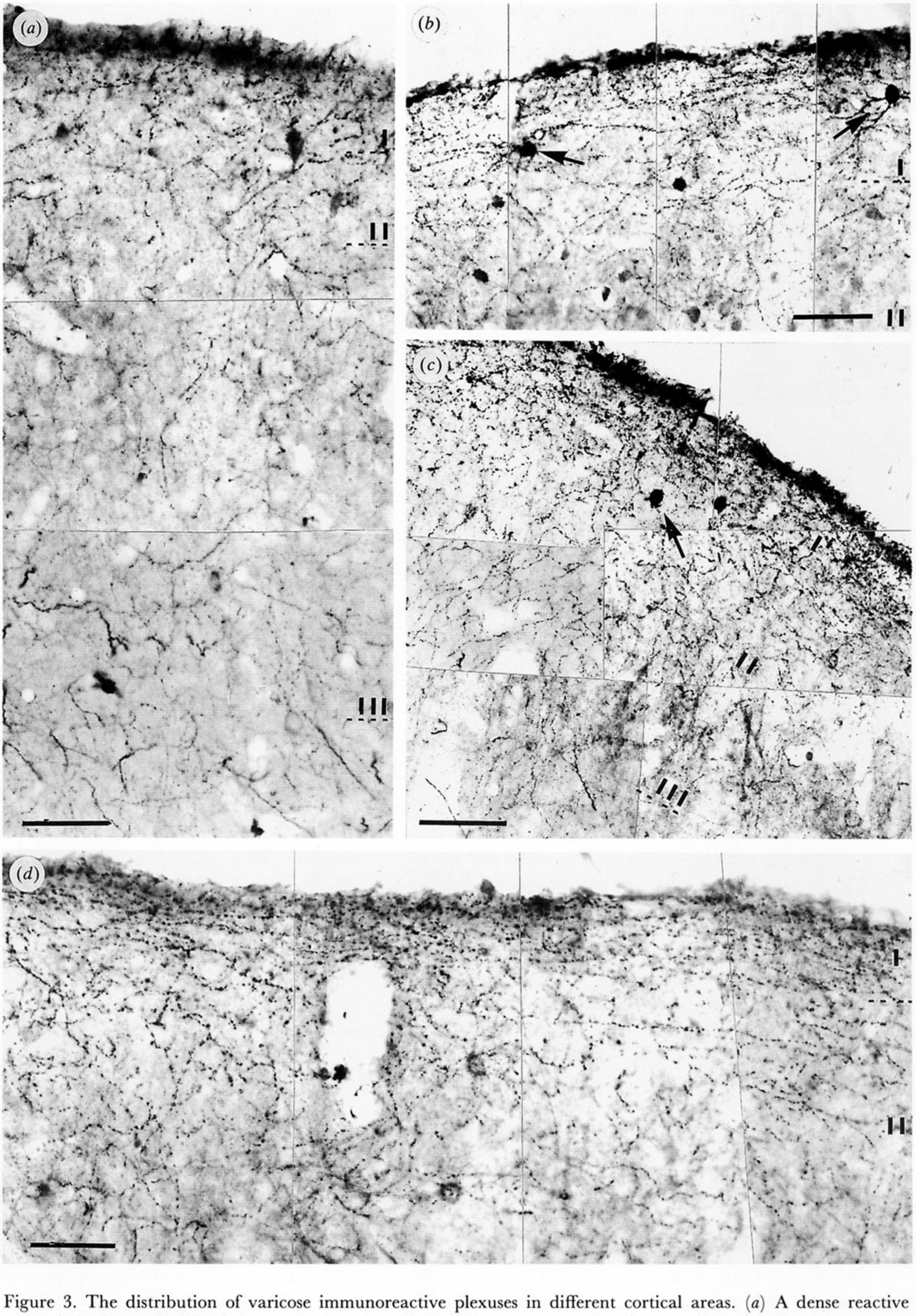

Figure 3. The distribution of varicose immunoreactive plexuses in different cortical areas. (*a*) A dense reactive network in layers I–III of the parietal cortex. Notice the strong density of nerve fibres in layer I, with the number of cNOS-IR fibres decreasing progressively in layers II and III. (*b*) The immunoreactive plexus in layers I and II of the temporal cortex. The long, horizontally orientated immunoreactive nerve fibres in layer I constitute a dense plexus. Notice in (*b*) the presence of a few, weakly immunoreactive neurons among the immunoreactive fibres. (*c*) An immunoreactive plexus made by horizontal nerve fibres in layer I of the dysgranular insular cortex which contains a few small immunoreactive neurons. (*d*) The distribution of immunoreactive nerve fibres in the perirhinal cortex. Notice in (*a*) the presence of some immunoreactive neurons in layer I and a dense plexus in layer II. Scale bars = 50 μm.

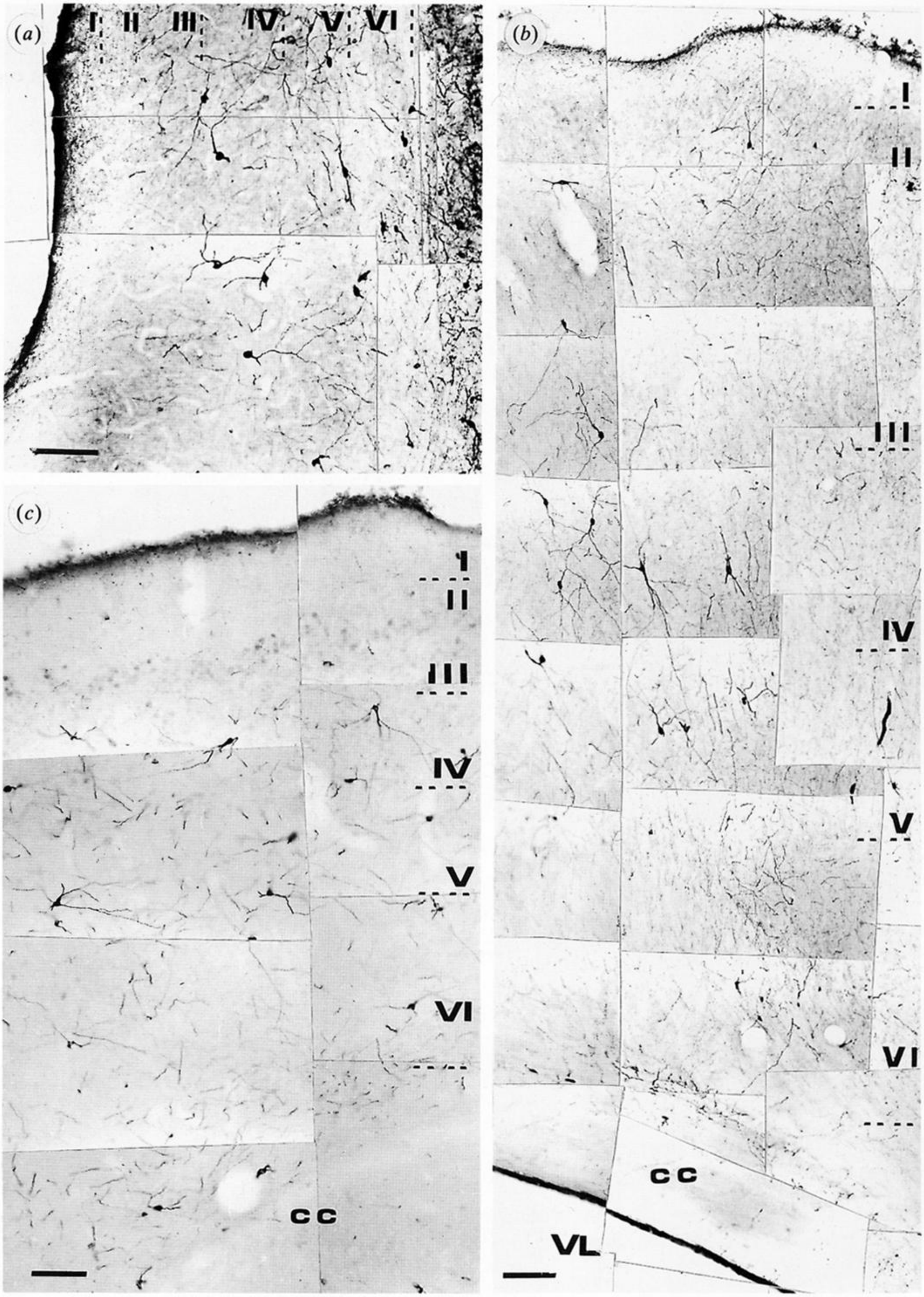

Figure 4. Photomontage showing a general view of the distribution of cNOS-IR in the infralimbic (*a*), frontal (*b*) and parietal (*c*) cortices. Scale bars = 100 μm.

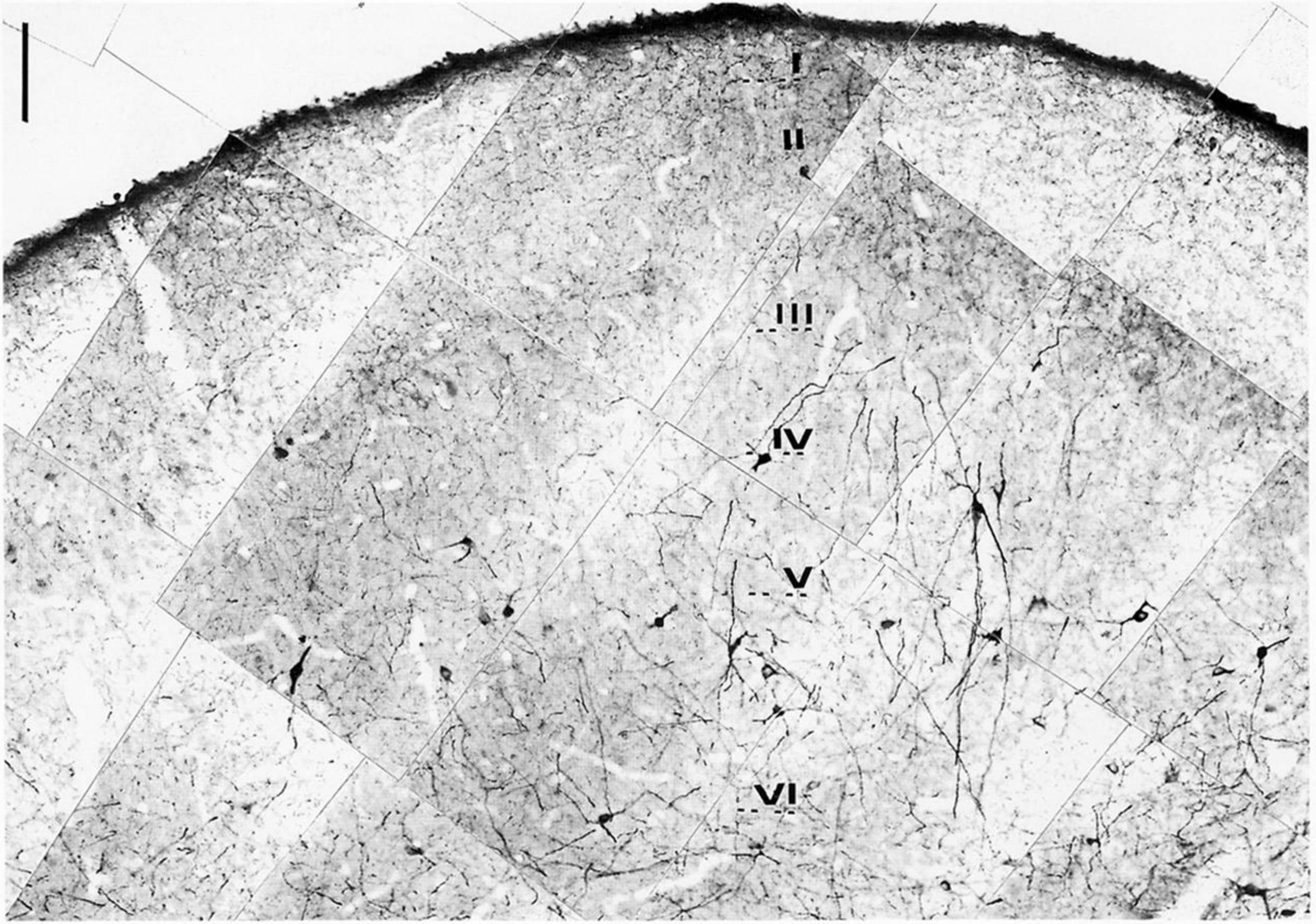

Figure 5. Photomontage illustrating the distribution of cNOS-IR in the entorhinal cortex. Notice that multipolar reactive neurons are located in layers IV and VI. Scale bar = 100 μm.

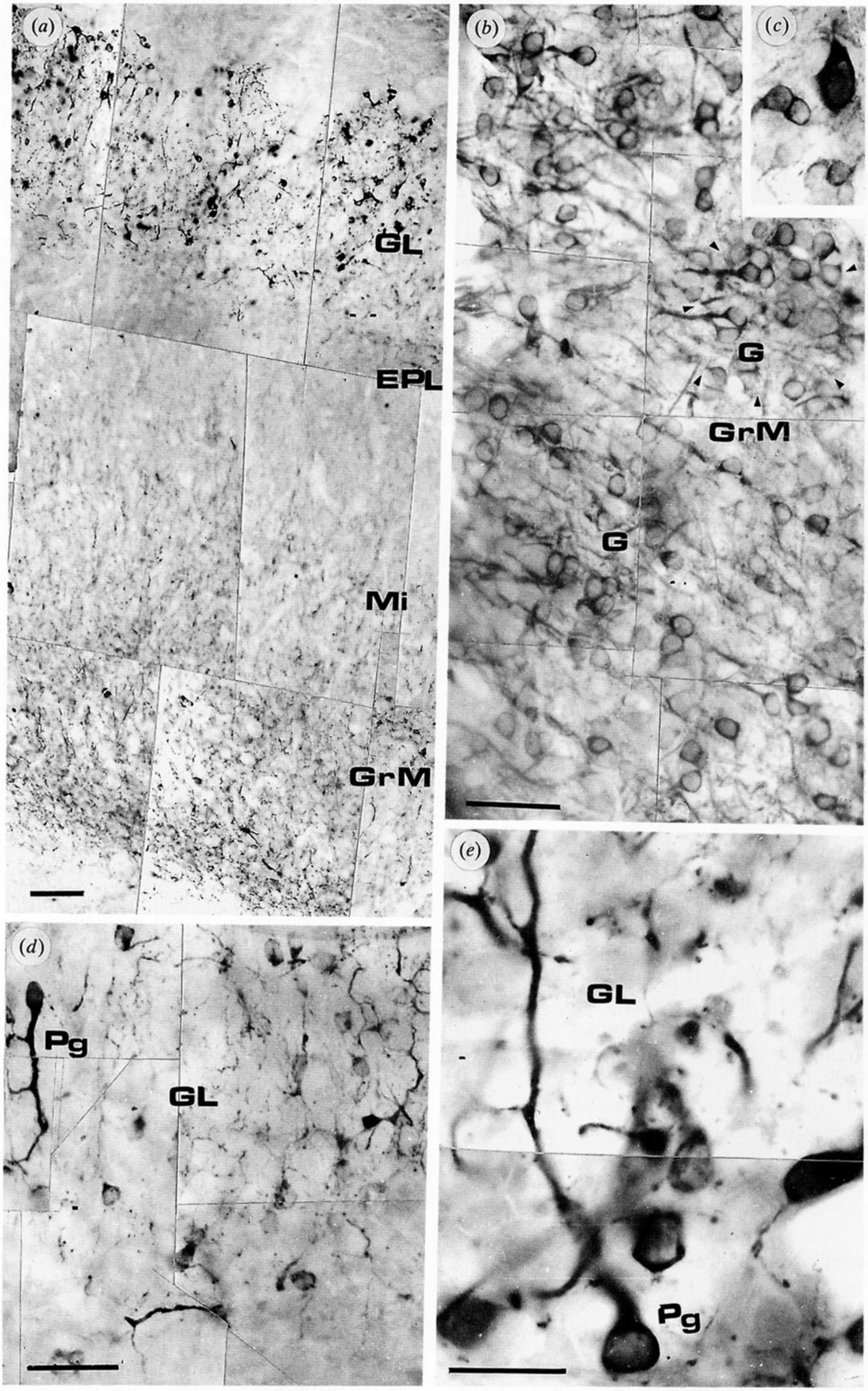

Figure 6. Photographs showing the distribution of cNOS-IR in the main olfactory bulb. (*a*) General view of the immunoreactive structures distributed in different layers of the main olfactory bulb, including the granule cell layer (GrM), mitral layer (Mi), external plexiform layer (EPL) and glomerular cell layer (GL). (*b*) Distribution and morphology of the granule cells (G) that form clusters (arrowheads) in the GrM, illustrated in more detail. (*c*) An immunoreactive neuron of the short-axon cell type. (*d*) Immunoreactive structures in the glomerular cell layer. Notice the periglomerular neurons (Pg) in (*d*). (*e*) A high-power magnification showing details of Pg cNOS-IR neurons. Scale bars: (*a*,*b*,*c*,*d*) = 100 μm; (*e*) = 50 μm.

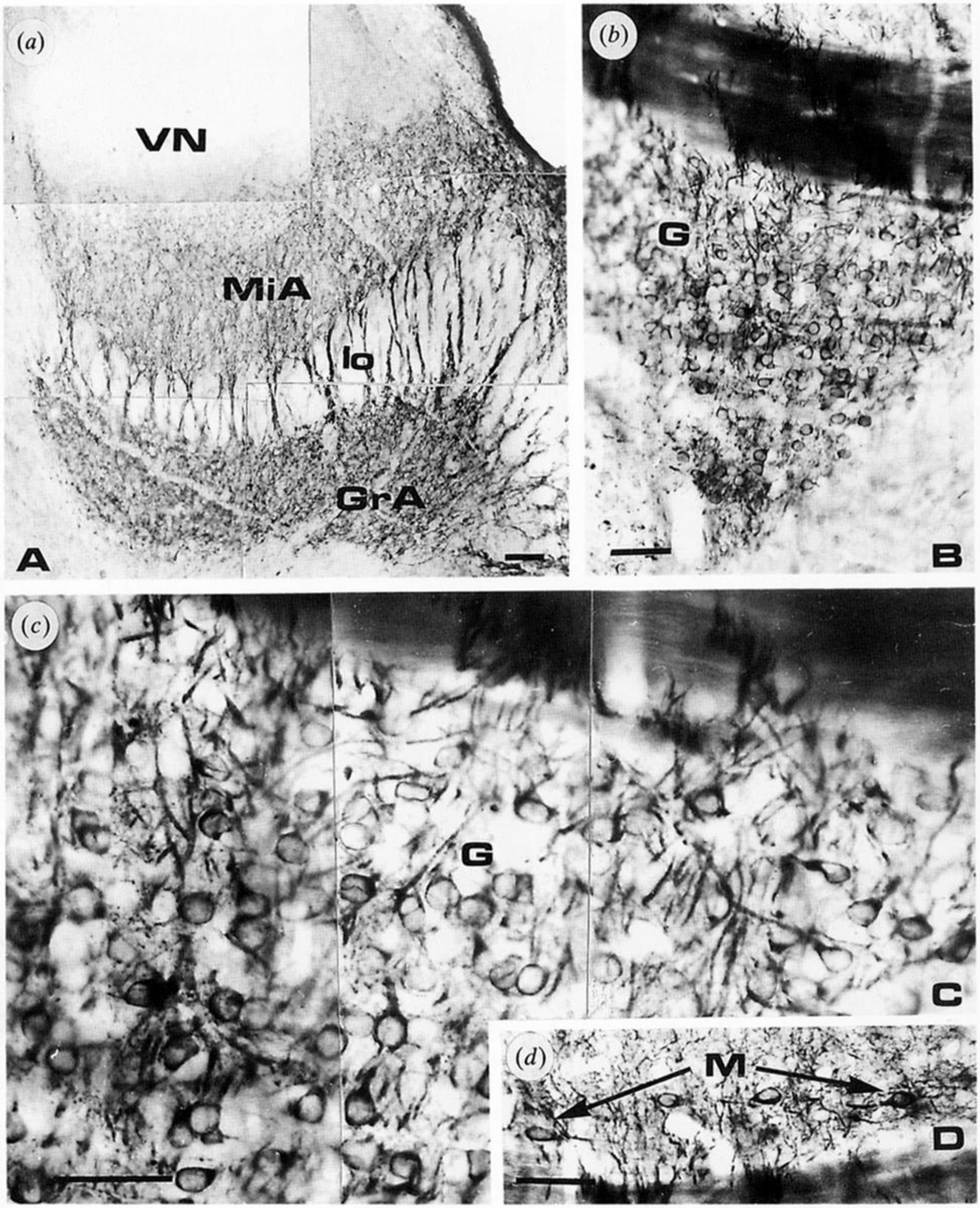

Figure 7. The distribution of cNOS-IR structures in the accessory olfactory bulb. (*a*) General view of the different immunoreactive layers that form the accessory olfactory bulb, including the granule cell layer (GrA), lateral olfactory tract (Io), mitral cell layer (MiA) and vomeronasal nerve layer (VN). (*b*) Details of immunoreactive granule cells (G) that form the granule cell layer. (*c*) A high-power magnification showing aspects of cNOS-IR granule cells. (*d*) Immunoreactive mitral-like cells (M) located in parallel to the olfactory tract. Scale bars = 100 µm.

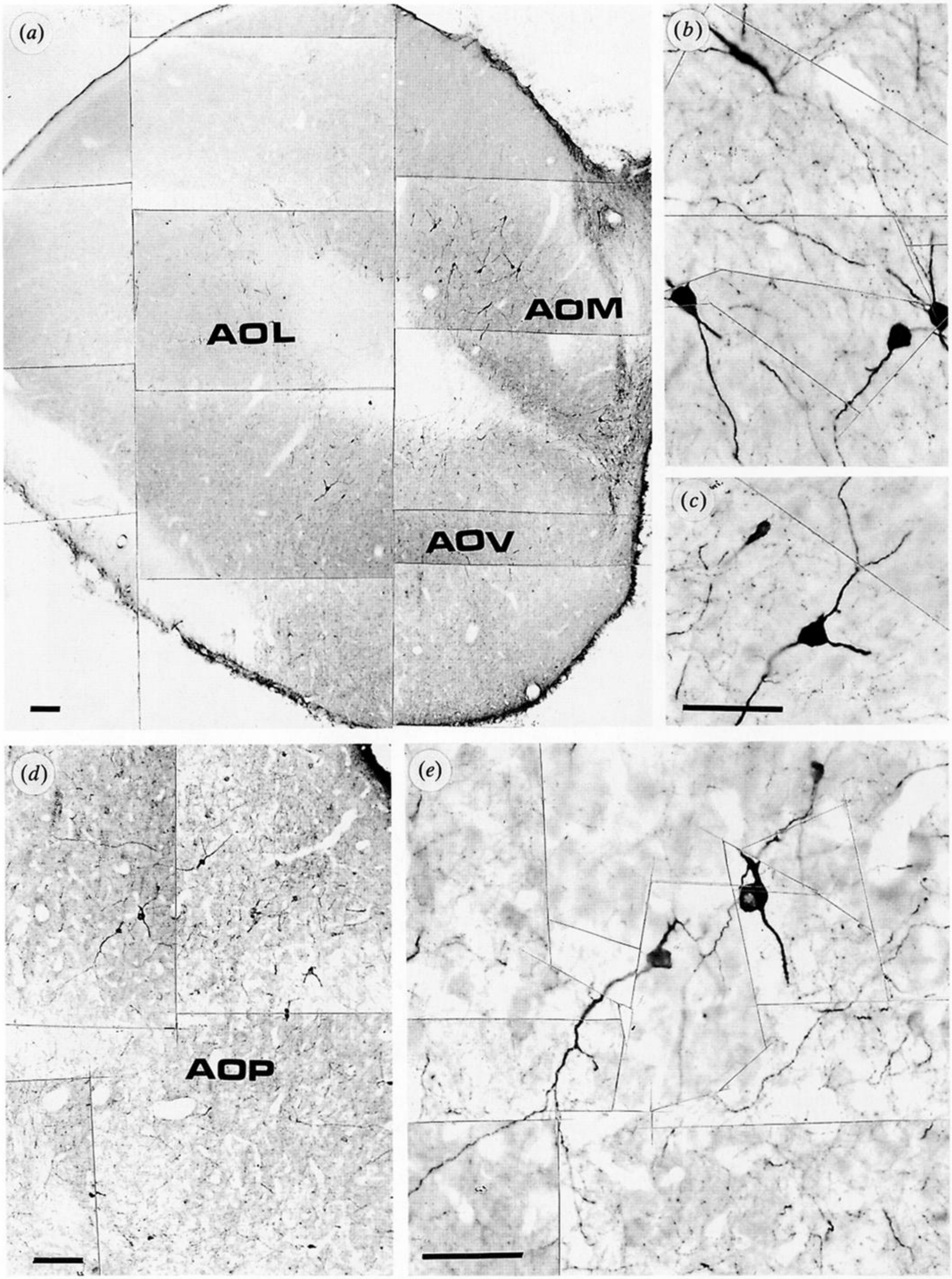

Figure 8. Photographs showing the distribution of cNOS-IR neurons and processes in the anterior olfactory nucleus. (*a*) A low power magnification, showing the medial (AOM), lateral (AOL) and ventral (AOV) groups of the anterior olfactory nucleus. (*b*,*c*) High-power magnifications showing features of immunoreactive neurons of the AOM and AOV, respectively. (*d*) Details of the localization of cNOS-IR in the posterior division of the anterior olfactory nucleus (AOP). (*e*) A high-power magnification of cNOS-IR neurons of the AOP. Scale bars = 100 μm.

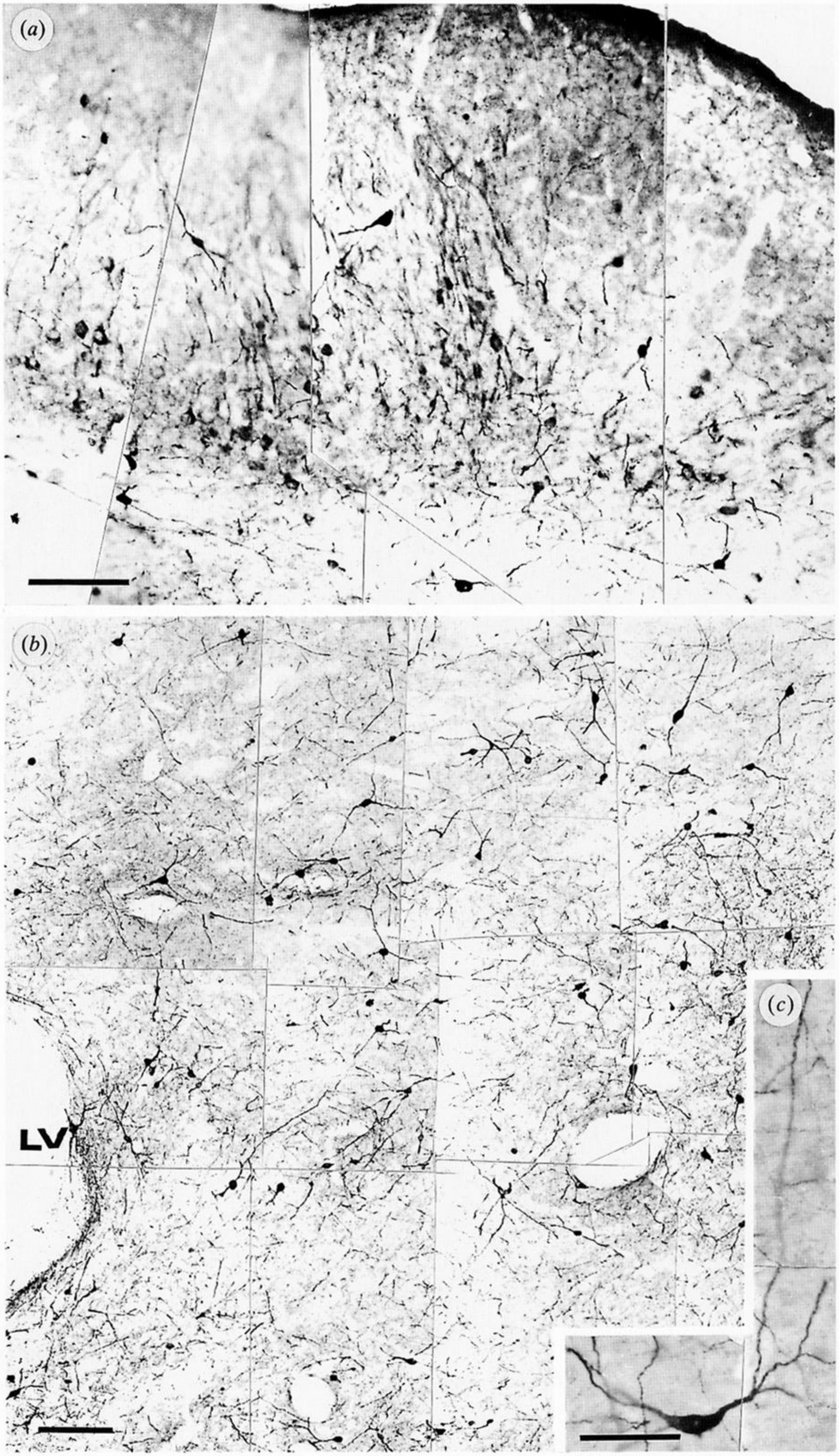

Figure 9. Photomontage of immunoreactive areas of the taenia tecta (*a*) and accumbens nucleus (*b*). (*c*) A high-power magnification of cNOS-IR neurons located in the accumbens nucleus. Notice that reactive neurons possess a few long, aspiny processes with a small number of collaterals. Scale bars: (*a*,*b*) = 100 μm; (*c*) = 50 μm.

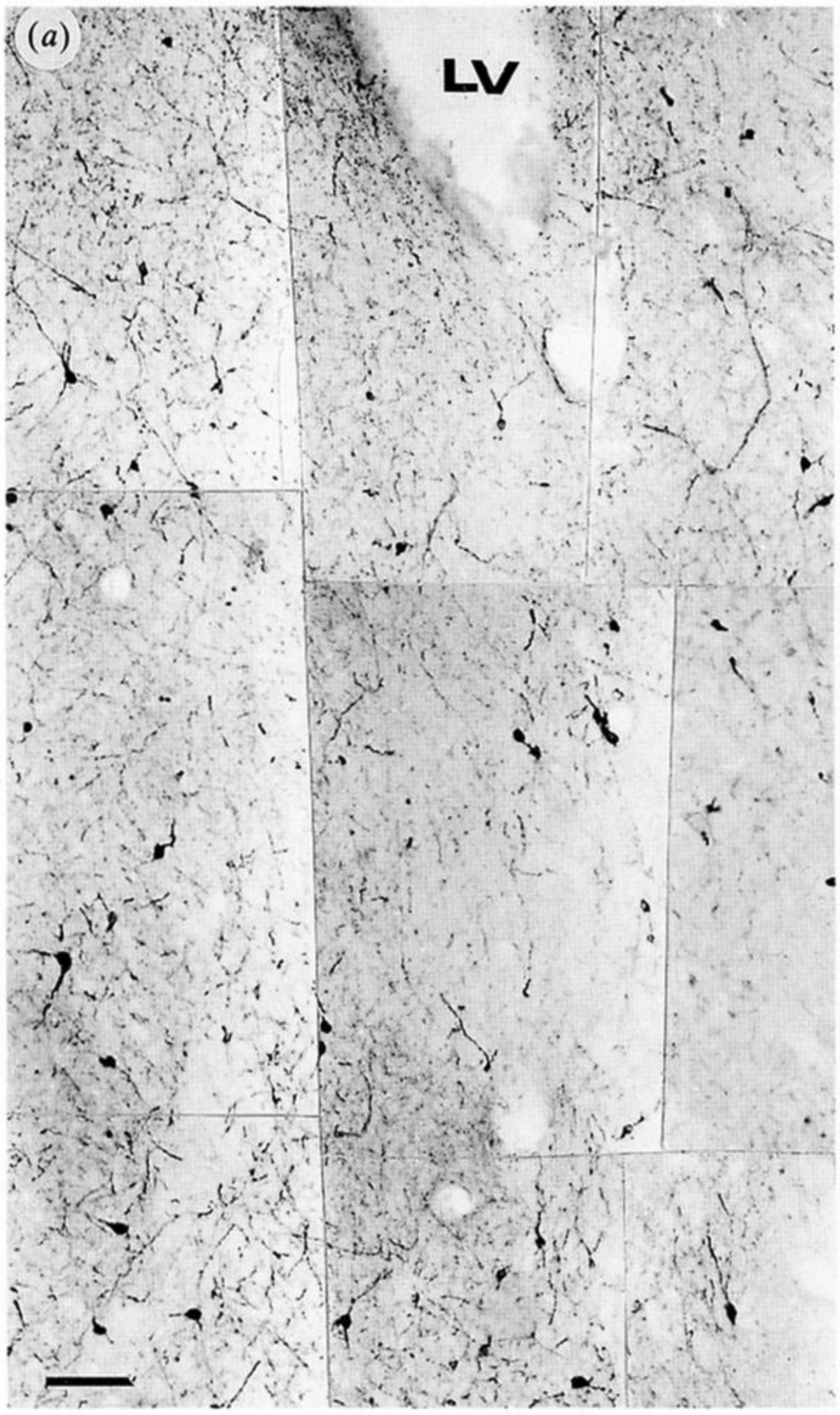

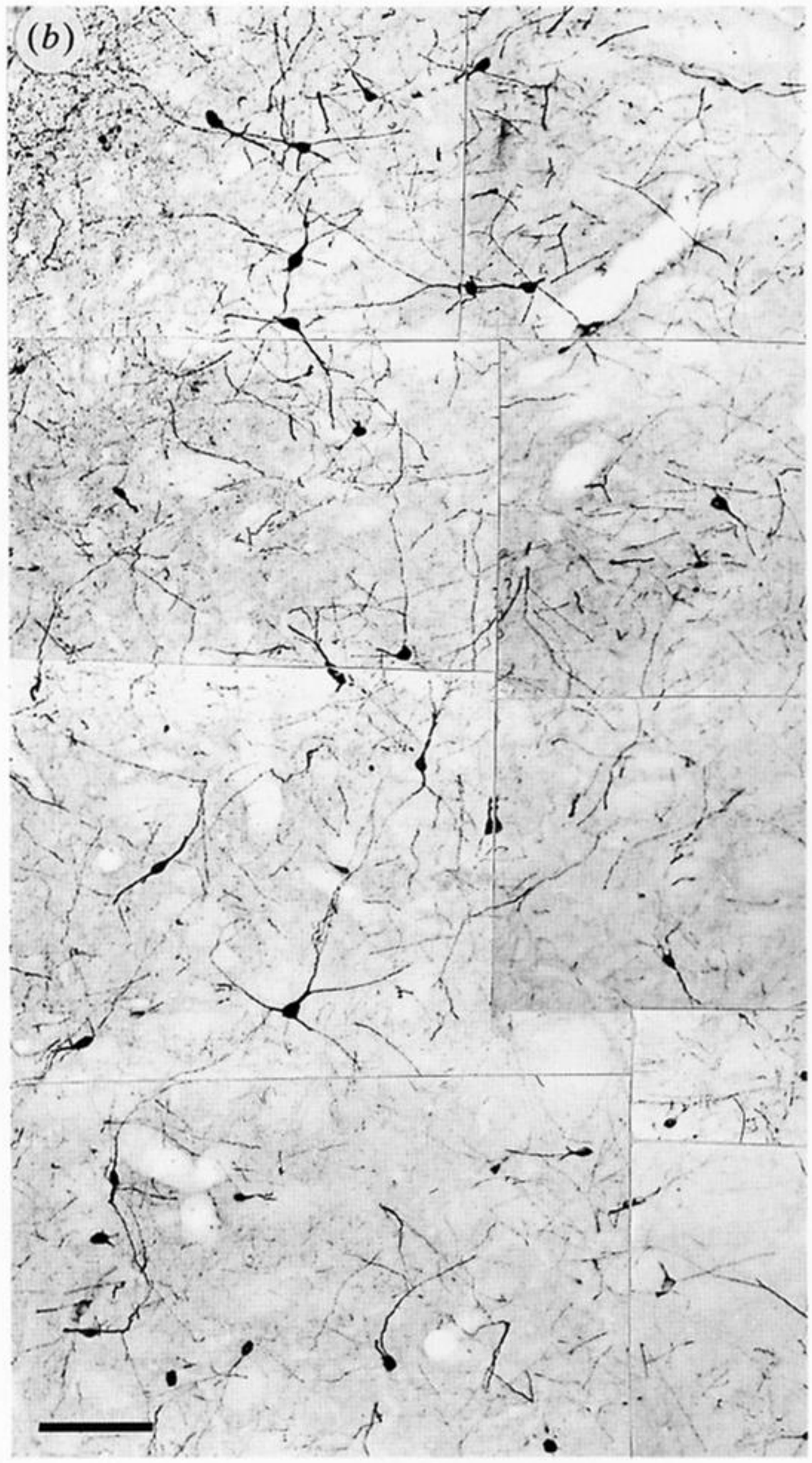

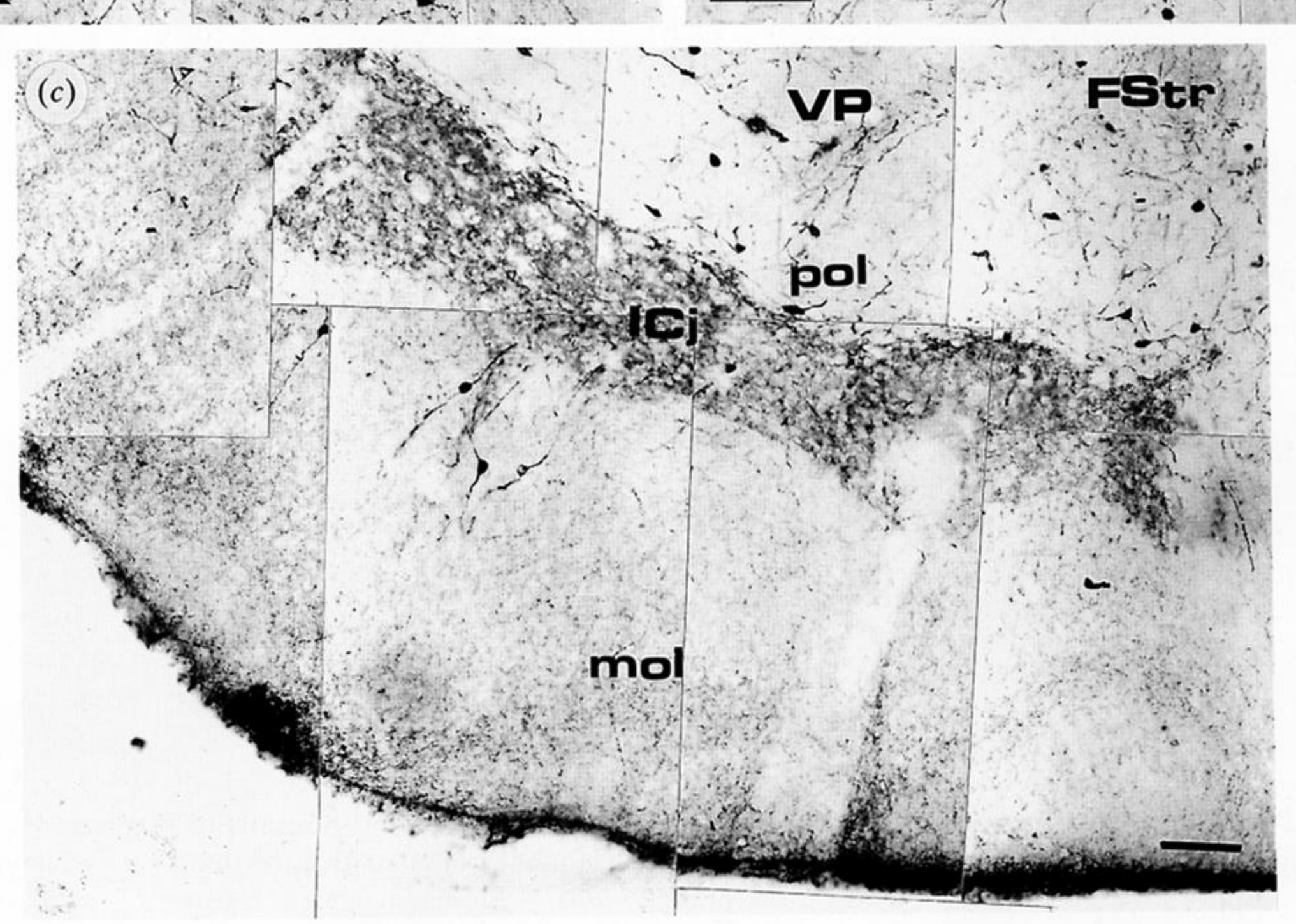

Figure 10. The distribution of cNOS-IR neurons and their long processes in the bed nucleus of the stria terminalis (*a*) and caudate-putamen (*b*). (*c*) Morphology of the island of Calleja located in the deepest portion of the polymorph layer of the olfactory tubercle. Notice that the island of Calleja contains a dense immunoreactive plexus and small immunoreactive neurons. The island of Calleja is surrounded by immunoreactive neurons of the polymorph layer. VP, ventral pallidum. Scale bars = 100 μm.

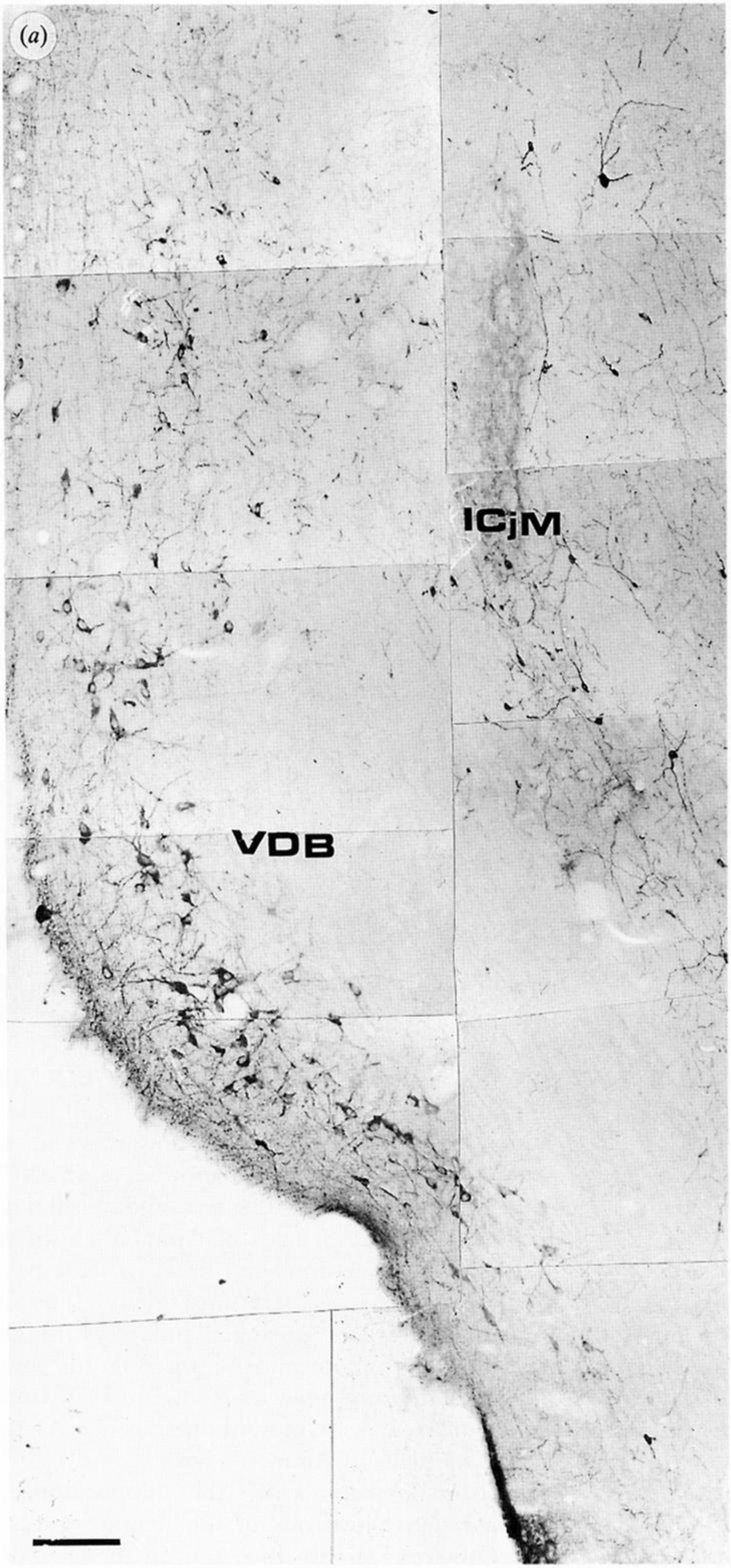

Figure 11. Photomontage showing the distribution of immunoreactivity in the middle line of the septal area. (*a*) Distribution of cNOS-IR neurons in the nucleus of the vertical limb of the diagonal band of Broca (VDB). ICjM is an island of Calleja major which contains many reactive fibres forming a dense immunoreactive plexus containing small immunoreactive neurons. (*b*) Medial septal nucleus (MS) containing cNOS-IR neurons. aca, anterior commissure; SHy, septohypothalamic nucleus; BSTV, ventral division of the nucleus of the stria terminalis; AMPO, anteromedial preoptic nucleus; MnPO, median preoptic nucleus. Scale bars = 100 μm.

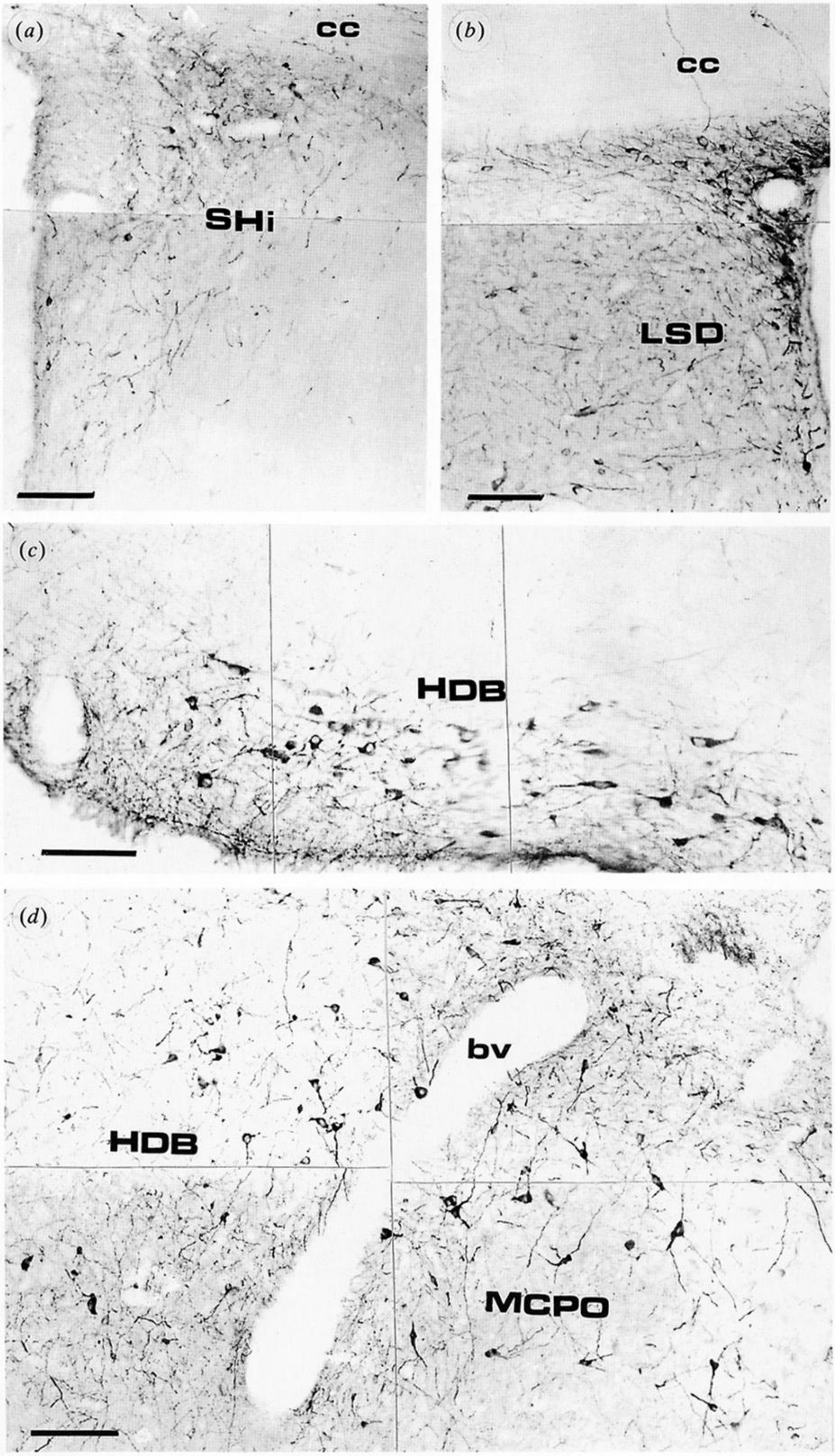

Figure 12. The distribution of cNOS-IR structures in the dorsomedial regions of the septal area and in the nucleus of the horizontal limb of the diagonal band of Broca. (*a*) Few immunoreactive neurons are present in the septohippocampal nucleus (SHi). (*b*) Distribution of immunoreactive neurons in the dorsal region of the lateral septum (LSD). (*c*) Distribution of immunoreactive neurons in the nucleus of the horizontal limb of the diagonal band of Broca (HDB). (*d*) cNOS-IR neurons in the most caudal portion of the nucleus of the HDB. Notice that the pattern of immunoreactivity present in the latter nucleus extends laterally into the magnocellular preoptic nucleus (MCPO). bv, blood vessel. Scale bars = 100 μm.

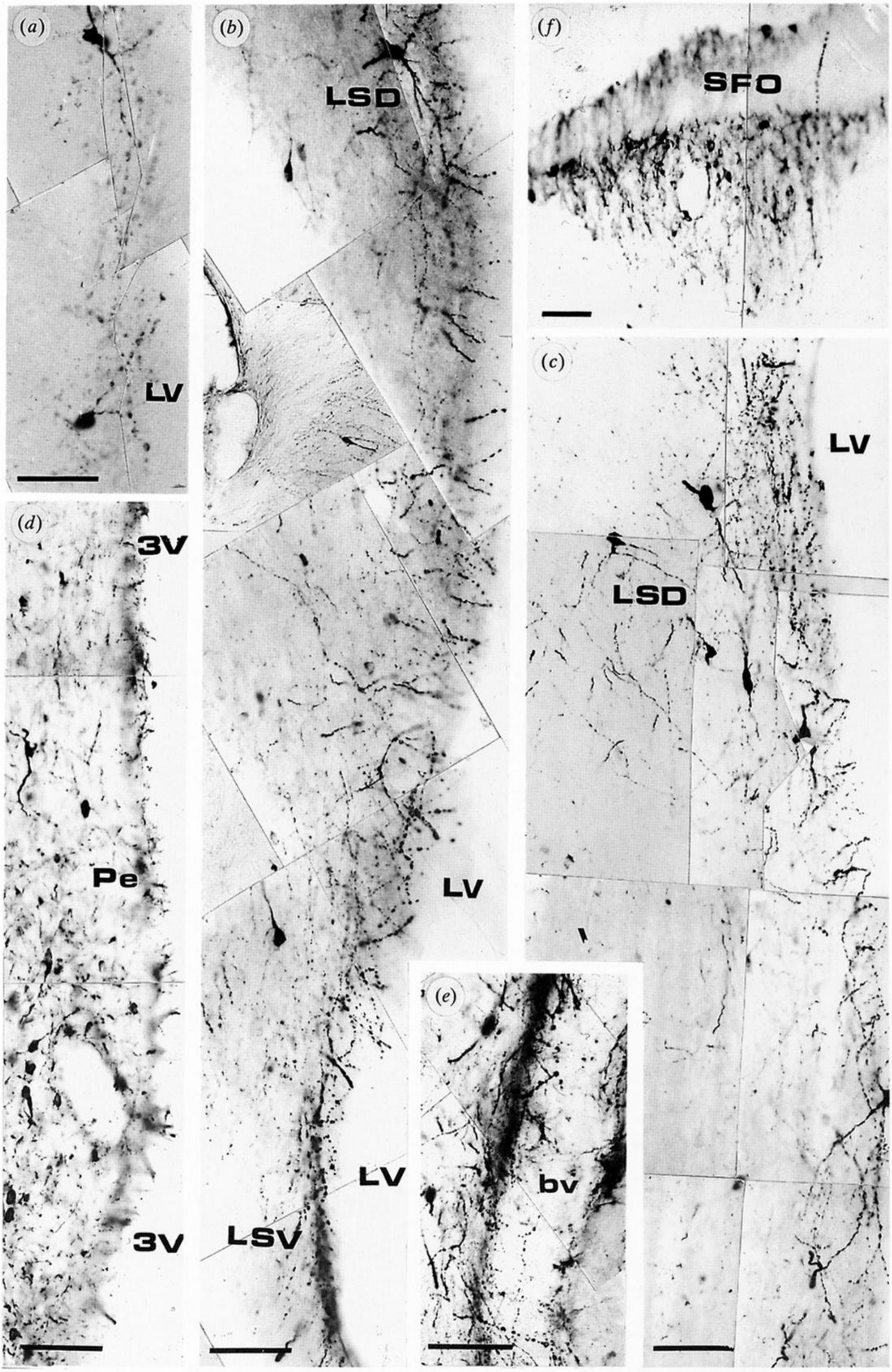

Figure 13. The distribution of cNOS-IR neurons and processes in the wall of the lateral and third ventricles, around blood vessels and in the subfornical organ. (*a–c*) Immunoreactive neurons and fibres penetrating into the wall of the lateral ventricle. Notice in (*a–c*) that some immunoreactive neurons located in the dorsal (LSD) and ventral (LSV) regions of the lateral septum exhibit varicose dendrites that contribute to the formation of a plexus in the subependymal region. (*d*) The dense innervation of the wall of the third ventricle. (*e*) Structure of a perivascular plexus. (*f*) Immunoreactive neurons in the subfornical organ (SFO). bv, blood vessel; LV, lateral ventricle; 3V, third ventricle. Scale bars: (*a–e*) = 50 μm; (*f*) = 100 μm.

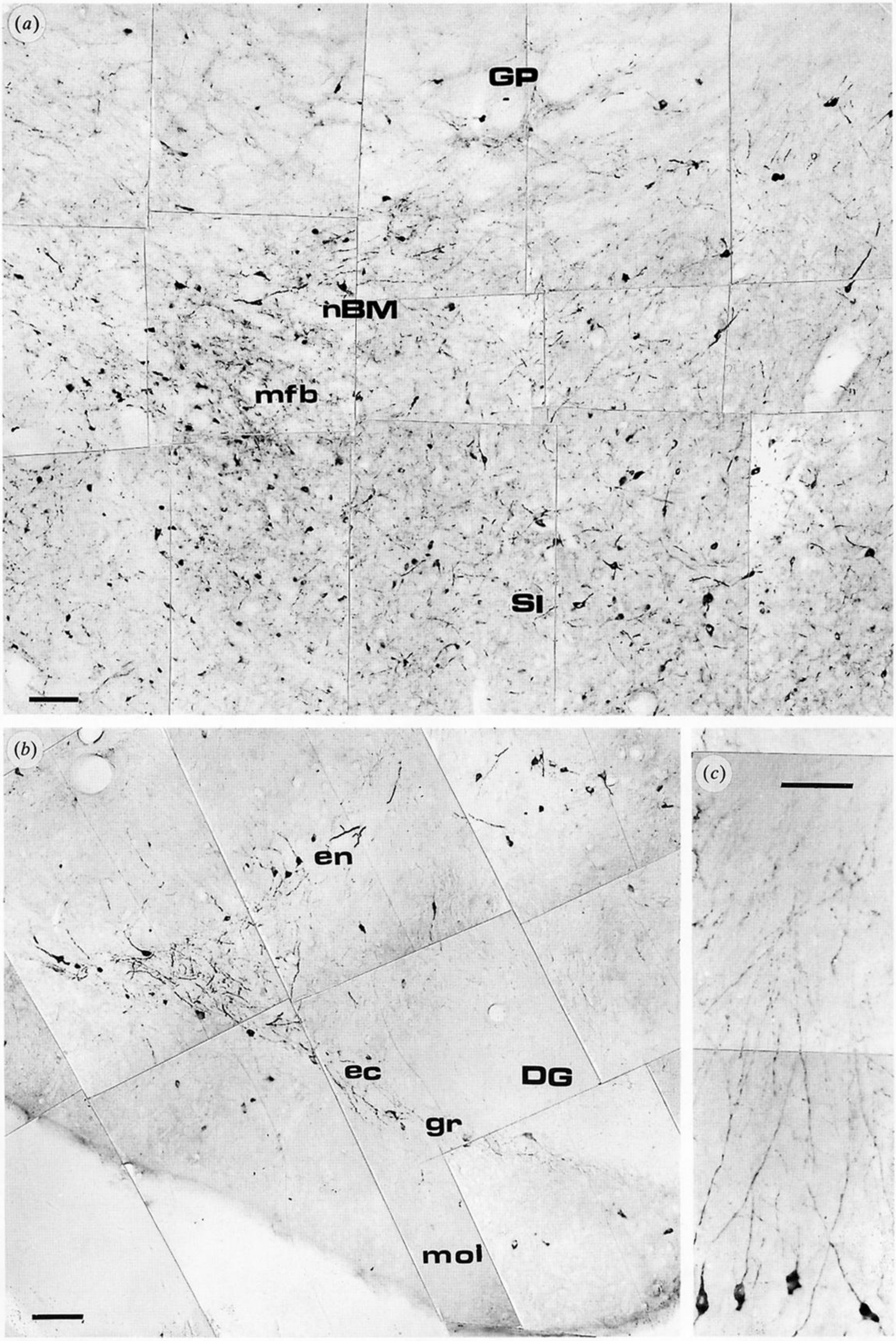

Figure 14. The distribution of cNOS-IR cell bodies and processes in the globus pallidus (GP) and rostral portion of the hippocampus. (*a*) A few immunoreactive neurons are located in the ventral portion of the GP. Notice in (*a*) that these neurons are mainly located in the area of the nucleus basalis magnocellularis (nBM), in the medial forebrain bundle (mbf) and in the substantia innominata (SI). (*b*) Distribution of immunoreactive neurons in the ectal (ec) and endal (en) regions of the dentate gyrus at the level of the granular cell layer. Notice that some small immunoreactive neurons are present in the molecular layer of the dentate gyrus. (*c*) Immunoreactive neurons located in the CA1 field of Ammon's Horn. Notice that the high power magnification used in (*c*) shows the distribution of neurons in the different layers that constitute this field. A large number of these neurons is found in the pyramidal cell layer. These cells have long basal processes distributed in the stratum oriens and their apical processes penetrate the stratum radiatum and lacunosum moleculare. Scale bars: (*a*,*b*) = 100 μm; (*c*) = 50 μm.

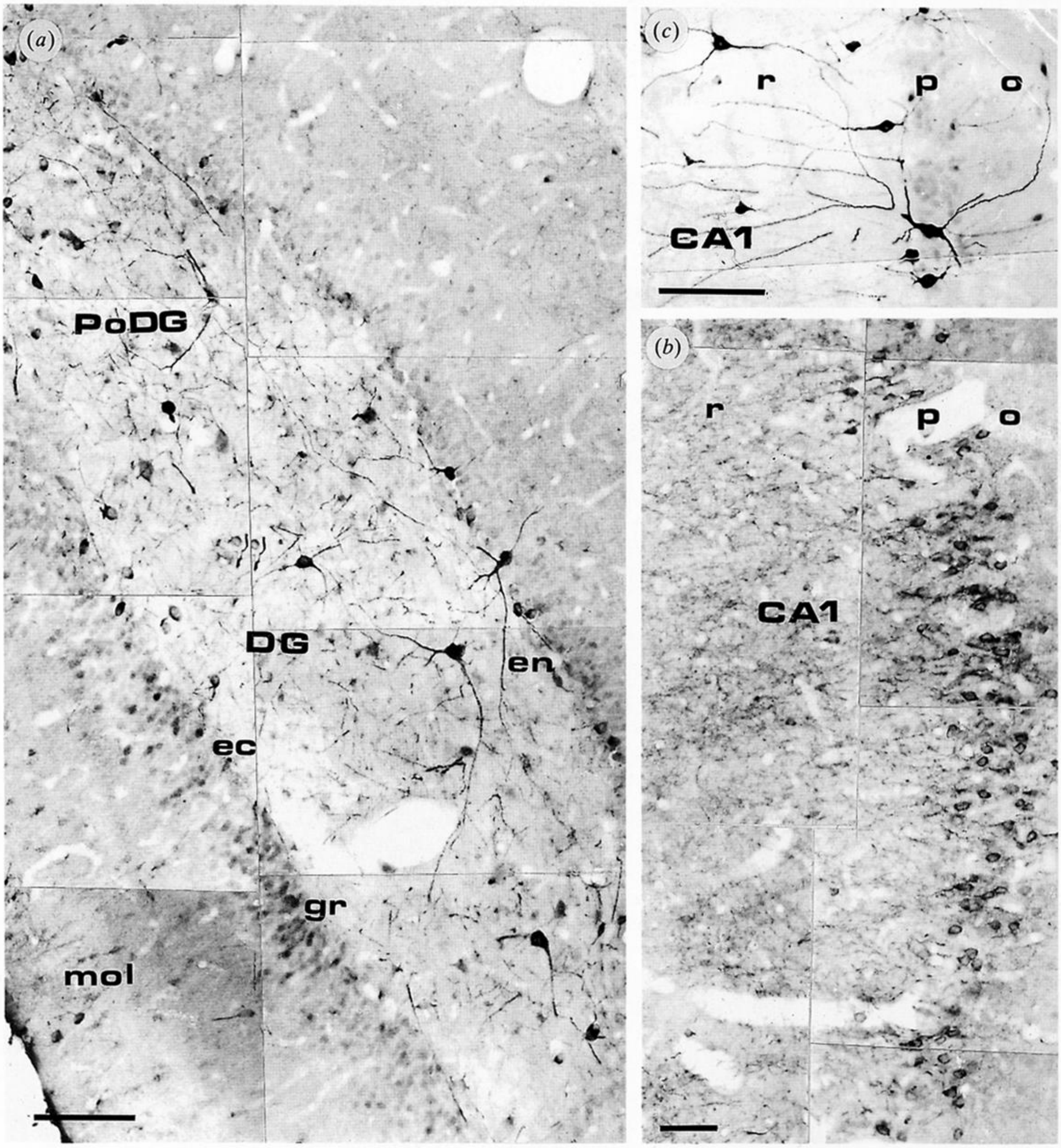

Figure 15. Photomontage of immunoreactive neurons distributed in the caudal hippocampus. (*a*) Immunoreactive neurons in the dentate gyrus. Notice the presence of neurons in the polymorph layer of the dentate gyrus. (*b*) Immunoreactive neurons in CA1 close to the parasubiculum. Notice in (*b*) that a large number of pyramidal cells can be found in the pyramidal cell layer. Details of the morphology of the latter cells can be seen in (*c–e*) taken from CA1–CA3 fields of Ammon's Horn. Scale bars = 100 μm.

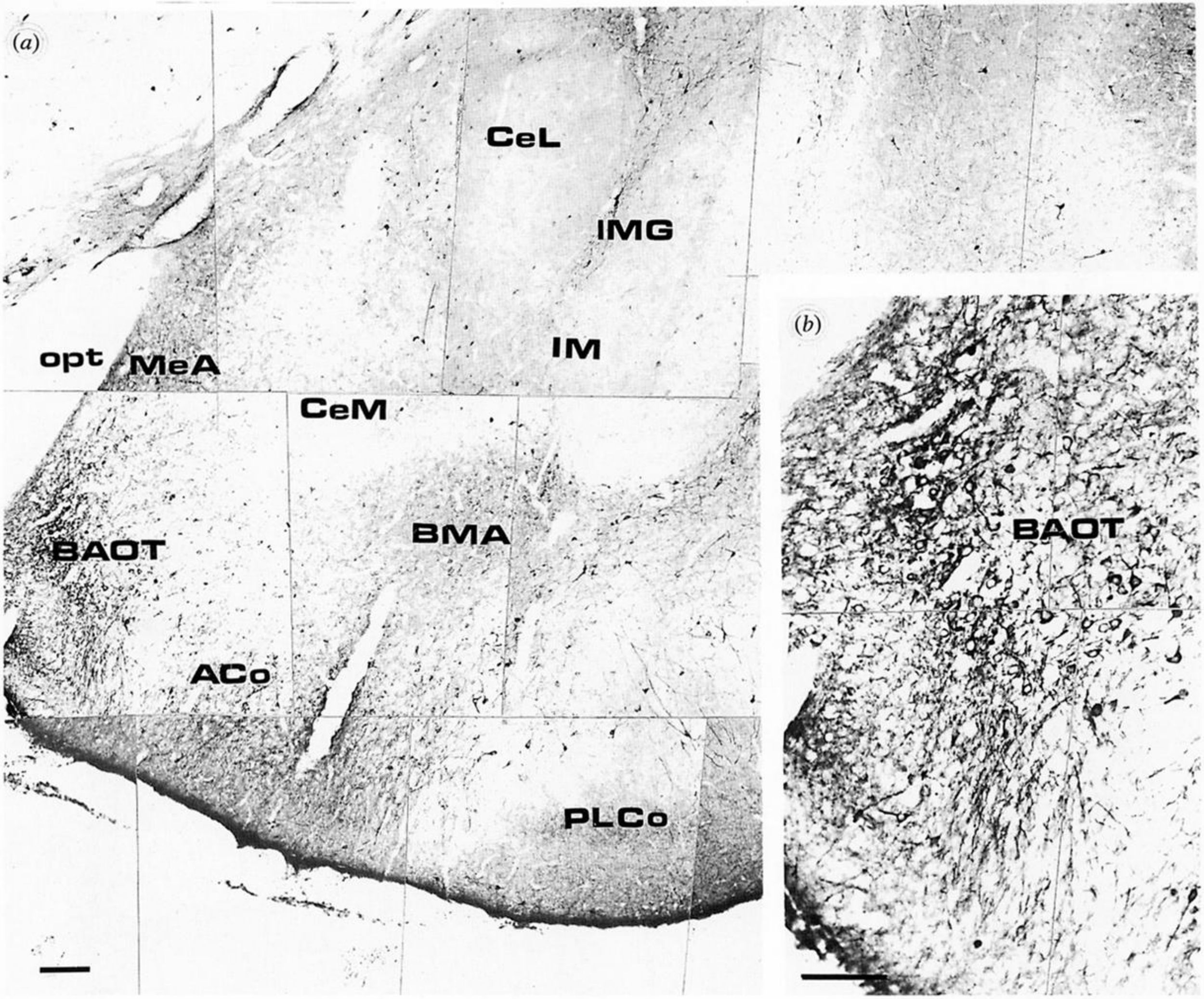

Figure 16. Photographs of cNOS-IR structures in different areas of the amygdala. (*a*) Immunoreactive neurons principally distributed in the medial amygdaloid nucleus as well as in the intercalated (IM) and basomedial amygdaloid (BMA) nuclei. Immunoreactive neurons are also detected in the bed nucleus of the accessory olfactory tract (BAOT), which are continuous with the immunoreactive neurons situated in the anterior cortical amygdaloid nucleus and the posterolateral cortical amygdaloid nucleus (PLCo). (*b*) High-power magnification showing aspects of immunoreactive neurons in the BAOT. Scale bars = 100 μm.

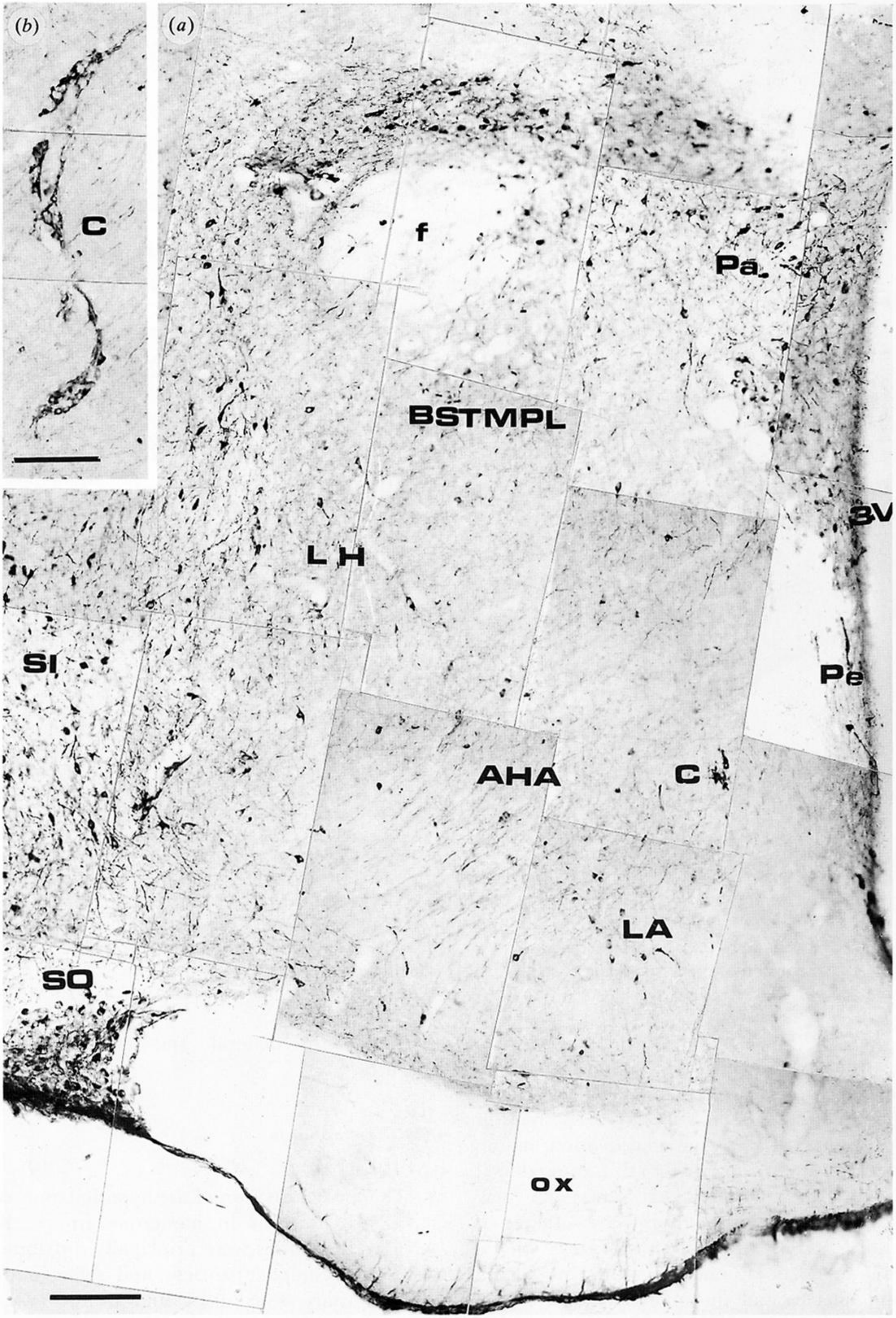

Figure 17. (*a*) Photomontage showing the distribution of immunoreactive neurons and processes in the hypothalamus. Notice that these are more abundant in the paraventricular (Pa) and supraoptic nucleus (SO) nuclei. (*b*) cNOS-IR neurons located around the blood vessels in the circularis nucleus (C). Scale bars: (*a*) = 100 μm; (*b*) = 50 μm.

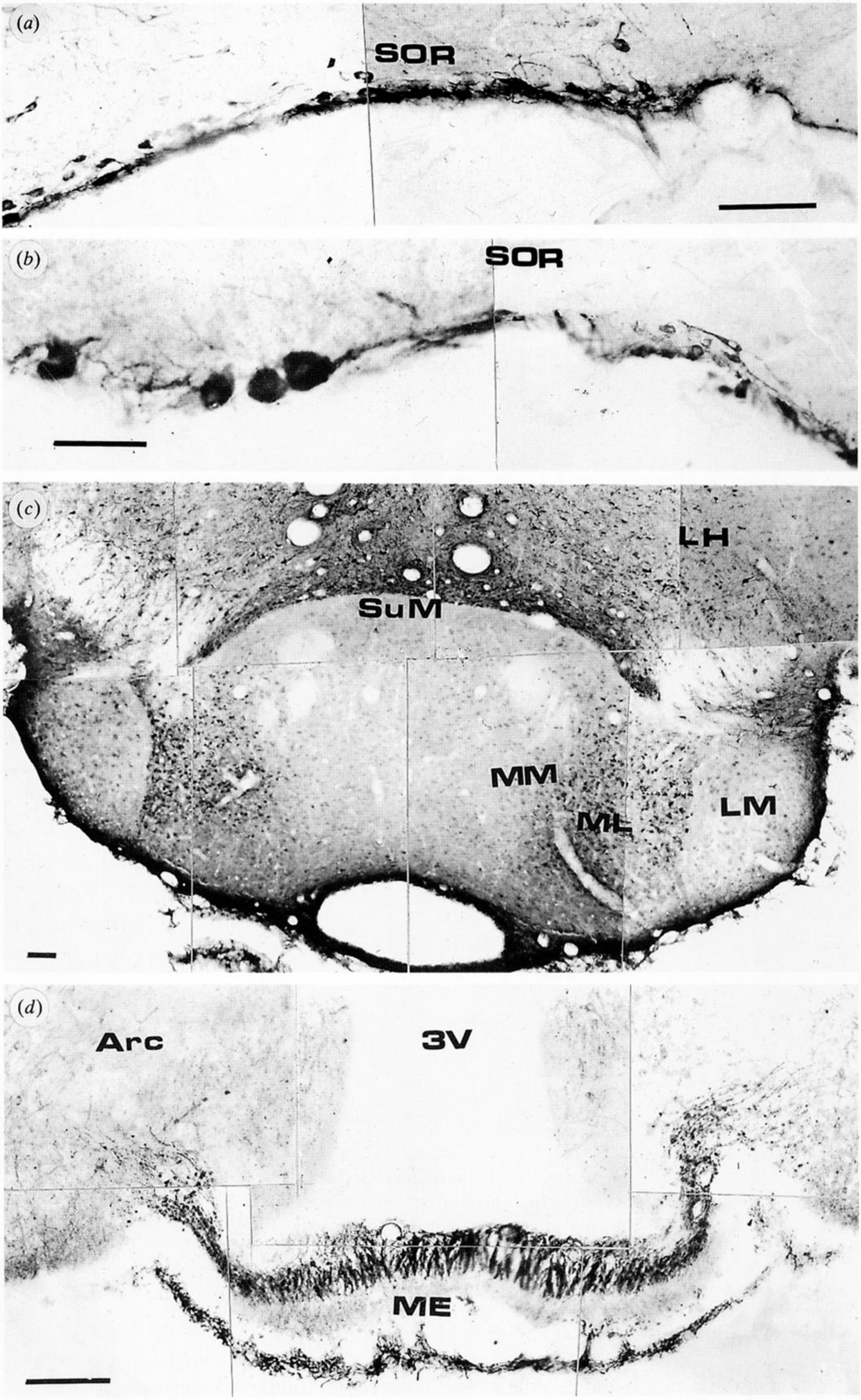

Figure 18. (*a*,*b*) Immunoreactive neurons forming the supraoptic retrochiasmatic nucleus (SOR) in the caudo-ventral part of the hypothalamus. (*c*,*d*) Distribution of cNOS-IR neurons in the mamillary nucleus and median eminence (ME), respectively. LH, lateral hypothalamus; SuM, supramamillary nucleus; MM, medial mamillary nucleus, medial division; ML, medial mamillary nucleus, lateral division: LM, lateral mamillary nucleus; Arc, arcuate hypothalamic nucleus. Scale bars = 100 μm.

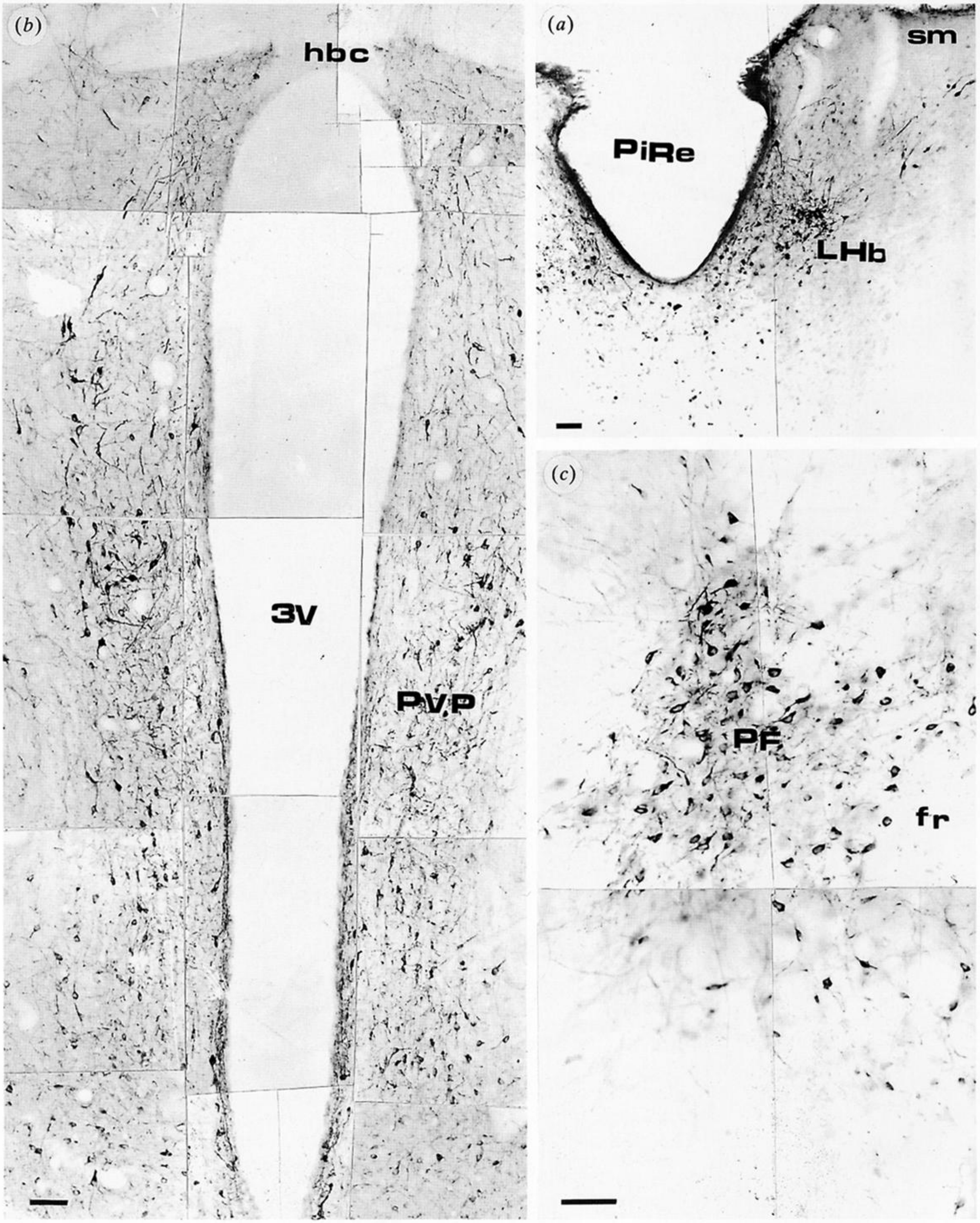

Figure 19. Distribution of cNOS-IR neurons in the mediodorsal thalamic region. (*a*) Immunoreactive neurons located in the lateral habenular nucleus (LHb). (*b*) Positive neurons located along the wall of the third ventricle (3V) forming part of the posterior portion of the paraventricular nucleus (PVP). (*c*) Immunoreactive neurons in the parafascicular nucleus (PF). fr, fasciculus retroflexus. Scale bars = 100 μm.

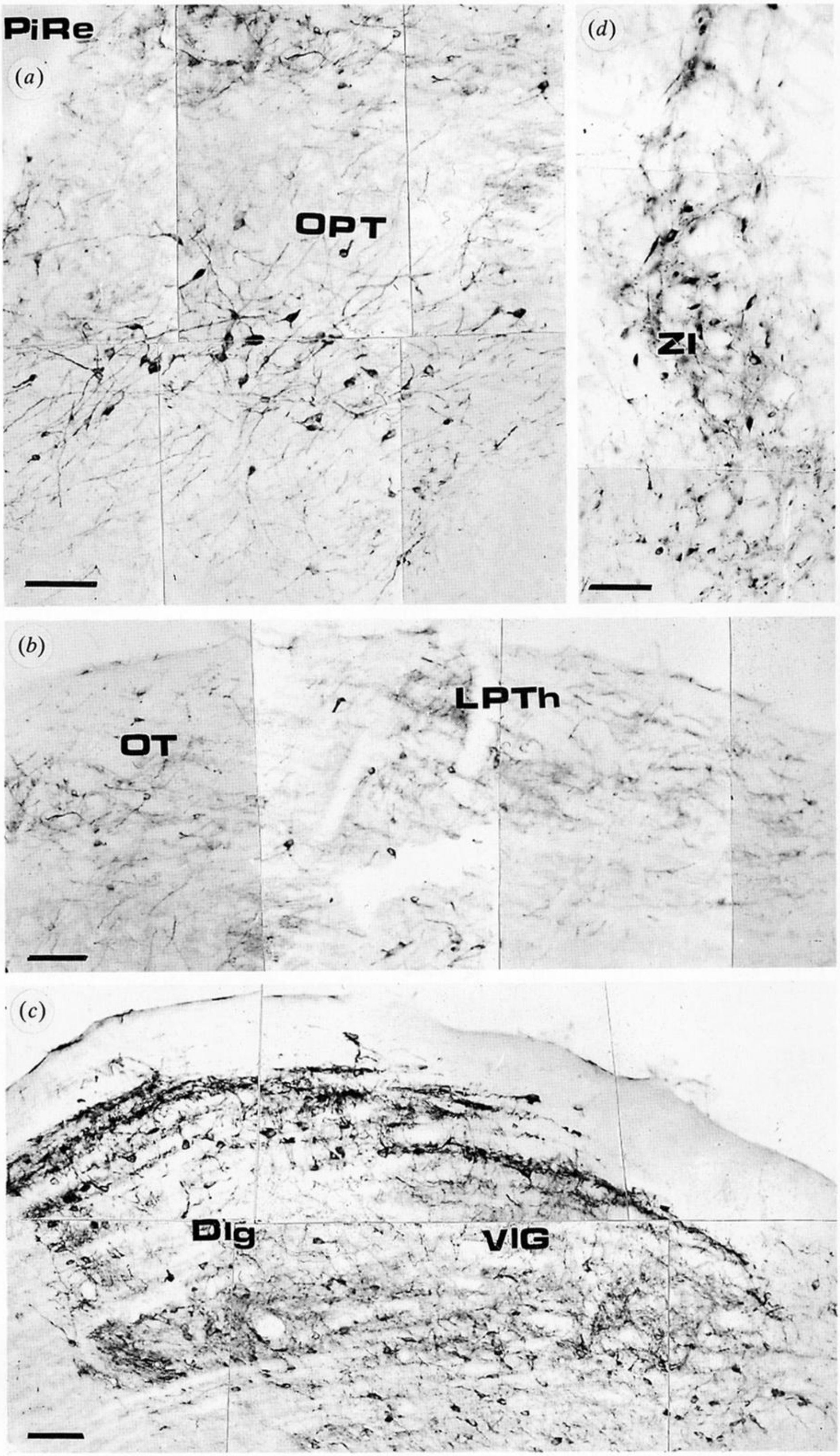

Figure 20. Micrographs illustrating the distribution of cNOS-IR neurons in the dorsolateral region of the thalamus. (*a*) Positive neurons in the olivary pretectal nucleus (OPT). (*b*) Positive neurons in the nucleus of the optic tract (OT) and in the lateroposterior thalamic nucleus (LPTh). (*c*) Distribution of immunoreactive nerve fibres and neurons in the dorsolateral geniculate (Dlg) and ventrolateral geniculate (VlG) nuclei. (*d*) Distribution of reactive nerve fibres and neurons in the zona incerta (ZI). Scale bars = 100 μm.

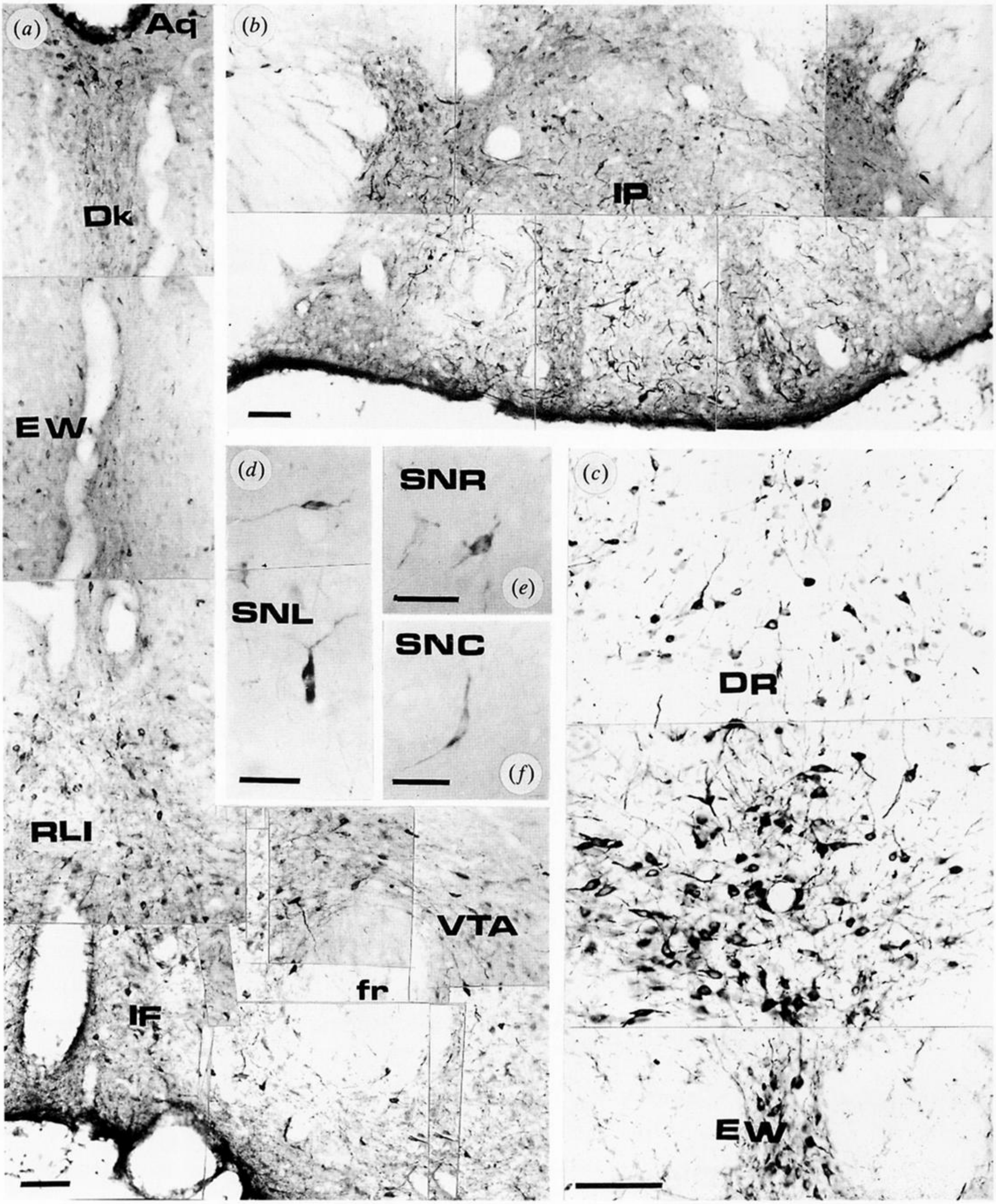

Figure 21. Photomontage showing the distribution of immunoreactive neurons in the mesencephalon. (*a*) Positive neurons in the ventral tegmental area (VTA), interfascicular nucleus (IF), rostral linear nucleus raphe (RLI), Edinger-Westphal nucleus (EW) and nucleus of Darkschewitsch (Dk). (*b*) Immunoreactive neurons in the interpeduncular nucleus (IP). (*c*) Reactive neurons in the dorsal raphe nucleus (DR). (*d–f*) Isolated immunoreactive neurons in the pars lateralis (SNL), pars reticulata (SNR) and pars compacta (SNC) of the substantia nigra. Scale bars: (*a–c*) = 100 μm; (*d–f*) = 50 μm.

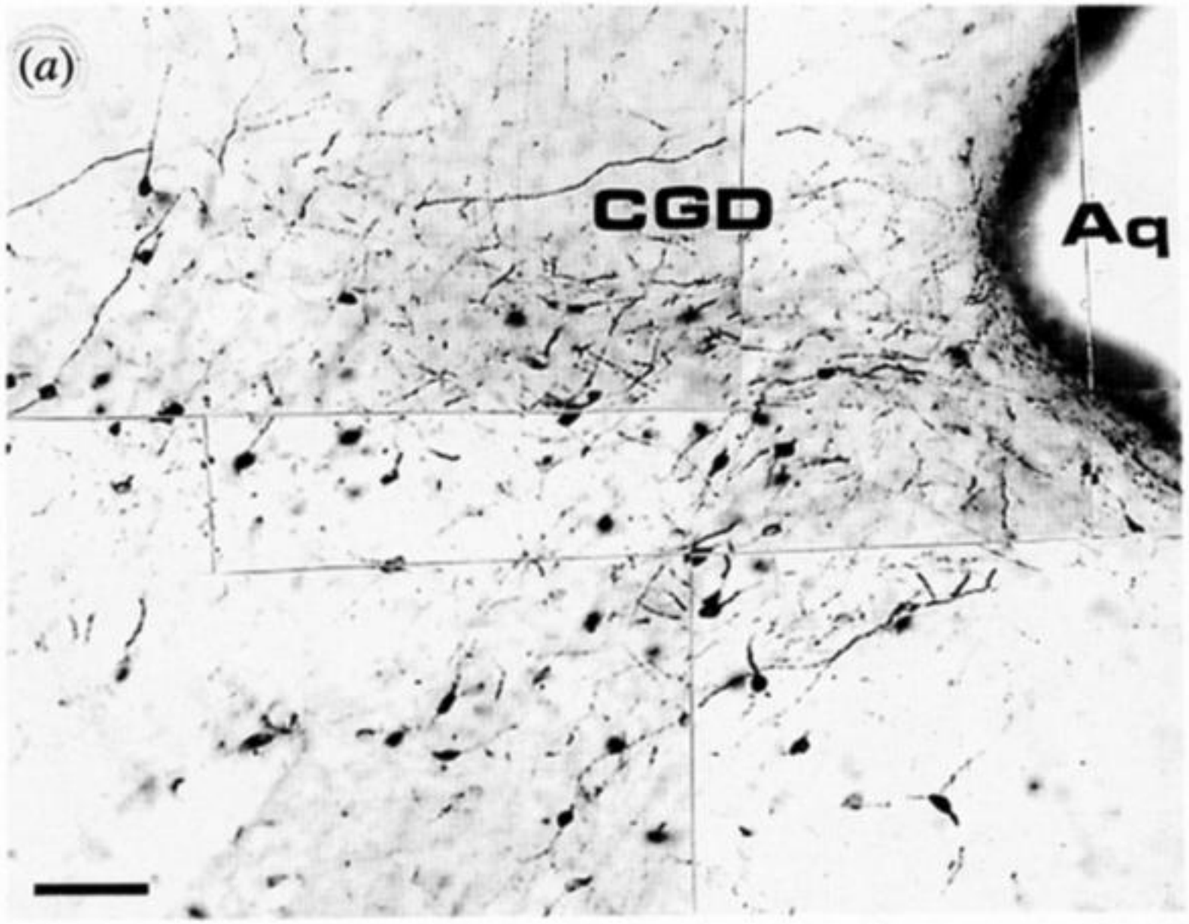

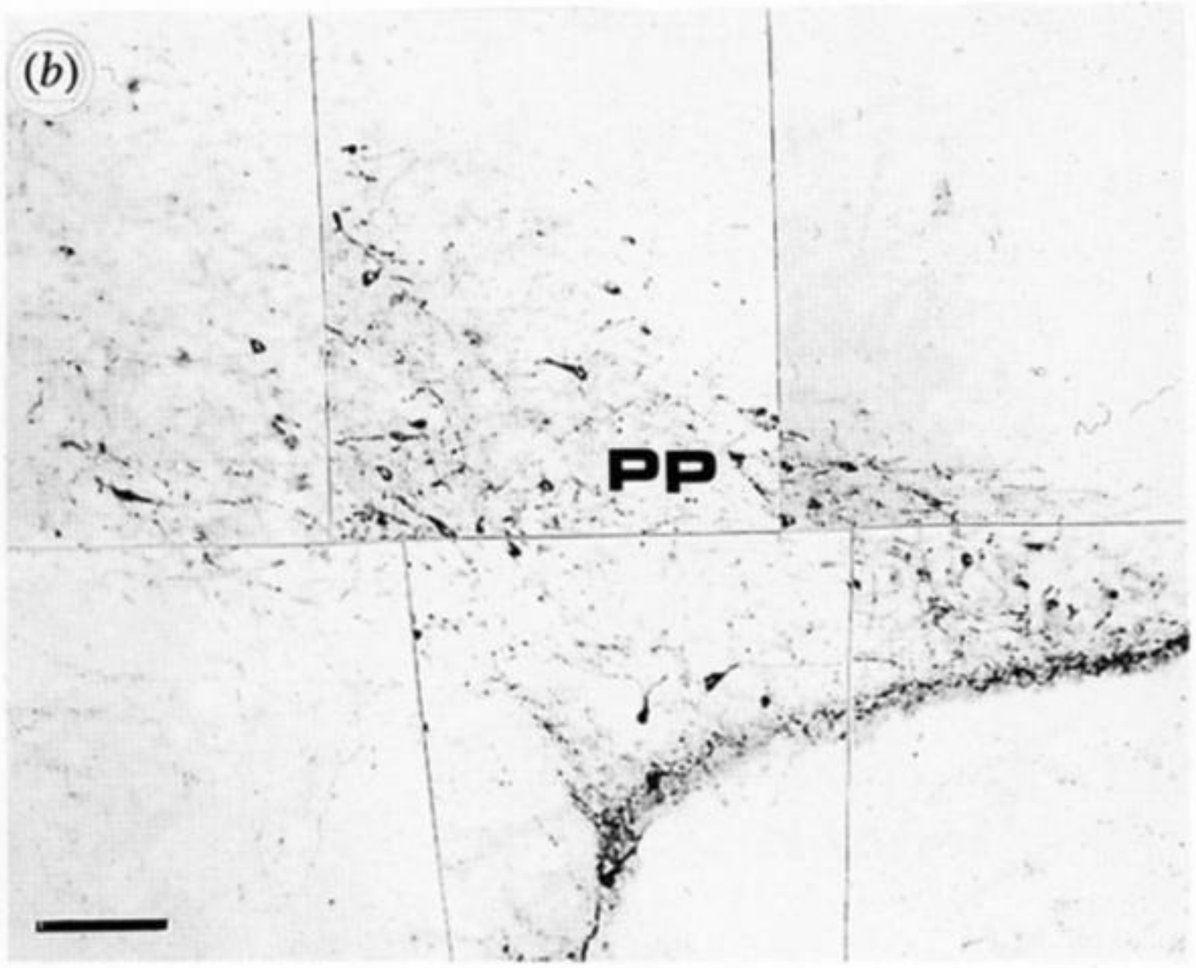

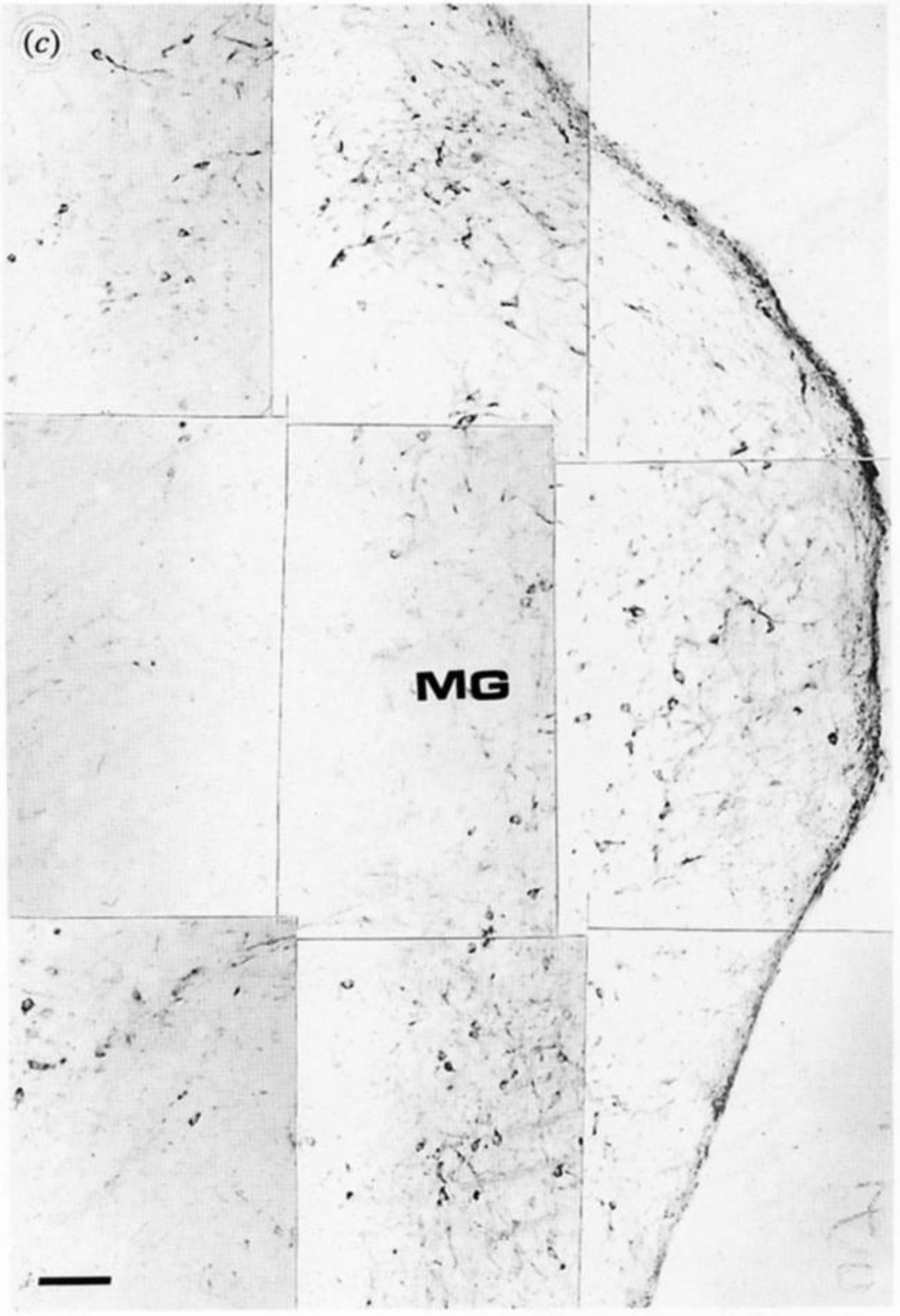

Figure 22. (*a*) Distribution of cNOS-IR neurons in the dorsal portion of the periaqueductal central grey (CGD). (*b*) Positive neurons in the peripeduncular nucleus (PP). (*c*) Positive neurons in the medial geniculate nucleus (MG). Scale bars = 100 μm.

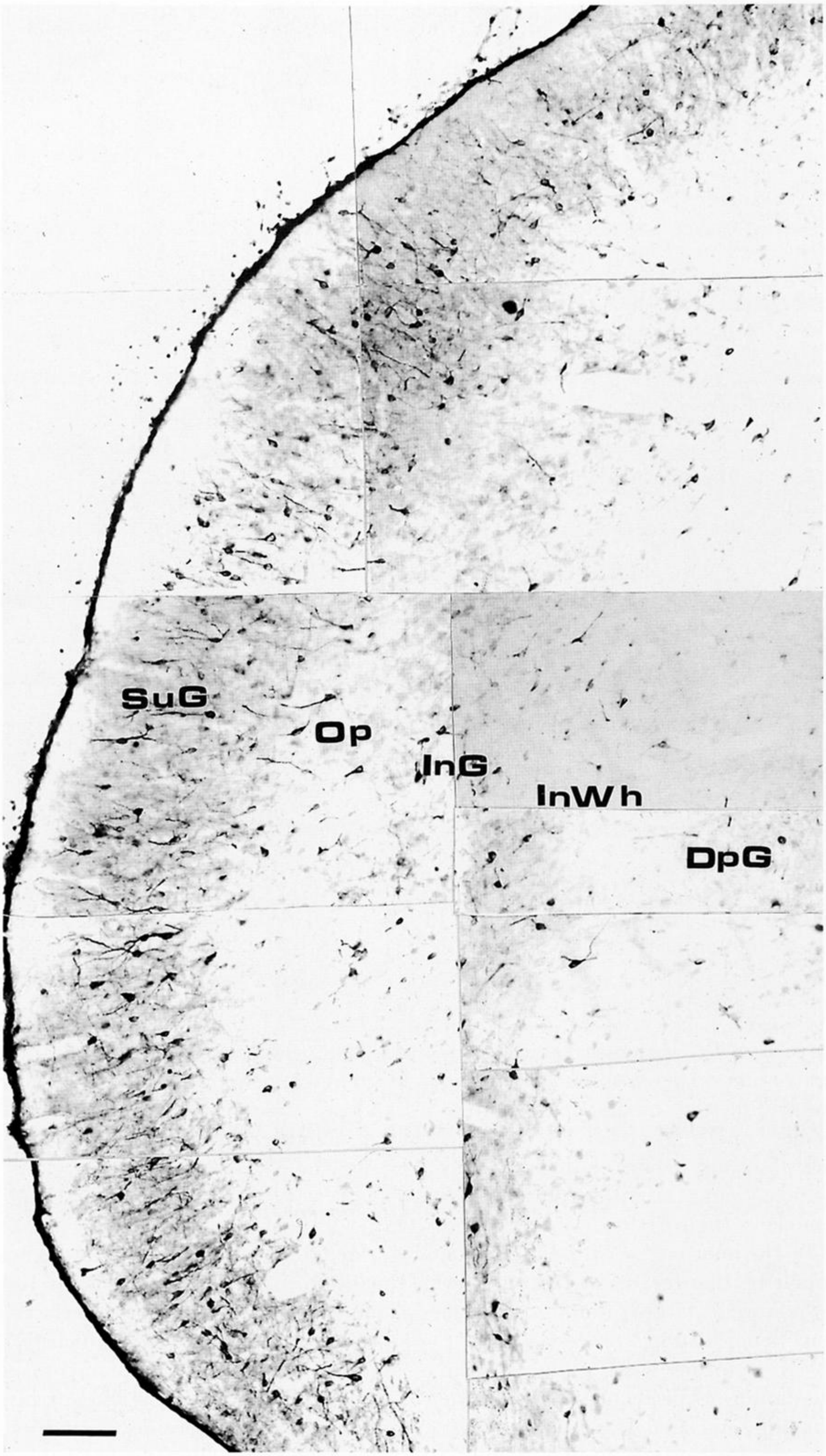

Figure 23. Photomontage showing the distribution of cNOS-IR neurons in the superior colliculus. A large number of positive neurons are present in the superficial grey layer (SuG); these neurons are less abundant in the optic nerve layer (Op), the intermediate grey layer (InG), intermediate white layer (InWh) and in the deep white layer (DpG). Scale bars = 100 μm.

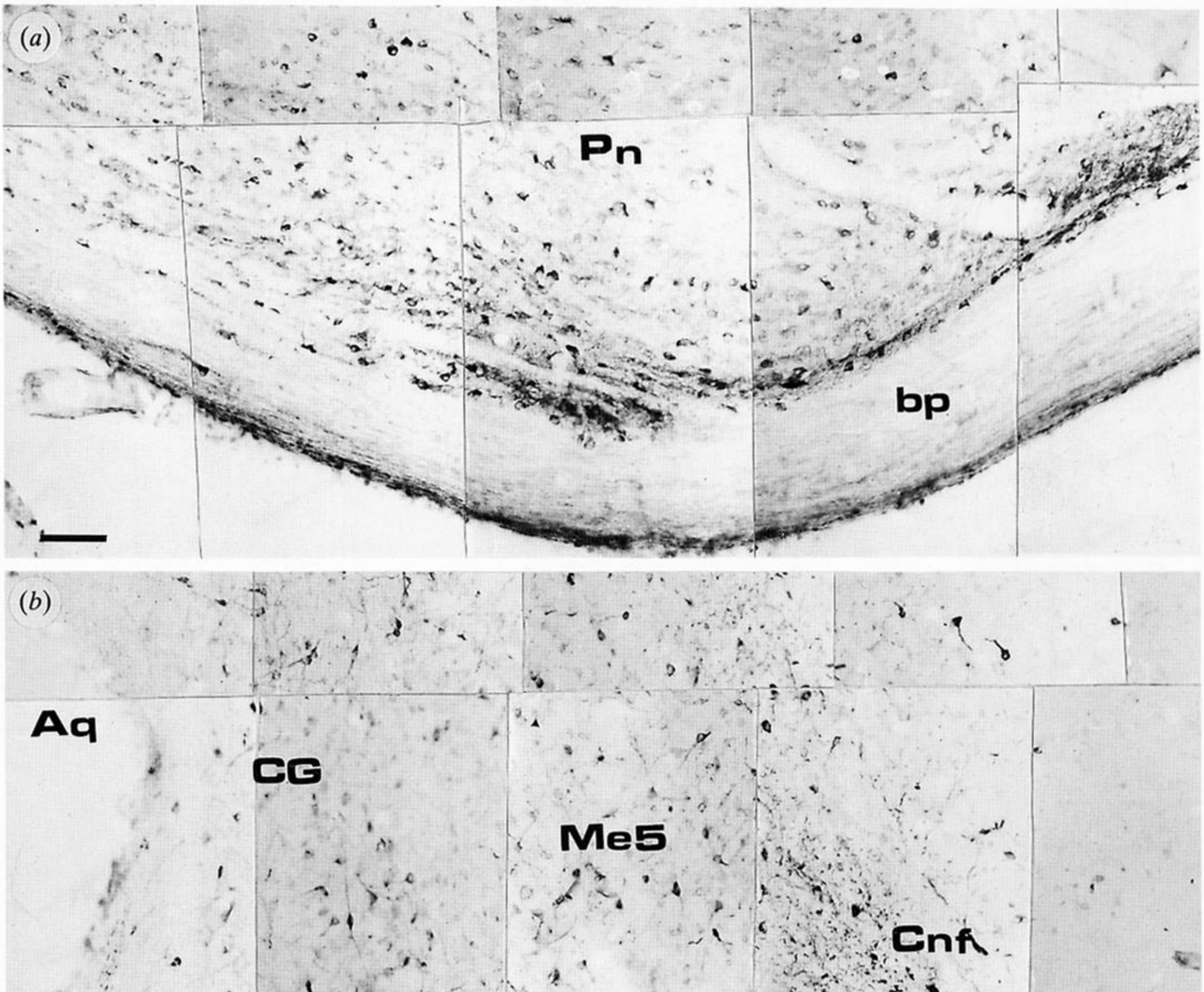

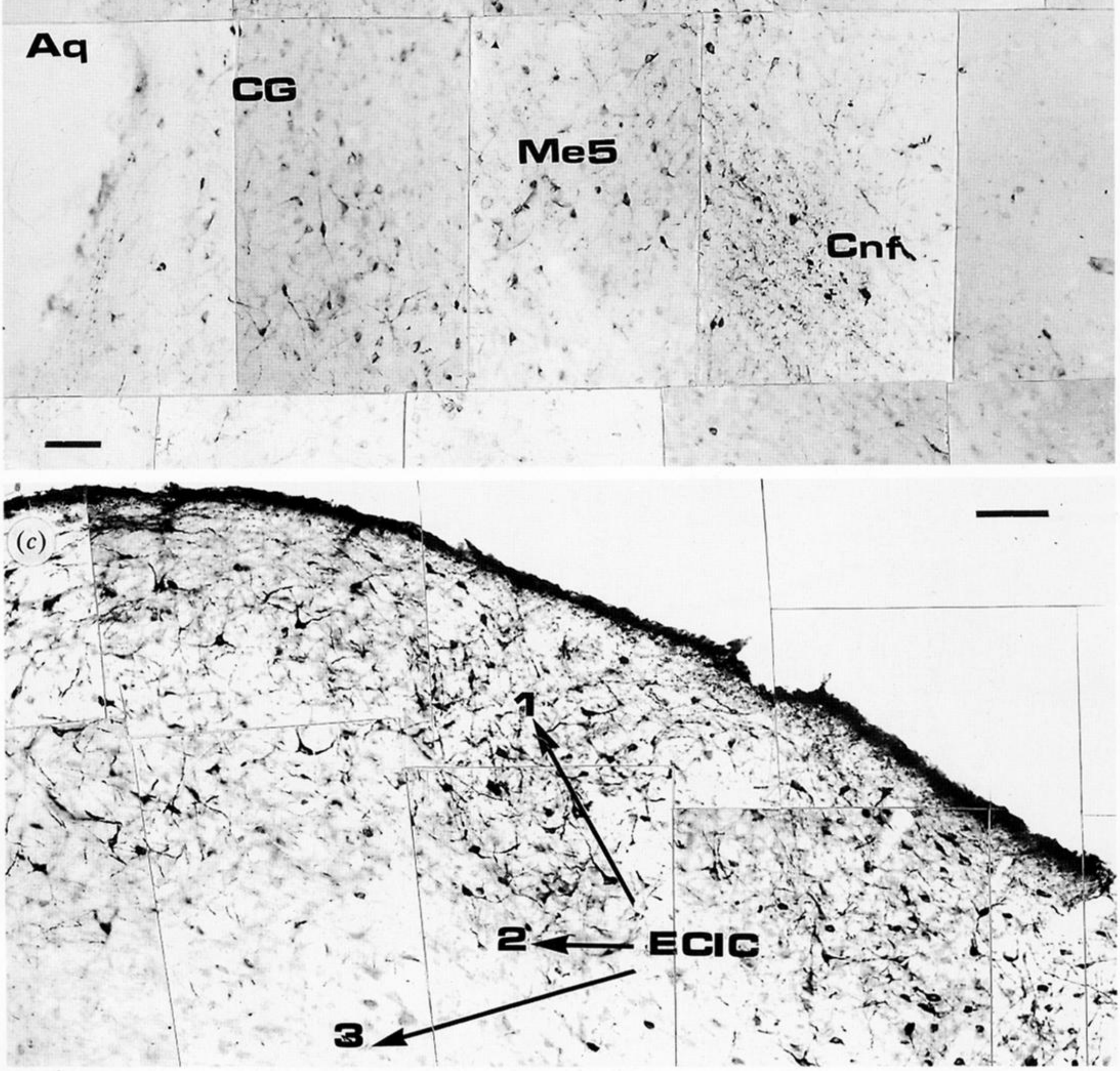

Figure 24. (*a*) Distribution of cNOS-IR neurons in the pontine nucleus (Pn). (*b*) Reactive neurons in the cuneiform (Cnf) nucleus and in the region of the mesencephalic trigeminal (Me5) nucleus. (*c*) Distribution of cNOS-IR neurons in the inferior colliculus. Notice that most reactive neurons in this nucleus are located in layer 1 of the external cortex (ECIC). Aq, aqueduct; CG, central grey; bp, brachium pontis. Scale bars = 100 μm.

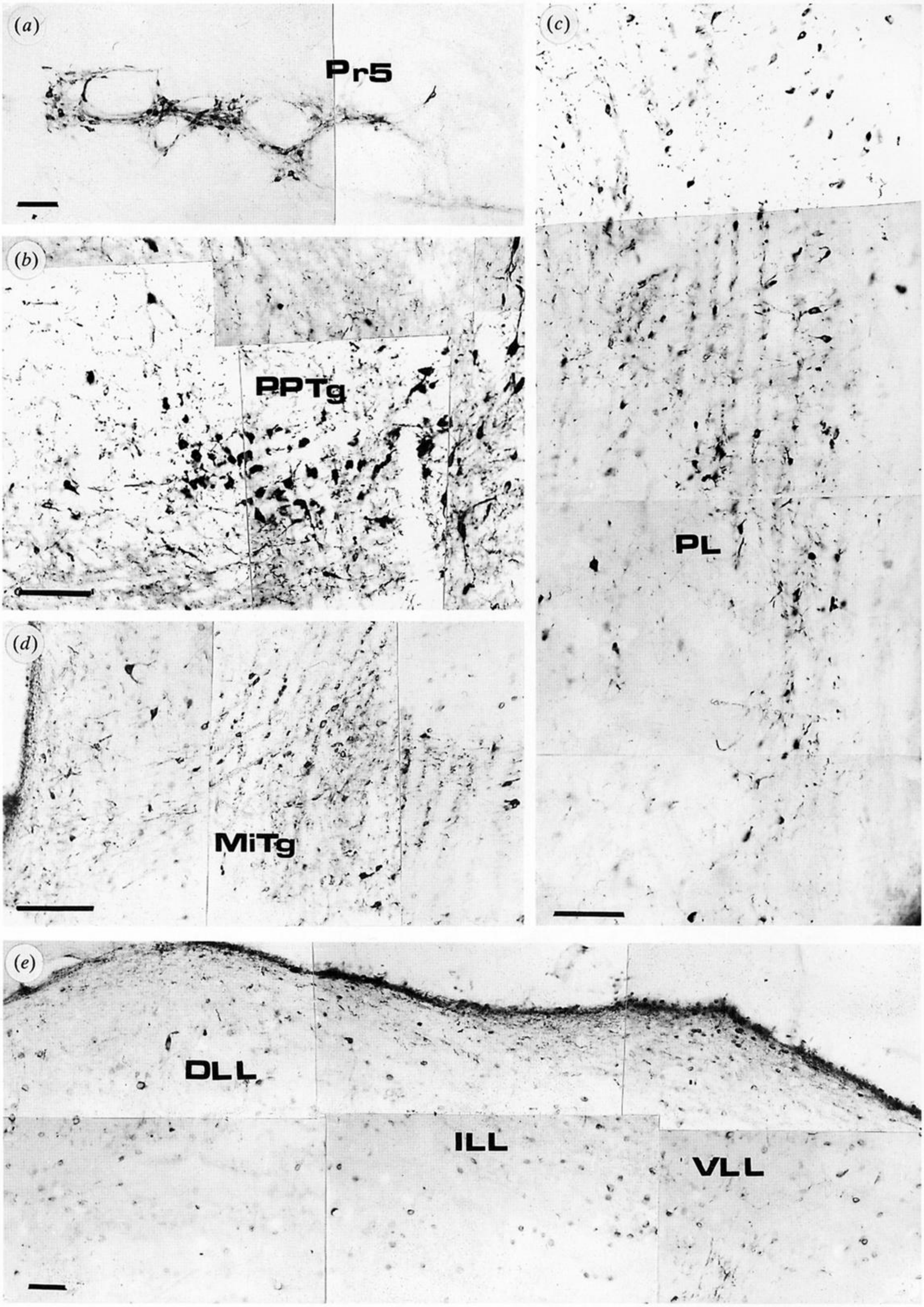

Figure 25. (*a*) Immunoreactive neurons in the principal sensory trigeminal nucleus (Pr5). (*b*) Reactive neurons in the pedunculopontine tegmental nucleus (PPTg). (*c*) Discrete distribution of immunoreactive neurons in the paralemniscal nucleus (PL). (*d*) Immunoreactive neurons distributed in the microcellular tegmental nucleus (MiTg). (*e*) A small number of reactive neurons distributed along the dorsal (DLL), intermediate (ILL) and ventral (VLL) nuclei of the lateral lemniscus. Scale bars = 100 μm.

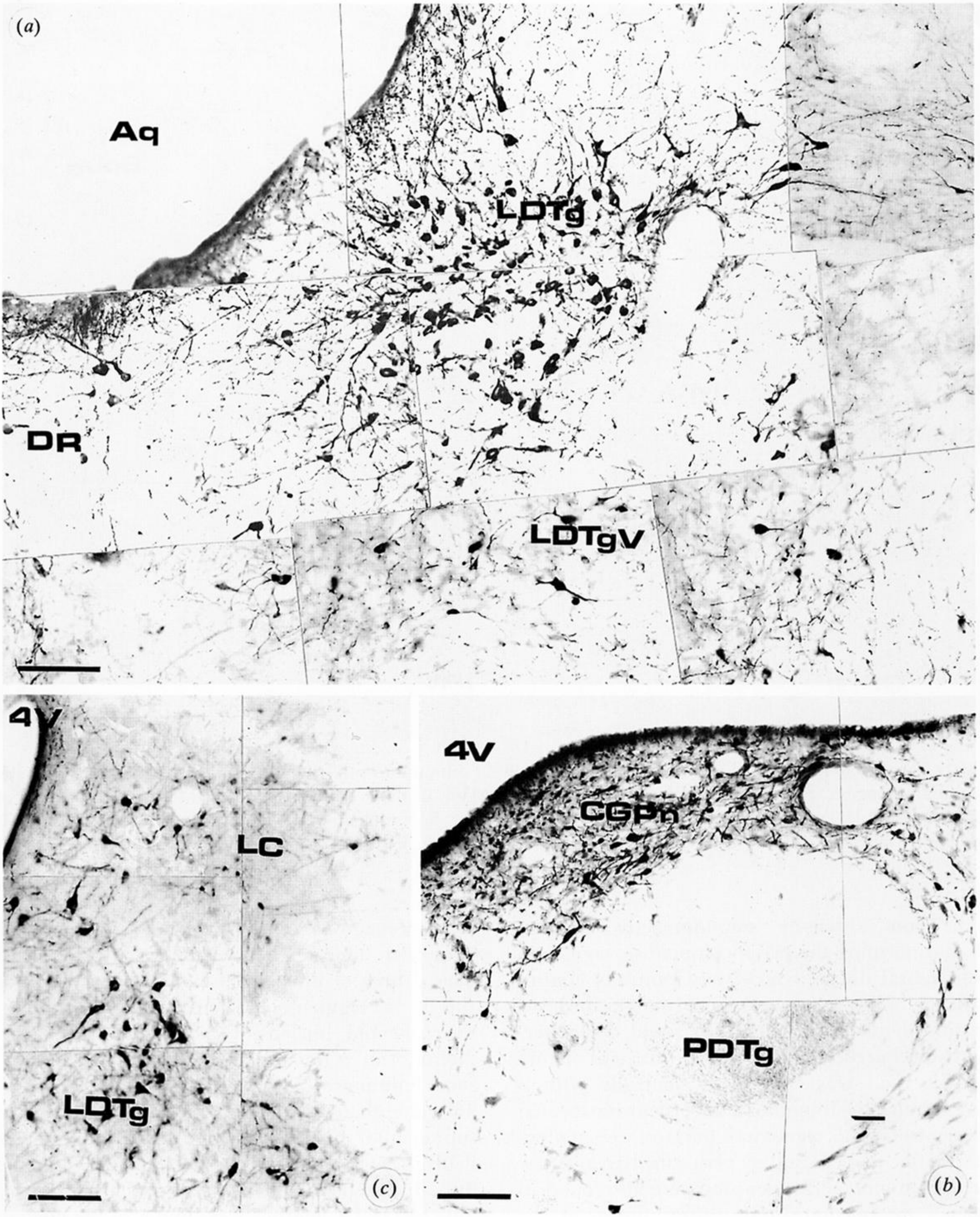

Figure 26. (*a*) Photomontage showing the distribution of cNOS-IR neurons in the rostral area of the laterodorsal tegmental nucleus (LDTg). Notice that reactive neurons are ventrally continuous with the ventral part of the laterodorsal tegmental nucleus (LDTgV). (*b*) Distribution of positive neurons in the central grey of the pons (CGPn) surrounding the posterodorsal tegmental nucleus (PDTg). (*c*) Immunoreactive neurons in the locus coeruleus (LC). 4V, fourth ventricle; DR, dorsal raphe nucleus; Aq, aqueduct. Scale bars = 100 μm.

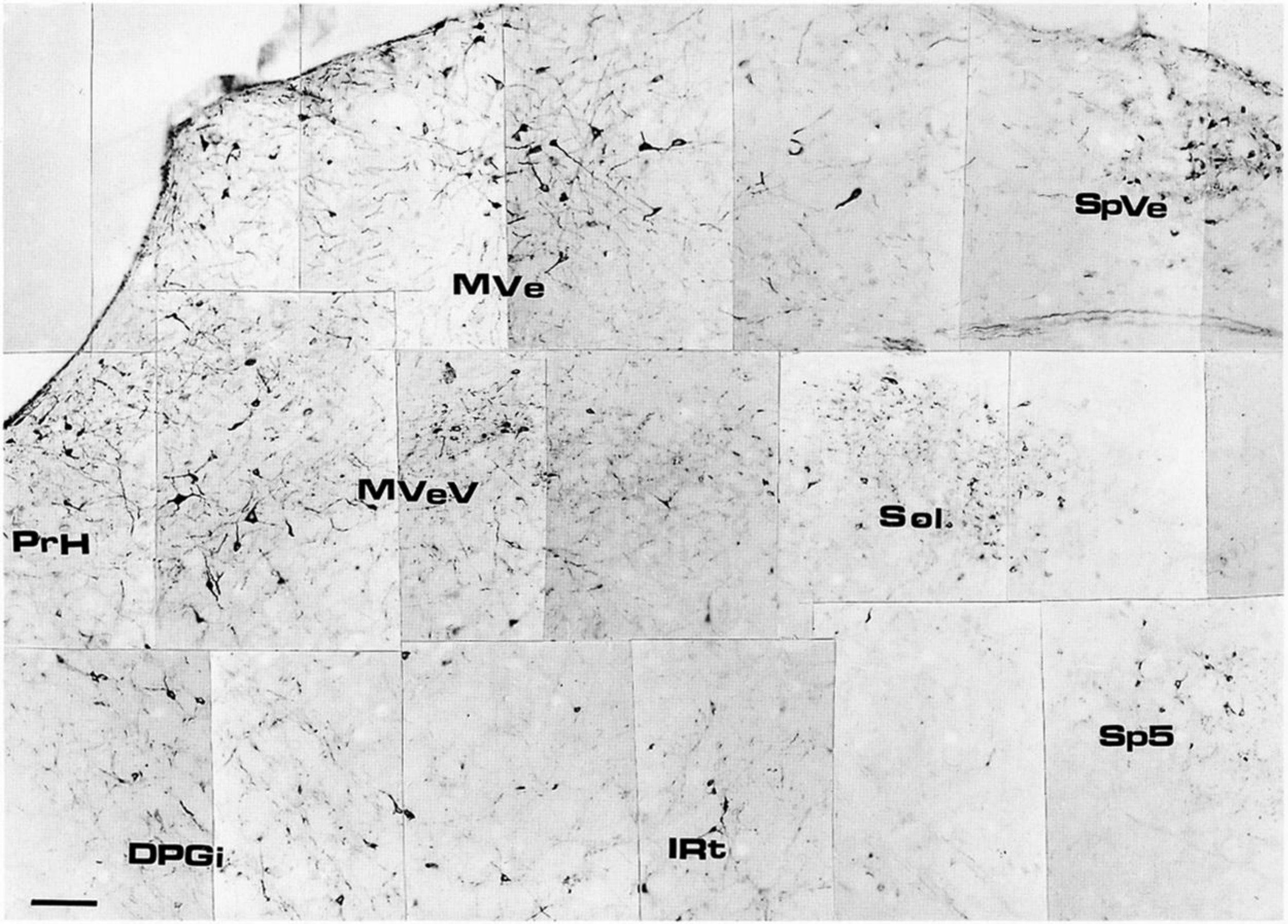

Figure 27. Photomontage illustrating the distribution of immunoreactive neurons of the dorsal area of the medulla oblongata. PrH, prepositus hypoglossal nucleus; MVe, medial vestibular nucleus; MVeV, ventral area of medial vestibular nucleus; SpVe, spinal vestibular nucleus; Sp5, dorsomedial spinal trigeminal nucleus; Sol, nucleus of the solitary tract; DGPi, dorsal paragigantocellular nucleus; IRt, intermediate reticular nucleus. Scale bar = 100 μm.

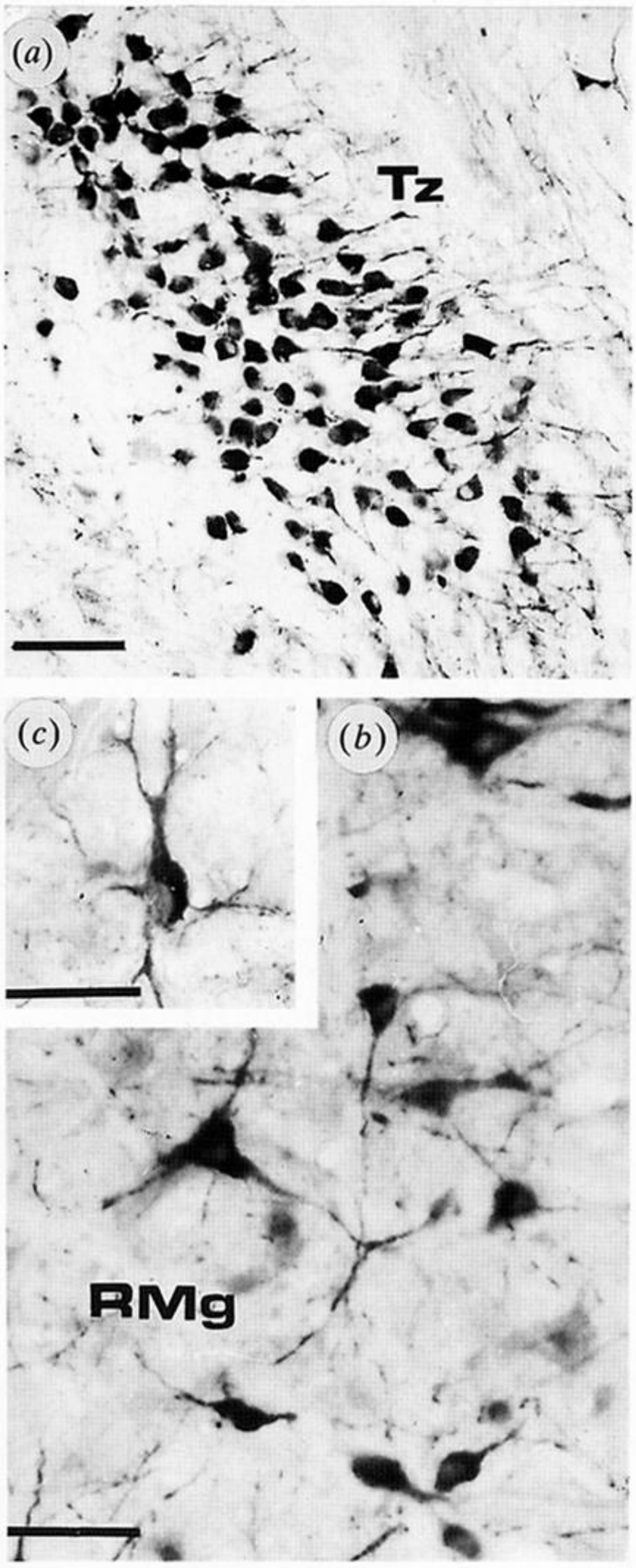

Figure 28. (*a*) Immunoreactive neurons in the trapezoid body (Tz). (*b*) Reactive neurons in the raphe magnus nucleus (RMg). (*c*) Morphological details of immunoreactive neurons of the RMg. (*d*) Distribution of cNOS-IR fibres in the lateral superior olive (LSO). Notice in (*d*) that varicose reactive fibres surround unreactive neurons. (*e*) Immunoreactive neurons distributed in the dorsal cochlear nucleus (DC). (*f*) cNOS-IR neurons forming the lateral paragigantocellular nucleus (LPGi). Scale bars: (*a*, *d*–*f*) = 100 μm; (*b*,*c*) = 50 μm.

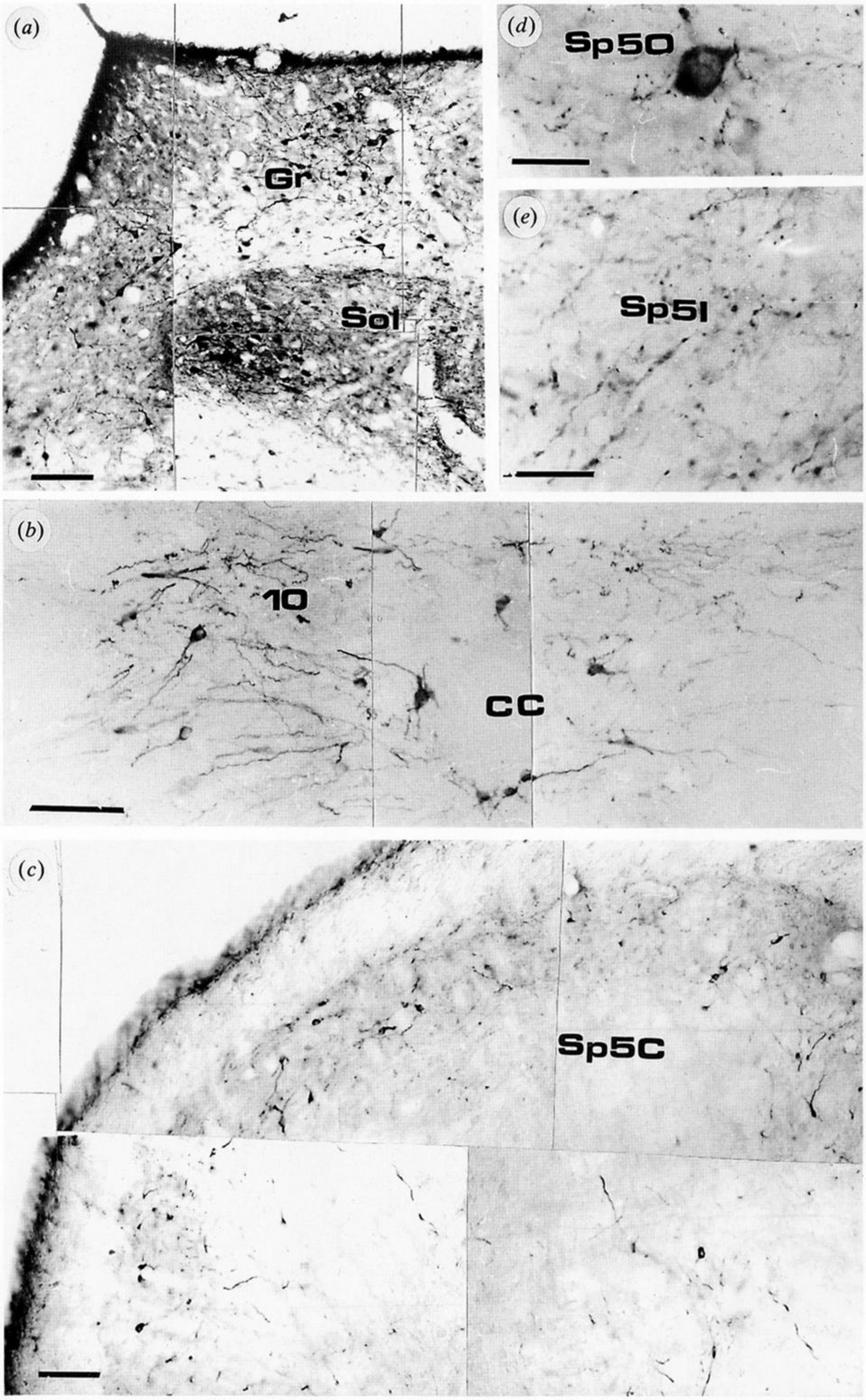

Figure 29. (*a*) Micrograph illustrating the distribution of immunoreactive neurons in the gracile nucleus (Gr) and caudal area of the nucleus of the solitary tract (Sol). (*b*) Immunoreactive neurons in the nucleus of the dorsal motor vagus nerve (10). (*c–e*) Distribution of immunoreactive neurons and processes in the pars oralis (Sp5O), interpolaris (Sp5I) and caudalis (Sp5C) of the spinal trigeminal nucleus. Scale bars: (*a–c*) = 100 μm; (*d,e*) = 25 μm.

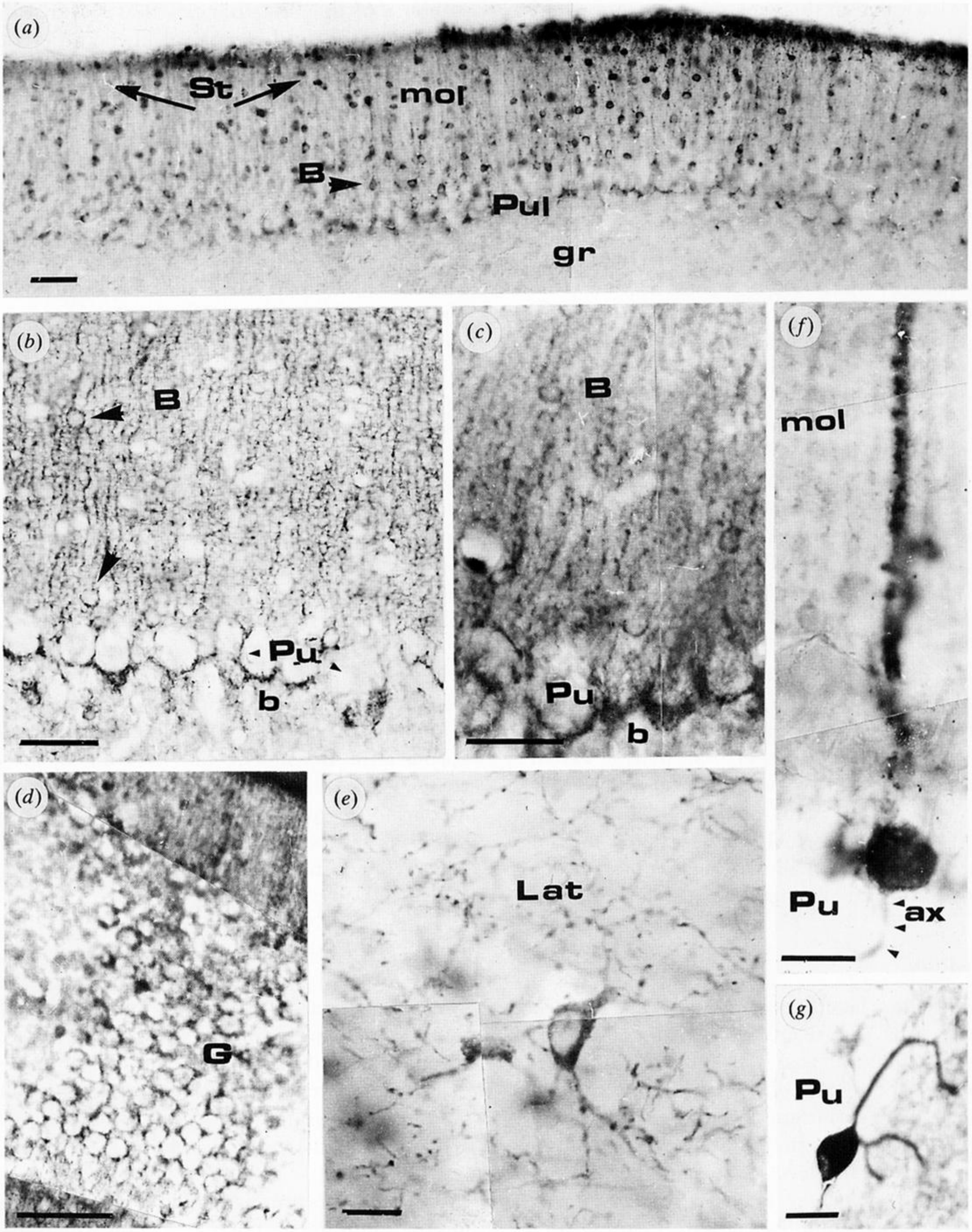

Figure 30. Distribution of cNOS-IR in the cerebellum. (*a*) General view of reactive structures in the different layers of the cerebellar cortex. Stellate cells (St) are located in the upper portion of the molecular layer (mol). Basket cells (B) are situated in the deep regions of the mol (arrow heads). Pul, Purkinje cell layer; gr, granular cell layer. (*b*) Distribution of basket cell bodies (arrowheads) and terminals (b). Pu, Purkinje cells. (*c*) High-power magnification of the molecular and Purkinje cell layers, providing details of the distribution of the basket terminals (b) which characteristically surround the initial portion of the Purkinje cell axons. (*d*) Granule cells exhibiting endogenous cNOS. (*e*) depicts the distribution of immunoreactive varicose nerve fibres and neurons in the lateral cerebellar nucleus (Lat). (*f,g*) Isolated immunoreactive Purkinje cells (Pu) located in the vermis and paraflocculus, respectively. ax, initial portion of Purkinje cell axon. Scale bars: (*a–d*) = 100 µm; (*e–g*) = 25 µm.